Mismatch Power Losses Minimization in Photovoltaic Array

by

Ahmed Al Mansur

DOCTOR OF PHILOSOPHY

IN

ELECTRICAL AND ELECTRONIC ENGINEERING

Department of Electrical and Electronic Engineering
Islamic University of Technology (IUT)
Board Bazar, Gazipur-1704, Bangladesh.

November, 2019.

CERTIFICATE OF APPROVAL

The thesis titled '**Mismatch Power Losses Minimization in Photovoltaic Array'** submitted by Ahmed Al Mansur, St. No. 112701 of Academic Year 2011-12 has been found as satisfactory and accepted as partial fulfillment of the requirement for the Degree DOCTOR OF PHILOSOPHY IN ELECTRICAL AND ELECTRONIC ENGINEERING on 1 November 2019.

Board of Examiners:

_____ **Dr. Md. Ruhul Amin** (Supervisor) Professor and Head, Electrical and Electronic Engineering Department, Islamic University of Technology (IUT), Gazipur.	Chairman (Ex-Officio)
_____ **Dr. Md. Ashraful Hoque** Professor and Dean, Electrical and Electronic Engineering Department, Islamic University of Technology (IUT), Gazipur.	Member
_____ **Dr. Syed Iftekhar Ali** Professor, Electrical and Electronic Engineering Department, Islamic University of Technology (IUT), Gazipur.	Member
_____ **Dr. Ashik Ahmed** Associate Professor, Electrical and Electronic Engineering Department, Islamic University of Technology (IUT), Gazipur.	Member
_____ **Dr. Md. Faruk Hossain** Professor and Head, Electrical and Electronic Engineering Department, Rajshahi University of Engineering and Technology (RUET), Rajshahi.	Member (External)
_____ **Dr. Muhammad Fayyaz Khan** Professor, Electrical and Electronic Engineering Department, Bangladesh University of Business and Technology (BUBT), Dhaka	Member (External)

Declaration of Candidate

It is hereby declared that this thesis report or any part of it has not been submitted elsewhere for the award of any Degree or Diploma.

_____

Dr. Md. Ruhul Amin
Professor and Head,
Electrical and Electronic Engineering Department,
Islamic University of Technology (IUT).
Date: 1 November, 2019.

_____

Ahmed Al Mansur
Student No.: 112701
Academic Year: 2011-12
Date: 1 November, 2019.

Dedicated to my parents and adorable wife.

Table of Contents

List of Figures

List of Tables

List of Abbreviations of Technical Terms

MML	**M**ismatch **P**ower **L**oss
MPP	**M**aximum **P**ower **P**oint
PV	**P**hotovoltaic
FF	**F**ill **F**actor
GA	**G**enetic **A**lgorithm
SP	**S**eries **P**arallel
LSS	**L**ong **S**eries **S**tring
LPB	**L**ong **P**arallel **B**anch
SCC	**S**hort **C**ircuit **C**urrent
TCT	**T**otal **C**ross **T**ied
BL	**B**ridge **L**inked
HC	**H**oney **C**ombed
LD	**L**adder **D**iagram
STC	**S**tandard **T**est **C**ondition
AM	**A**ir **M**ass
IEC	**I**nternational **E**lectrotechnical **C**ommission
RE	**R**ecoverable **E**nergy
KVL	**K**irchhoff **V**oltage **L**aw
KCL	**K**irchhoff **C**urrent **L**aw

GMPP	**G**lobal **M**aximum **P**ower **P**oint
MPPT	**M**aximum **P**ower **P**oint **T**racking
SD	**S**tandard **D**eviation
GDP	**G**ross **D**omestic **P**roduct
GB	**G**lobal **B**est
RSD	**R**emote **S**olar **D**etector
OPC	**O**utdoor **O**perating **C**ondition
PVSA	**P**hotovoltaic **S**ystem **A**nalyzer
ESPL	**E**lectro **S**olar **P**ower **L**imited
IDCOL	**I**nfrastructure **D**evelopment **C**ompany **L**imited
SE4ALL	**S**ustainable **E**nergy for **A**ll
CIF-SREP	**C**limate **I**nvestment **F**unds **S**caling Up **R**enewable **E**nergy **P**rogram
NDC	**N**ationally **D**etermined **C**ontribution
SREDA	**S**ustainable and **R**enewable **E**nergy **D**evelopment **A**gency
IPPs	**I**ndependent **P**ower **P**roducers
IFC	**I**nternational **F**inance **C**orporation
USAID	**U**nited **S**tates **A**gency for **I**nternational **D**evelopment
UNDP	**U**nited **N**ations **D**evelopment **P**rogram
TSEL	**T**echnaf **S**olartech **E**nerg**y** **L**td

ACKNOWLEDGMENTS

I would like to first acknowledge my thesis supervisor Professor Dr. Md. Ruhul Amin, for his help and guidance in the past three years. Three years ago, I was a novice in research paper writing. Three years later, I feel like a serious researcher and feel prepared to enter the next stage in my academic career. He not only taught me how to do research, but also showed me, by his own example, how to be a great educator and a caring advisor. I am grateful for all his help both in my research work and in many other aspects. It is always a pleasure to have a supervisor with such knowledge, insights and patience.

I would also like to express my sincere appreciation to the Dean, Faculty of Science and Engineering, IUT, Professor Dr. Md. Ashraful Hoque for providing all kinds of supports to accomplish the work. I want to thank Professor Dr. Kazi Khairul Islam, UU for spending much of his precious time on my works. I am also grateful to Professor Dr. Md. Fayyaz Khan, VC, BUBT and Professor Dr. Abdur Razzak, IUB for their fruitful comments and suggestions. There are many people who helped me a lot with the work in this thesis. Professor Dr. Ashik Ahmed, EEE, IUT helped me to develop the genetic algorithm and Md. Mozaharul Mottalib, CIS, University of Delaware, USA wrote a very neat simulation code that I used in this work. I also want to thank Dr. Rakibul Hasan Sagor, Md. Thesun Al-Amin, Fuad Adnan, from IUT for their help, sharing their knowledge and great ideas. I also want to thank all my office mates, who make it a fun place to work. A special thanks to my office roommates Mr. Shamim Mondol, and Dr. Aminur Rahman, GUB, for their supports and cooperation for helping me during various stages of my thesis. There are many more people than I can list here.

I would like to convey my thanks to my parents, my brothers for supporting me the whole way through, especially my father, Tajuddin Ahmed for his constant encouragement and support during these past years.

Most of all, I want to thank my wife, Afroza. The delicious food she cooked and her constant love and comfort provided the strongest support in all my endeavors. I am always grateful for her joyful company.

Ahmed Al Mansur
November, 2019.

ABSTRACT

The mismatch in current-voltage (*I-V*) characteristics of Photovoltaic (PV) modules causes significant power loss in a large PV array, which is known as mismatch power loss (MML). In a PV array MML depends on several factors, such as partial shading, manufacturing tolerance and non-uniform aging. Recent investigations have reported that in PV array MML varies from 1% to 10% due to manufacturing tolerance (±3% to ±5%) and power degradation is typically 0.8% per year due to aging of PV modules and the economic loss is very significant. In this work, different conventional MML reduction techniques are investigated and an adaptive genetic algorithm (GA) based module rearrangement technique has been proposed for MML reduction both in new and aged PV arrays. For new PV arrays, MML due to manufacturing tolerances is investigated using 400 W, 3400 W, and 9880 W PV arrays with different (1×40, 2×20, 4×10, 5×8 40×1, 20×2, 10×4, and 8×5) series-parallel (SP) configurations. MML due to non-uniform aging is investigated using 400 W, 1.6 kW, 3.2 kW, and 10 kW aged PV arrays with the same SP configurations. Simulation and experimental results show that GA based module rearrangement technique performed better than conventional techniques both for new and aged PV arrays. For new PV array a maximum percentage of recoverable energy %RE of 4.15 % is recorded for 5×8 SP array by applying *GA* based MML reduction method. The GA based technique yields a maximum %RE of 4.67% for two years aged 8×5 SP array configuration. In addition, the performance of conventional array configurations (SP, TCT, BL, HC, and LD) and hybrid array configurations (HC-TCT, LD-TCT, TCT-S, S-TCT, SP-LD, LD-SP, and SP-TCT) are also investigated for MML reduction using non-uniformly aged PV array with different dimensions. Experimental results show that most of the hybrid array configurations are performed better than conventional interconnection topologies with respect to MML% mitigation for non-uniformly aged PV array. A maximum %RE of 15.94% is recorded for LD-SP configuration compared with most conventional SP configuration for a 400 W PV array. Moreover, a case study is performed to investigate the daily, monthly and yearly economic benefit of GA based MML reduction of a 28 MW PV plant both at new and aged conditions. The results show that %RE is 1.2% at the time of installation and 1.5% after three years and accordingly the annual extra revenue will be BDT 6585463.64 and 7935299.22 respectively for the 28 MW plant.

CHAPTER 1

Introduction and Background

This chapter provides an overview of the mismatch power losses in Photovoltaic array due to current-voltage (*I-V*) mismatch of array modules. The identification of different reasons of *I-V* mismatch are discussed here. The relevant background and literature reviews are also provided in this chapter. The motivation of this work with problem statements are given afterward. The objectives and methodology of the work are presented sequentially. Finally, the outline of the thesis organization is summarized the last section.

1.1 Mismatch in I-V Characteristics of PV Modules in an Array

Power loss in photovoltaic arrays due to mismatch in cell current-voltage (I-V) characteristics is first time introduced by Louis L. Bucciarelli in 1979 [1]. The maximum output power available from a PV array will be less than the sum of the maximum output power of the individual modules due to I-V mismatch of the modules, given that all operate at common cell-temperature and constant light-intensity levels. I-V mismatch refers to the variation in maximum power point (MPP) voltage, and MPP current of same power rated PV modules. In a PV array, individual PV modules are connected in both series and parallel. Mismatch losses are caused by the interconnection of solar modules which do not have identical properties or which experience different conditions from one another. For example, if two modules are connected in series having non-identical current then they compromise to operate at lower current and similarly two parallel-connected modules have different voltage work towards the smaller voltage [2]. The explanations are given below.

1.1.1 Mismatch for Modules Connected in Parallel

Consider an array with two modules are connected in parallel, and their I-V curves are shown in Figure 1.1. Where, Module 1 (V_{oc1} = 61V and I_{sc1} = 4A) and Module 2 (V_{oc2} = 65V and I_{sc2} = 4.5A) are connected in parallel with mismatch condition. Therefore, the array open-circuit voltage (V_{oc} = 62V) is compromised to operate towards Voc1. But the array short circuit current (I_{sc} = 8.5A) is the sum of the currents in the individual modules. The method of calculating the combined V_{oc} is shown in Figure 1.2.

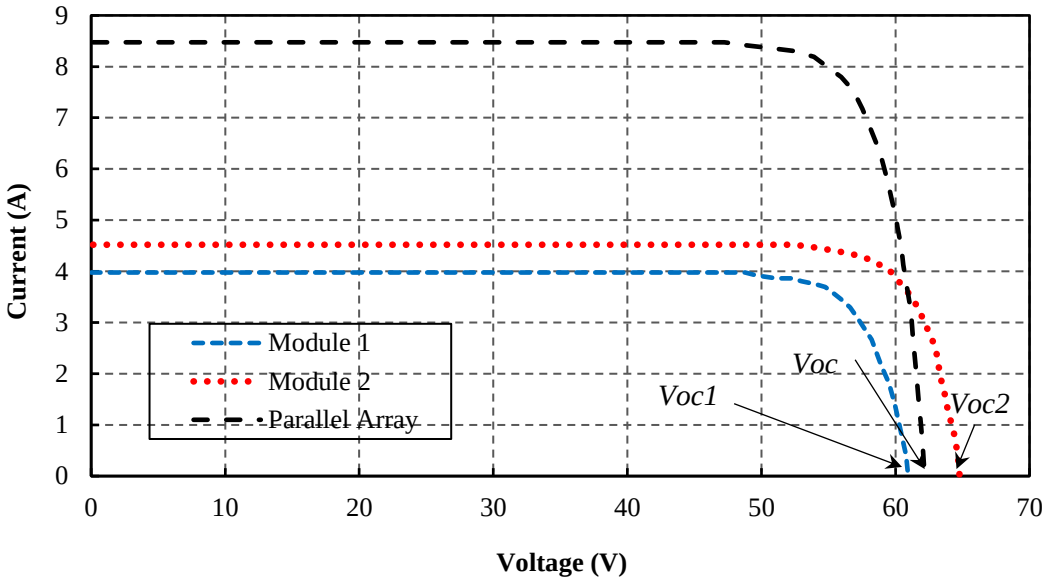

Figure 1.1: Voltage mismatch for two modules in parallel. The individual cells are in red and blue. The black curve is the IV curve of the combination. The V_{OC} of the combination lies between the V_{OC}'s for the individual cells [2].

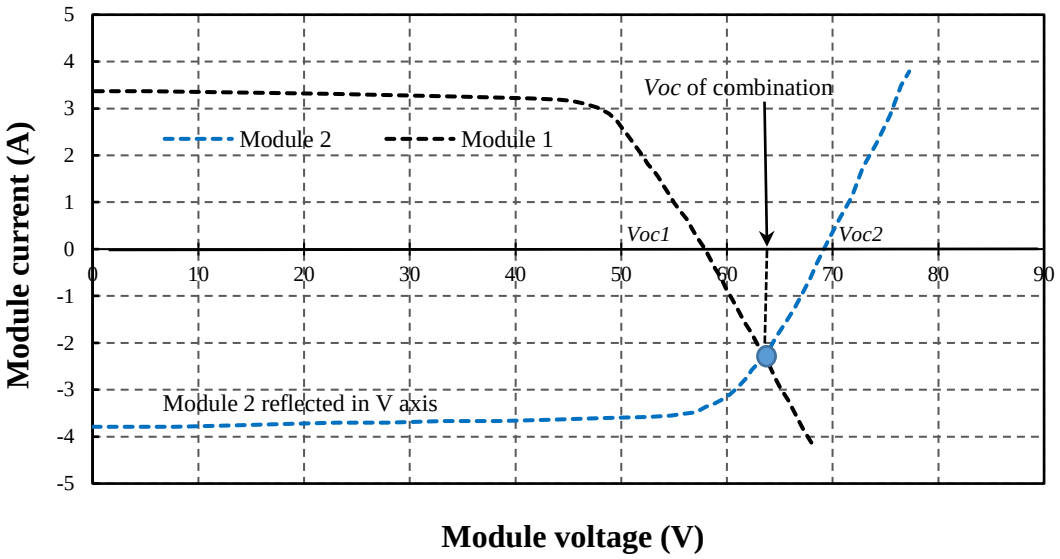

Figure 1.2: An easy method of calculating the combined open circuit voltage (*Voc*) of mismatched modules in parallel. The curve for one of the cells is reflected in the voltage axis so that the intersection point (where I1+I2=0) is the *Voc* of the parallel array [2].

1.1.2 Mismatch for Modules Connected in Series

Consider an array with two modules are connected in series with mismatch condition and their I-V curves are shown in Figure 1.3. Where, the array short circuit current is compromised to operate towards Isc1. But the array open circuit voltage is the sum of the voltage in the individual modules. The method of calculating the combined Isc is shown in Figure 1.4. There is a minor change in the open-circuit

voltage due to the logarithmic dependence of open-circuit voltage on short-circuit current. In a series connected array with current mismatch, severe power reductions are experienced if the poor module produces less current than the maximum power current of the good modules and also if the combination is operated at short circuit or low voltages, the high-power dissipation in the poor module can cause irreversible damage to the module [2].

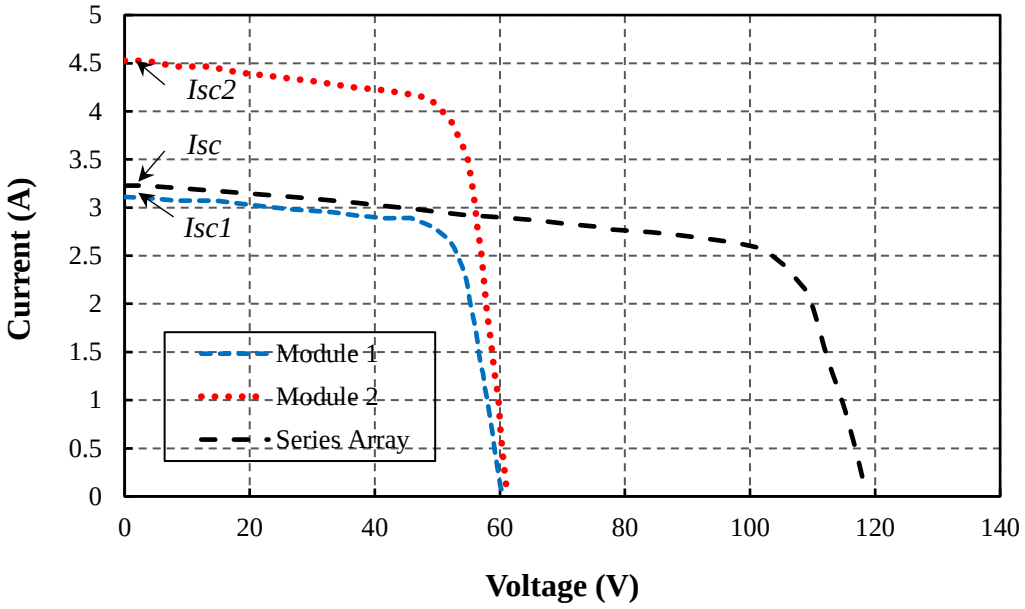

Figure 1.3: Current mismatch for two modules in series can be quite serious and quite common. The I_{sc} of the combination is limited to the I_{sc1} of the lowest module [2].

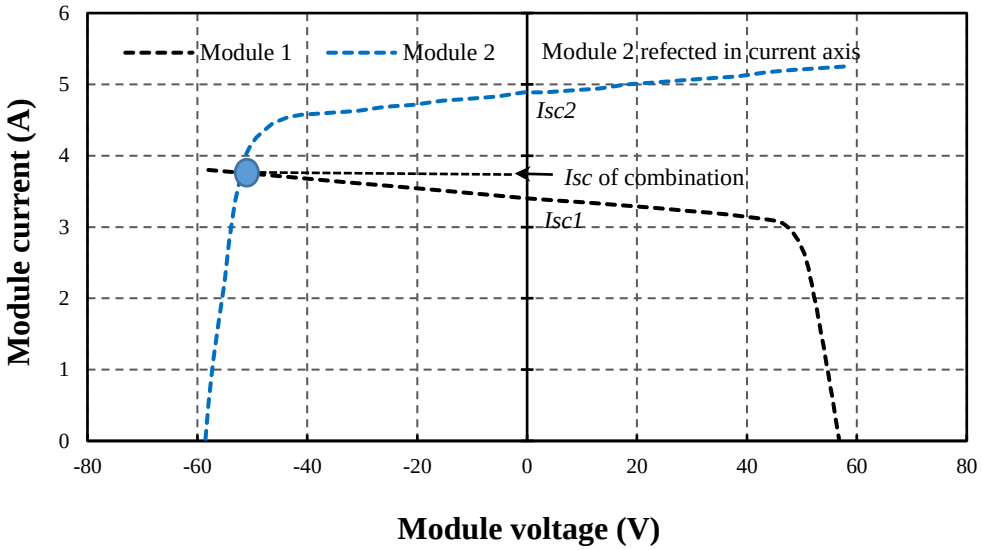

Figure 1.4: An easy method of calculating the combined short-circuit current of series connected mismatched modules. The current at the point of intersection represents the short-circuit current of the series combination (where *V1+V2*=0) [2].

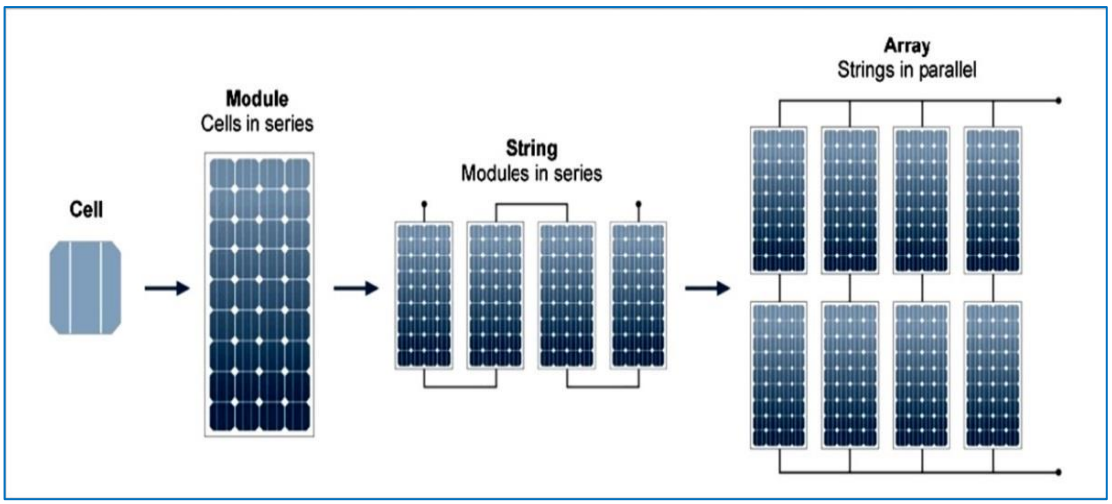

Figure 1.5: Modularity of PV systems

1.2 Reasons of Mismatch Losses in Photovoltaic Array

A PV array consists of a series and parallel combination of PV modules. The same way PV modules are composed of PV cells, shown in Figure 1.5. This modular nature of PV systems is advantageous when it helps to wire the system up to a desirable level of current, voltage, and power. But the fact that PV modules with the same brand and same ratings are not precisely identical turns the modularity of PV systems to be disadvantageous when it causes sort of power losses known as mismatch losses [3, 4]. Hence, investigation and mitigation of mismatch losses among cells inside modules are of PV module manufacturers' interest, whereas such an investigation among modules in arrays is of system operators and installers' interest. This work deals with mismatch losses among modules at the array level.

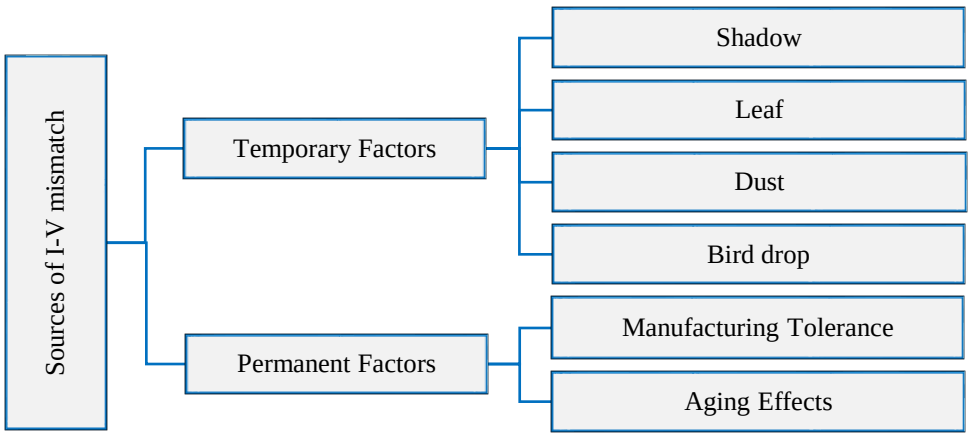

Figure 1.6: Classification of factors that cause mismatch losses in PV array

A group of modules of the same brand and the corresponding nominal ratings is not identical. Their differences are understood by comparing and contrasting their characteristic parameters such as fill factor (FF), maximum power (P_{MPP}), current at maximum power (I_{MPP}), voltage at maximum power (V_{MPP}), short circuit current (I_{SC}) and open circuit voltage (V_{OC}). The difference in modules characteristic parameters is called *I-V* mismatch since it results in different electrical performances. *I-V* mismatch comes from either temporary or permanent sources as classified in Figure 1.6.

1.2.1 Temporary Factors of I-V Mismatch

Shading or non-uniform illumination might happen by fallen leaves of trees, scattered clouds moving over the PV array, shadow of an object situated around the PV array or other reasons [5, 6]. This factor can temporarily result in mismatch losses in a PV array.

1.2.2 Permanent Factors of I-V Mismatch

A. I-V Mismatch for Manufacturing Tolerance

Manufacturing processes are not uniform. The nature of growing crystals and processing wafers and cells makes it nearly impossible to produce cells with no variance between them. Inconsistencies in the semiconductor materials themselves (whether silicon or CdTe), impurities in the air, residue buildup in the manufacturing tools, and thermal drift all contribute to inconsistencies in manufactured modules. No two cells are ever identical [7]. This problem is well-understood, and has a standard solution: manufacturers "bin" their modules, selling them in ranges of power (typically ± 3% to ±5%). Thus, when an integrator buys module of a given power rating, they are buying modules with a range of power defined around a reference value (the nameplate rating). As shown in Table 1.1, a survey of the top modules shows that typical binning ranges are in the ±3% to ±10% range. Since these bins are a cross-section of a normal manufacturing distribution, the module power within a binned range is typically evenly spread through the promised range. While these binning ranges are an elegant fix to the problem of manufacturing inconsistencies, they also represent a significant and measurable source of module mismatch. Table 1.2 shows that when the deviation of modules power rating is ± 3%, then MML is considered 3% theoretically, but practically it is found 4-7% for a commercial PV array at unshaded condition [8].

Table 1.1: Typical Module Binning of Top Module Manufacturers

Bin Power Range	Number of Manufacturers Surveyed
3% total	2
5% total	3
6% total	3
10% total	2
Mean	5.9% range
Median	5.5% range

Table 1.2: Performance deviation of I-V parameter and MML in a commercial PV array

Parameters	Value
Performance deviation of Pm	± 3%
Performance deviation of V_{OC} and V_{MPP}	± 10%
Performance deviation of I_{SC} and I_{MPP}	± 10%
MML (theoretically)	3%
MML (practically)	(4- 7) %

B. I-V Mismatch for Aging Effects

Aging is one of the primary sources of *I-V* mismatching [9]. The module degradation is not uniform, and recent studies have revealed that the power drop of a crystalline module is due to current and FF reductions, but not to significant changes in the voltage [10]. The PV module parameters are subjected to a change over time that is quantified utilizing the ratio between the standard deviation (σ) and the mean value (μ) of the parameter value itself σ/μ. This value increases from 1% to 10% for the module short-circuit current over 25 years of working time [11]. It is greatly affected by the working temperature and humidity, which have an effect on delamination and discoloration of the materials used as encapsulants. These dependencies are analyzed in detail, by means of experimental data, by Jordan in [12]. The mismatching among the short-circuit currents of the modules in the PV field, which increases with plant aging, determines a power loss, but it also increases the probability of hot spots, and thus permanent damage to the affected cells. Figure 1.7 shows different effects on PV array modules due to aging.

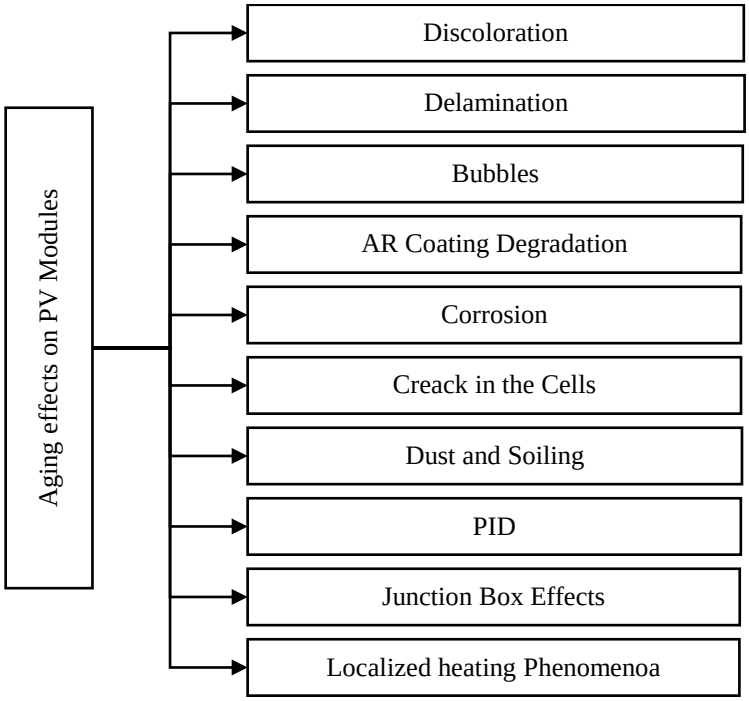

Figure 1.7: Different effects on PV array modules due to non-uniform aging

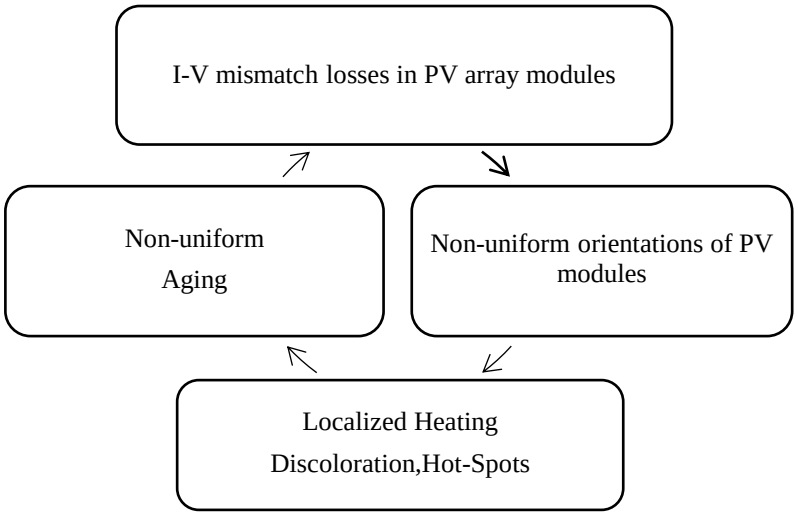

Figure 1.8: Close loop link exists between mismatch loss and aging

A simplified block diagram illustrating the close-loop links existing among PV modules degradation phenomena is shown in Figure 1.8, where the closed-loop link connecting aging with mismatching is also clearly indicated [13]. This work focuses on finding a solution for mismatch losses occurs due to all permanent factors. Thus, from now on term mismatch losses address the mismatch power loss coming from permanent factors, and term mismatch refers to permanent I-V mismatch in PV modules.

1.3 Power Loss due to *I-V* Mismatch

In practical PV generators, a central Maximum Power Point Tracker (MPPT) system is applied to lead the system to work at its' possible maximum power. In the presence of such a system, all modules are supposed to work at their MPP and MPP which are not precisely identical for all modules as previously explained. Simply put, under a central MPPT, when two modules with different MPP are connected in series, they compromise to work at the lower MPP and similarly two modules with different MPP connected in parallel work at the lower MPP. Generalization of these conditions to a vast array of PV modules connected in series and parallel results in the following equation:

$$Mismatch\ \ Loss\ \% = \left(\frac{\sum Modules\ Power\ \ - Array\ Power}{\sum Modules\ Power}\right) \times 100 \qquad (1.1)$$

Since arrangement of PV modules in an array affects the system energy losses and system yield, finding the optimal arrangement of the modules that returns the lowest possible mismatch losses and highest possible energy yield is worthy of investigation.

1.4 Literature Review on Mismatch Power Loss (MML)

The utilization of solar energy has received remarkable attention across the globe over the last decades [14]. Researchers are continually working to find the means and ways for further improving the performance of the existing technologies and developing more efficient methods of utilization of solar energy [15, 16]. Currently, PV technology is one of the widely used renewable energy technologies that is being motivated by the global scenario of increasing energy demand [17]. In many applications, such as hybrid solar power plants , building-integrated photovoltaic (BIPV) [18]systems, solar-powered vehicle battery charging system, grid-connected PV systems, Solar powered water pumping systems, micro-grid PV system, solar PV arrays are used in different dimensions and configurations according to the system requirements [19, 20] .

The MML of a PV array modules depends on several factors [21], such as the availability of solar radiation and its spectral distribution, PV module operating temperature (causes 9% power loss due to a 20-degree temperature differences

between hot and cold modules), shading, uneven soiling (causes 1 to 4% power loss) PV modules manufacturing tolerance (causes 4 to 7% power loss in new array), and PV power degradation (averagely 0.8% per year) by aging [22]. Among them, MML due to manufacturing tolerance is one of the significant factors, which is a common phenomenon in a new PV array [23, 24].

In a new PV array, the output power is undoubtedly less than the summation of individual module's ability because new PV modules with same power rating and even from the same manufacturer are not precisely identical due to manufacturing tolerances [25]. In PV modules manufacturing technology, manufacturing tolerances of ±3% to ±5% in their maximum power rating are generally allowed [26].

To maximize the PV array output power, by minimizing MML due to manufacturing tolerances, module sorting techniques had gained popularity among the researchers. To obtain minimum MML, photovoltaic maximum power parameters, such as max-power current, *Im*; short circuit current, *Isc;* max-power point power, *Pm*; max-power voltage, *Vm;* and open circuit voltage, *Voc* are typically used as PV module sorting parameters for the arrangement of newly installed PV array at uniform radiation condition [27].

In [28], MML due to manufacturing tolerances in PV array modules is first introduced, where the parameters *Im* and *Vm* are used to analyze both series and parallel PV string power losses at uniform radiation condition. In [29], three max-power parameters *Im*, *Vm* and *Pm* are used as a module sorting variable for a 700 V, 400 kW PV array, where the result shows that *Im* based method reduces MML and produces more array power than *Vm* and *Pm* methods. In [30], MML is compared by arranging 40 PV modules between *Im* based arrangement with most commonly used random arrangement technique. Here, the result shows that minimum MML is obtained by *Im* based method. In above literature, it is clear that MML in PV array depends on modules sorting (arrangement) technique, hence, further investigation is required to find an optimal arrangement technique to achieve minimum MML in new PV array output.

The GA based optimal arrangement technique was first adopted in [31] for arranging new PV modules in an array to minimize MML at uniform irradiance condition. A simulation-based performance is investigated by using different LSS-SP

array (3×6, 4×10, 5×13 and 5×18) configurations of 95 W modules and compared with conventional module arrangement techniques (*Im*, *Isc*, and *Pm*). Where, the simulation results show that MML can be minimized less than 1% using GA technique whereas MML is always higher than 1.02% for other conventional module arrangement techniques by *Im*, *Isc*, and *Pm*.

The above literature review shows that PV modules arrangement technique using maximum power parameters is a prevalent practice to reduce MML in new PV array with SP configuration. Besides, GA is also gained popularity as a PV array modules rearrangement technique mostly at partial shading condition. To the best of the author's knowledge, to minimize the MML in a large PV generation at uniform irradiance condition the GA based module arrangement technique has only investigated on LSS-SP array configurations, not for LPB-SP array configurations. Furthermore, experimental validation has not been performed yet [31]. Therefore, applying and experimentally validating GA as a module arrangement technique is one of the main objectives of this work.

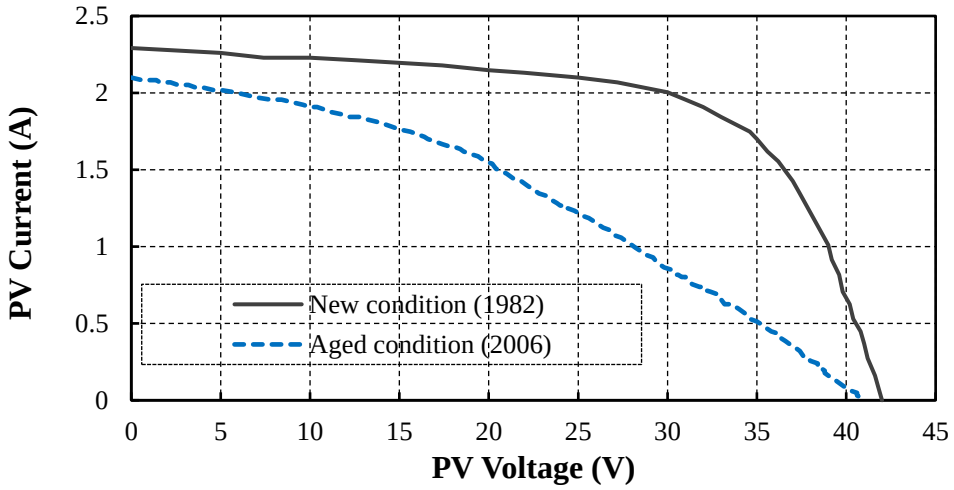

Figure 1.9: Electrical characteristics of a PV module, which have been tested at new and aged condition in 1982 and 2006, respectively.

On the other hand, *I-V* mismatch due to aging of PV modules is another significant factor in large PV array causes massive power losses [32]. The aging of PV panels causes the change of the slope of the *I-V* curve due to the variation of series and shunt resistances close to open circuit voltage and short circuit current respectively, [33, 34] as shown in Figure 1.1. Therefore, the fill factor decreases and consequently reduces the peak power point of the PV module [35]. Aging of the PV module is a

continuous process, but it is not uniform in nature. In an array, the non-uniform aging of PV modules increases mismatch in the *I-V* curves [36]. In [37], it has been shown that, in a PV array, the aging speed of modules is non-uniform, and power loss is averagely 0.8% per year. The power degradation of PV modules can vary from 0.5% to 1% per year due to different aging effects [12]. In [38], it has been shown that a closed-loop relation exists among MML and non-uniform aging of PV modules in an array. Therefore, it is beneficial to investigate the MML reduction methods for old PV array to maximize power.

In [39], a new rearrangement technique is proposed for aged PV array to obtain maximum output power using an extensive searching method based on the Munkres algorithm. In [40], three rearrangement methods are investigated for non-uniformly aged PV arrays to obtain maximum output power, but MML is not analyzed. In [41], GA based module rearrangement method is first time applied on non-uniformly aged PV array for energy maximization, except MML investigation; where, an experimental study is carried out by using artificially old PV modules, and plastic films are used to cover the surface of the modules to make non-uniform aging condition.

In [42], the SCC based new rearrangement strategy is tested on different size of PV arrays (4×4, 10×10, and 100×10), considering non-uniformly aged PV modules. In [43], the SCC based module rearrangement method is also investigated for non-uniformly aged PV array; where SCC is compared with the RA based method, while the output power is 13.5% improved by the SCC method. But, the MML minimization process is not effectively analyzed here. However, to maximize the array power, MML reduction by rearrangement techniques (RA, SCC, and GA) has been investigated in [44], using modules at new condition only.

Though aged modules are used to investigate rearrangement techniques, in [41-43], those are artificially aged or non-uniformly aged, but experiments are not carried out using the real aged PV modules. In the literatures, no comparison is performed among the rearrangement techniques (RA, SCC, and GA), and the investigation of MML reduction by rearrangement processes utilizing the real aged PV array is still very scanty. Therefore, this work aims to fill the gap by investigating the MML reduction by the rearrangement techniques (RA, SCC, GA) for real aged PV arrays (400 W, 1.6 kW, 3.2 kW, and 10 kW) to maximize the output power. Six different

array dimensions, 2×20, 4×10, 5×8, 20×2, 10×4, and 8×5 are used for each PV arrays to find the useful comparison and performance of MML reduction techniques on array size.

MML due to partial shading is another significant factor in vast PV system [45-47]. In order to maximize the PV array output power by minimizing MML due to partial shading, module interconnection schemes had gain popularity among the researcher [48-50]. The most popular interconnection schemes are: total-cross-tied (TCT), bridge-linked (BL), series-parallel (SP), and honey-combed (HC) [48, 51, 52]. In addition, some hybrid array configurations are also available in literature, such as SP-TCT, HC-TCT, BL-TCT etc [53-56].

In [57], a simulation-based comparison is made to extract the maximum power by mitigating MML from Series (S), Parallel (P), S-P, TCT, BL, and HC PV array topologies under partial shading conditions. In [58], a mathematical analysis is performed among SP, TCT, BL and HC configurations in terms of output power maximization and MML reduction under partial shading condition. It has been shown that TCT configuration is performed better than others. In [59], a simulation-based comparison is made for SP, BL and TCT configurations under shading condition using different size of array dimensions (2×6, 6×2, 4×3 and 3×4), where TCT configuration is performed higher output power in all respects. In [60], different array configurations (TCT, BL, SP, HC and HC-TCT) are experimentally investigated to minimize MML due to partial shading. Where, TCT configuration is performed lower MML for different type of shading patterns. In [61], various types of 4×4 array configurations (TCT, SP-TCT, BL-TCT and BL-HC) are studied for MML minimization due to different shading cases using MATLAB/Simulink. In, the performance of four conventional array configurations (SP, TCT, BL and HC) and three hybrid array configurations (SP-TCT, BL-TCT and HC-TCT) are investigated under different types of moving shading patterns for mismatch loss reduction. Where, results show that MML depends on shading patterns and hybrid array topologies are comparatively performed batter in MML reduction than conventional topologies. In [62], a novel structure (NS) PV array topology is proposed and compared with classical hybrid PV array topologies (SP-TCT, BL-TCT, BL-HC) under diagonally shading scenario using MATLAB/Simulink. Where, simulation results show that NS configuration is found superior for some cases of shading effects. From the above works [55-60], it is found

that during shadow condition, the hybrid interconnection schemes performed better than conventional interconnection schemes with respect to array output power maximization and MML minimization.

To the best of the authors' knowledge, in literature, hybrid array configurations are not investigated yet for nonuniformly aged PV array. This work aims to fill up the gap by investigating different conventional and hybrid array configurations on aged PV array to extract maximum power. Moreover, the performance of some novel hybrid configurations is also investigated here. Furthermore, a comparative analysis has been performed among classical and novel array configurations with respect to array output power, mismatch loss and recoverable energy.

1.5 Problem Statements

- For new and aged PV arrays: Experimental validation of GA based module rearrangement technique for MML minimization is not investigated for both LSS-SP and LPB-SP arrays.
- For new and aged PV arrays: Comparative analysis of MML reduction by different (*Ra, Im, Isc, Pm, Vm, Voc and GA* based) techniques of module arrangement is not performed yet for various power rating of PV Arrays.
- For aged PV array: Different standard (SP, TCT, BL, HC, LD) and hybrid (SP-TCT, HC-TCT, BL-TCT) array configurations are not investigated yet for MML minimization.
- For partially shaded PV array: LD configuration is not investigated and compared with SP, TCT, BL and HC configurations for MML minimization with different shading patterns.

1.6 Motivation

The utilization of solar energy has received remarkable attention across the globe over the last decades. Researchers are continually working to find the means and ways for further improving the performance of the existing technologies and developing more efficient methods of utilization of solar energy. Currently, PV technology is one of the widely used renewable energy technologies that is being motivated by the global scenario of increasing energy demand. To maximize the PV array output power by minimizing mismatch loss under *I-V* mismatch condition, different rearrangement techniques with different interconnection schemes are

investigated by the researchers. Since the rearrangement of PV modules in an array affects the system energy losses and system yield, finding the optimal method of the modules that returns the lowest possible mismatch losses and highest potential energy yield is worthy of investigation. Further development is possible for MML reduction both for new and aged condition of PV arrays to maximize the energy production.

1.7 Thesis Objectives

The main objectives of this study are specified as follows:

- To develop an adaptive GA based PV modules rearrangement technique for both newly installed PV array and aged PV array configurations. And experimental validation in the outdoor weather condition.
- To make a comparative analysis among the proposed and convention techniques of module rearrangement with respect to array output power, %MML, and percentage of recoverable energy (%RE) for both new and aged PV arrays.
- To investigate the performance of some novel PV array configurations to yield maximum power by Minimizing MML in aged PV arrays and comparison with standard array configurations to justify the novelty of the work.
- To make a comparative investigation of standard PV array configurations for MML minimization in PV arrays at partially shaded condition.

1.8 Outline of Methodology

As mentioned earlier, the mismatch power loss is a significant problem in PV array, has been investigated by many researchers using different techniques. In this work GA based module arrangement technique has been proposed for MML minimization in large PV arrays. The proposed technology will be applied to new PV array and also on the aged PV array configuration. This working process will include the following significant steps:

(i) Selection of PV Modules: To investigate the MML in any PV array due to I-V mismatch, same brand and same power ratted photovoltaic modules are required both for new and aged condition. Referring to the datasheet of PV modules are currently available in the market, it is found that despite all advancements of PV modules production technology, there still exists a manufacturing tolerance of ±3% to ±5% in their power rating.

(ii) Data Sets of Modules: Each module of the target PV array (new or old) needs to have all the required specification to calculate MML. Hence, to get the dataset of PV modules at new or aged condition, *I–V* measurements are suggested to be performed under STC (25°C, 1000W/m^2, AM 1.5G) according to IEC 60904-1 standard.

(iii) Simulation of Different Techniques: Sorting modules based on *Isc, Im, Vm, Voc,* and *Pm* parameters are the conventional techniques of MML mitigation for SP configured PV array. In order to perform the simulation, for traditional methods, module rearrangement can be achieved by using Microsoft Excel software, while for the proposed GA based technique a programming software is required. To investigate the performance of the MML reduction techniques, MML% should be calculated for each of the arrangements coming from conventional methods and also by the proposed *GA* based method. Therefore, the well-established mathematical model of MML% both for new and aged PV array configurations will be used in this work.

(iv) *Hardware Experimentation*: To perform the experimental investigation of the MML reduction techniques, a set of PV modules are required with tasted datasets. The position of the modules will be determined from the simulation, and then a practical array connection will be made according to the simulation result. And the output characteristics will be measured using any commercial I-V tracking device. The same process will be repeated to validate all the techniques. Finally, a comparative analysis will be performed among the proposed and the conventional methods to justify the performance of the work.

1.9 Thesis Organization

Chapter 2 presents different techniques of module arrangement to minimize the MML in PV arrays both at new and aged condition. At new condition of PV modules MML is investigated due to manufacturing tolerances using different conventional techniques during uniform irradiance condition. An adaptive GA based module arrangement technique is proposed here as a new solution of MML reduction both for long series string (LSS) and long parallel branch (LPB) in SP array configurations. A comparative analysis is made to find the performances of MML reduction techniques for new PV arrays with three different power ratings (400 W, 3400W and 9880 W). Simulation and Experimental investigation are performed to find out the usefulness of

the proposed method with respect to MML% reduction and improve the %RE for newly installed PV arrays. At aged condition of PV modules MML minimization is investigated to maximize the output power using different rearrangement technique. GA based and short circuit current (SCC) based module rearrangement techniques are investigated in this chapter to obtain an optimal arrangement that yields maximum output power from the aged array. Besides, the performance of these two techniques is compared with randomly module arrangement technique (RA) to find the effectiveness of the rearrangement techniques on the aged PV arrays considering the four different power ratings (400 W, 1.6 kW, 3.2 kW, and 10 kW).

Chapter 3 shows an experimental investigation of MML minimization of Aged PV array using different standard and hybrid array configurations. Four conventional configurations (SP, TCT, BL, and HC) are investigated using on a 4×6 aged PV array at indoor test condition. Different standard (SP, TCT, BL, HC, and LD) and hybrid (HC-TCT, LD-TCT, TCT-S, S-TCT, SP-LD, LD-SP, and SP-TCT) array configurations are investigated at outdoor weather condition using an artificial nonuniformly aged 4×10, 400 W PV array.

Chapter 4 investigates the performances of different PV array configurations to obtain maximum output power for six different sizes of shading patterns. The experimental investigation is carried out using a 4×6 PV array with series-parallel (SP), total-cross-tied (TCT), ladder-diagram (LD), honey-comb (HC) and bridge-linked (BL) configurations. A comparative analysis is performed among the five configurations under different shading conditions for MML reduction and improvement of the percentage of recoverable energy (%RE).

Chapter 5 shows a case study on 28 MW grid connected PV plant in Teknaf, Cox-Bazar, Bangladesh to investigate the GA based MML minimization in a large PV plant. The description of the PV array size, MPPT charge controller, Inverter system of the 28 MW PV plant is also presented in this chapter. GA based module arrangement technique is compared with RA based technique using a 21×21 PV array of 28 MW PV plant. Extra energy obtained by GA based module arrangement technique is also calculated on the basis of daily, monthly and yearly.

Finally, Chapter 6 reviews the conclusions and contributions of the work and suggests areas for future related work.

CHAPTER 2

MML Minimization Techniques for Photovoltaic Arrays

The mismatch in current-voltage (*I-V*) characteristics of Photovoltaic (PV) modules causes significant power loss in large PV array both at new and aged condition of PV modules. The primary sources of *I-V* mismatching in the PV array are briefly described in chapter 1. In chapter 2, the MML is analyzed due to manufacturing tolerances and due to aging of PV modules. The PV array output power generation can be improved by minimizing MML using different techniques of module arrangement. An adaptive genetic algorithm-based module arrangement technique is proposed here as a new solution of MML reduction both for new and aged PV arrays with different dimensions. A comparative analysis is made to find the effectiveness of MML reduction techniques a 400 W PV array at three different aging conditions.

2.1 Mismatch Power Loss in New PV Array

In a PV array, all modules do not have identical *I-V* characteristics even from the same manufacturer and same power ratings. *I-V* characteristic parameters are considered as *Voc*, *Isc*, *Vm*, *Isc*, and *Pm.* The *I-V* mismatch means differences of these *I-V* parameters between individual modules, which cause MML in PV array. There are some constant factors such as manufacturer tolerance, light-induced power degradation, uneven surface soiling, discoloration, and cracking are responsible for *I-V* mismatch in new PV array modules; causes typically 4-7% energy loss [63]. The manufacturing process of PV modules are developing competitively day by day to minimize the manufacturing variance of *I-V* parameters in same power rated modules, but still, now the available crystalline PV modules in the market contain manufacturing tolerances ±3% to ±5% in their power rating. Due to this manufacturing tolerance level in case of the high volume of PV modules in an array, the MML increases significantly.

Figure 2.1 shows that before connecting the modules in the array, the summation of individual modules power is higher than the array power, and their corresponding power difference is defined as mismatch power. Therefore, to minimize

MML due to manufacturing *I-V* mismatch in PV modules, this is essential to maximize the array power, by arranging array modules applying optimal configuration technique.

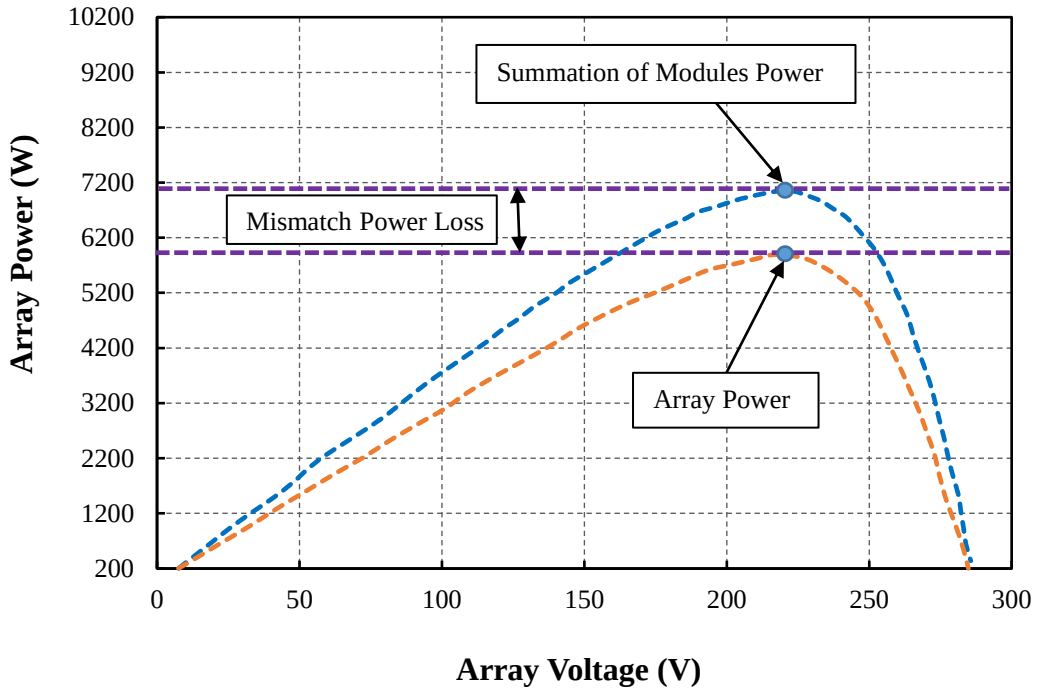

Figure 2.1: MML in new PV array due to modules *I-V* mismatch at uniform irradiance

2.2 Mathematical Model of MML in New PV Array

In SP array configurations, series connected modules are work at the same amount of current in a string, and parallel strings are work at the same amount of voltage at a time. As a rule, Kirchhoff voltage law (KVL) is applied for string voltage calculation, and Kirchhoff current law (KCL) is used for the array current calculation. Therefore, according to KVL, the string voltage equals the summation of modules voltage in the string, and according to KCL, the array current equals the summation of string current in the array [31]. However, in a practical PV array, a central maximum power point tracker (MPPT) [64-67] is used to get its maximum global power (GMPP) [68-71]. Therefore, all modules are led to work at their maximum potential, which is not exactly same for all modules even from same power rating due to the manufacturing tolerances, which causes MML in the PV array. For example, if two modules are connected in series having non-identical *Im*, then they compromise to operate at lower *Im* and similarly two parallel connected modules are having different *Vm* work at smaller *Vm* [31, 72, 73].

Now, consider a PV string be made up of X series-connected PV modules, with string voltage, $V_{String}^{mpp}$and string current, I_{String}^{mpp} The string voltage and current of the *Pth* PV module can be denoted by $V_{Module,P}^{mpp}$ and $I_{Module,P}^{mpp}$ respectively. With this notation, maximum string voltage and current can be expressed as follows.

$$V_{String}^{mpp} = \sum_{P=1}^{X} V_{Module,P}^{mpp} \tag{2.1}$$

$$I_{String}^{mpp} \leq min\{I_{Module,P}^{mpp} : 1 \leq P \leq X\} \tag{2.2}$$

Again, consider a PV array has Y number of parallel connected string; identify its terminal voltage, and current for *Qth* PV string are $V_{String,Q}^{mpp}$and $I_{String,Q}^{mpp}$ respectively. With this notation maximum array current and maximum array voltage can be expressed as;

$$I_{Array}^{mpp} = \sum_{Q=1}^{Y} I_{String,Q}^{mpp} \tag{2.3}$$

$$V_{Array}^{mpp} \leq min\{V_{String,Q}^{mpp} : 1 \leq Q \leq Y\} \tag{2.4}$$

Now, consider an *X*×*Y* PV array has *X* number of series connected modules in a string and *Y* number of parallel connected strings; identify its output terminal power, and *Zth* PV module is P_{Array}^{mpp} and $P_{Module,Z}^{mpp}$ respectively. With this notation maximum array output power, the summation of modules power and percentage of MML in the PV array can be expressed as;

$$P_{Array}^{mpp} = V_{Array}^{mpp} \times I_{Array}^{mpp} \tag{2.5}$$

$$P_{Module}^{Sum} = \sum_{Z=1}^{XY} P_{Module,Z}^{mpp} \tag{2.6}$$

$$MML\% = \frac{P_{Module}^{Sum} - P_{Array}^{mpp}}{P_{Module}^{Sum}} \times 100 \tag{2.7}$$

The array power decreases because the array voltage is equal to the minimum voltage of the string connected in parallel and array string current is similar to the

minimum current of the module connected in series. Therefore, the array output power is always less than the summation of individual modules power in the array.

2.3 Simulation Work for New PV Arrays

In order to make a comparative analysis, among the different module arrangement techniques, regarding array output power and MML, three different power 400 W, 3400 W, and 9880 W arrays are used in this chapter. Where each array contains 40 PV modules of 10 W, 85 W, and 247 W respectively. Therefore, three datasets are collected from a PV module manufacturer company. These datasets are used in simulation work to calculate array output power and MML using NetBins software. Consequently, after obtaining the datasets, the PV modules are arranged with different LSS-SP array arrangements (1×40, 2×20, 4×10, 5×8) and LPB-SP array arrangements (40×1, 20×2, 10×4, 8×5) according to the unusual arrangement techniques. The techniques of PV modules arrangement are described in the following section. For each PV array arrangement, array output voltage, current, and power are calculated to find out the MML of that array arrangement. The mathematical model of MML and corresponding MML calculation process are already described in the above section. Finally, the performance of MML reduction techniques are compared by using three different case studies on 400 W, 3400 W and 9880 W arrays are described in the following sections.

2.3.1 Datasets of Three Different PV Arrays at New Condition

In this section, three different flash test datasets of 40 polycrystalline PV modules of three separate power rating, 10 W, 85 W, and 247 W are collected from a PV manufacturer company, Electro Solar Power Limited (ESPL). PV modules are tested using the PV test system in ESPL at standard test condition (STC), 25°C, 1000 W/m2, AM 1.5G, according to the IEC 60904-1 standard [74, 75]. The tested data of three datasets have been tabulated in Table 2.1; which contains the value of electrical characteristics of *Voc, Isc, Pm, Vm* and *Im* for each PV modules. Also, their average value and standard deviation (SD) are calculated and tabulated in the following table.

Table 2.1 Datasets of 10 W, 85 W and 247 W modules for generating 400 W, 3400 W, and 9880 W PV array respectively

PV Array Power	PV Module Power	PV Module No	Electrical characteristics of PV modules				
			Voc (V)	Isc (A)	Pm (W)	Vm (V)	Im (A)
400 W	10 W	1	10.464	1.309	10.118	8.569	1.181
		2	10.396	1.295	10.032	8.570	1.171
		3	10.454	1.307	10.150	8.588	1.182
		⋮	⋮	⋮	⋮	⋮	⋮
		40	10.453	1.320	10.238	8.630	1.186
		Average	10.425	1.295	10.191	8.617	1.183
		SD	0.116	0.020	0.194	0.123	0.013
3400 W	85 W	1	21.241	5.298	85.133	16.925	5.03
		2	21.492	5.314	86.392	17.147	5.038
		3	21.299	5.328	85.198	16.906	5.04
		⋮	⋮	⋮	⋮	⋮	⋮
		40	21.339	5.347	86.569	16.988	5.096
		Average	21.382	5.354	86.035	16.995	5.063
		SD	0.064	0.031	0.407	0.075	0.022
9880 W	247 W	1	40.556	7.516	249.606	34.62	7.21
		2	40.599	7.512	245.324	33.858	7.246
		3	40.665	7.545	247.991	33.788	7.34
		⋮	⋮	⋮	⋮	⋮	⋮
		40	40.763	7.487	250.885	34.628	7.245
		Average	40.538	7.544	247.107	34.094	7.248
		SD	0.173	0.088	2.305	0.385	0.039

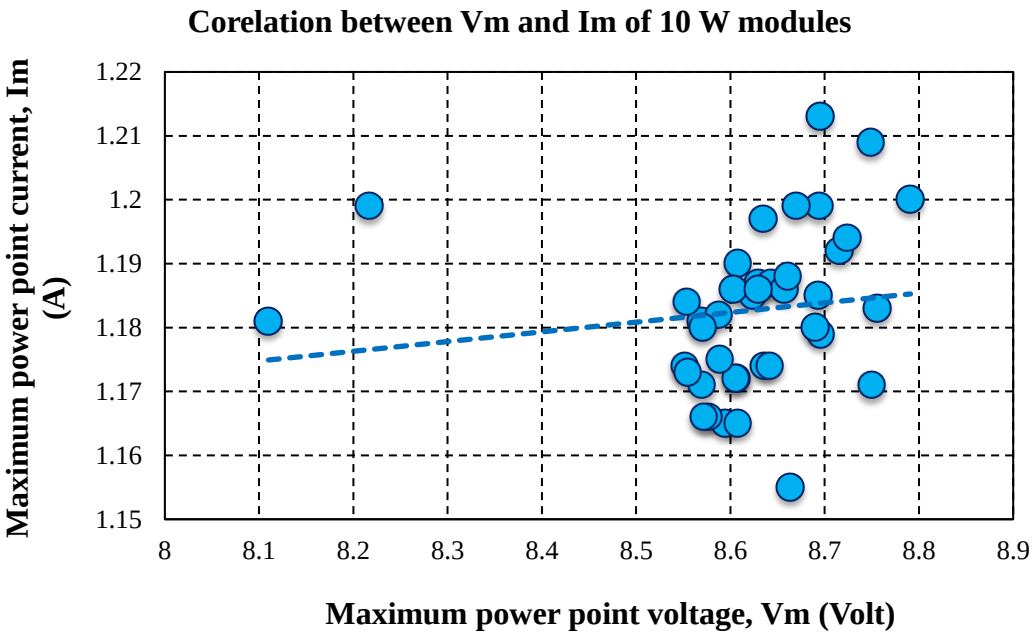

Figure 2.2: Correlation between Vm and Im of 10 W modules in 400 W array

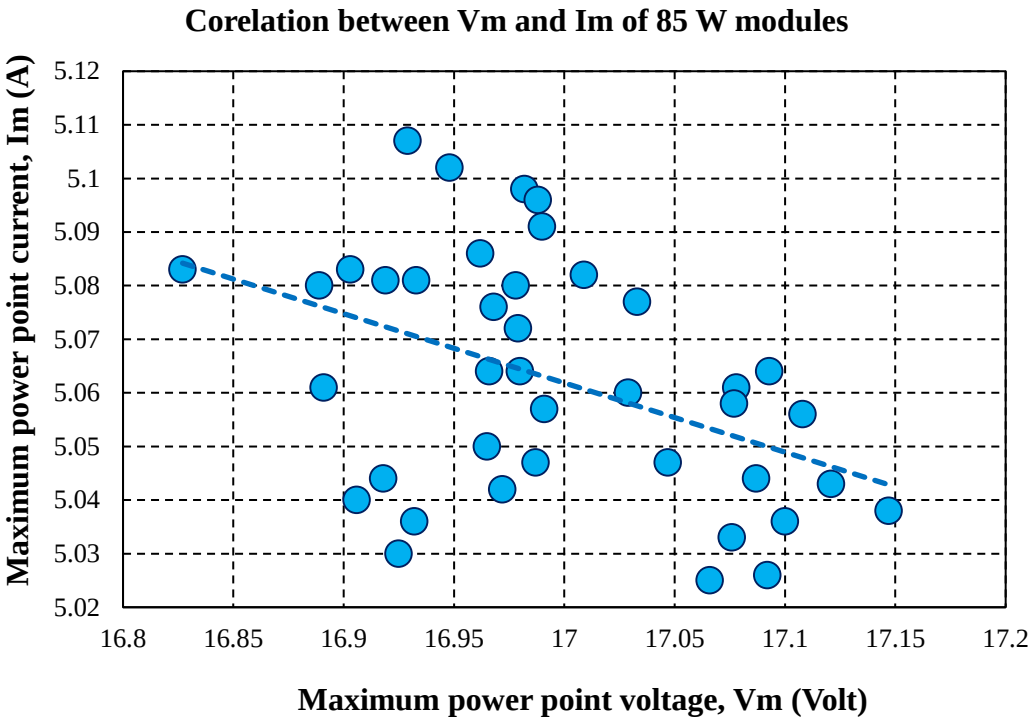

Figure 2.3: Correlation between Vm and Im of 85 W modules in 3400 W array

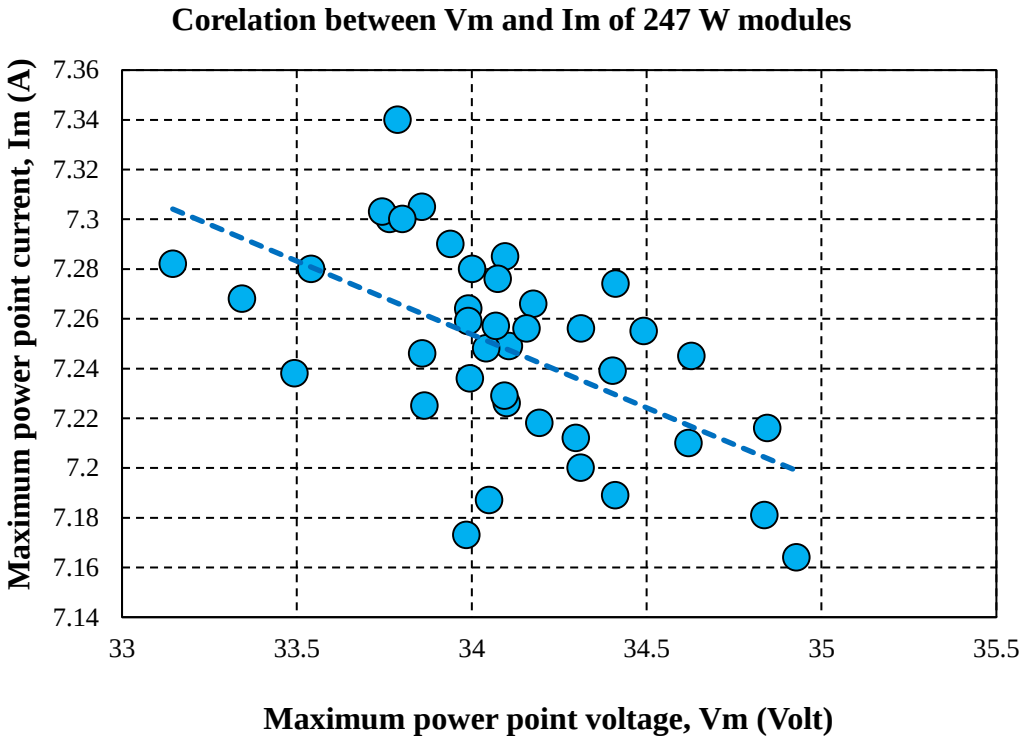

Figure 2.4: Correlation between Vm and Im of 247 W modules in 9880 W array

The correlation between the parameters Vm and Im of the datasets of 10 W, 85 W, and 247 W PV modules are shown in Figure 2.2, 2.3 and 2.4, respectively. The

dotted line in the figures represents the trend line of the dataset. Figure 2.2 shows the positive correlation, and the value of the correlation coefficient is +0.148 and Figures 2.3, and 2.4 show the negative correlation and the number of correlation coefficients are -0.435 and -0.567, respectively.

2.3.2 Conventional Techniques of Module Arrangement

The conventional techniques of SP PV array modules arrangement are based on *I-V* parameters such as *Im, Isc, Pm, Vm,* or *Voc* [29, 76, 77]. Therefore, the arrangement techniques are named according to the selected *I-V* parameter: i) *Im*_method; ii) *Isc*_method; iii) *Pm*_method; iv) *Vm*_method and v) *Voc*_method. For Im based method, let's consider an LSS-SP array of dimension, 4×10 with 40 modules as shown in Figure 2.5, which are arranged by *Im* values. The arrangement has been made from lower values to higher values of *Im;* as a result, module number 1 has the lowest value of *Im* while module number 40 has the highest. The similar process is also used to arrange the modules by the other methods stated above. The difference of I_{Module}^{mpp} in strings and difference of V_{Module}^{mpp} of strings are the factors causing MML in an array [7, 28]. The current-based module arrangement techniques (*Im* and *Isc*) minimize MML by greedily reducing the difference of I_{Module}^{mpp} in strings [29, 77]. Consequently, string current (I_{String}^{mpp}) increases gradually from the first row to the last row. This arrangement increases the total array current (I_{Array}^{mpp}) as in (2.3) and consequently, the output power increases. The voltage-based modules arrangement techniques (*Vm* and *Voc*) reduce the differences of V_{Module}^{mpp} in strings but increases the string voltage (V_{String}^{mpp}) from the first row to the last row. Consequently, the array voltage (V_{Array}^{mpp}) decreases as in (2.4). Therefore, the array output power in voltage based methods (*Vm* and *Voc*) are comparatively smaller than current based methods (*Im* and *Isc*) [28, 29]. On the other hand, in power-based method *Pm*, both array voltage and array current increase averagely, hence the array power increases than voltage-based method but not more than current based method elaborately described in [31]. Another typical technique of module arrangement is the random method (*Ra*_method), which is mostly used in the small size PV array. In this method, modules are arranged randomly by considering all modules with identical power in the PV array.

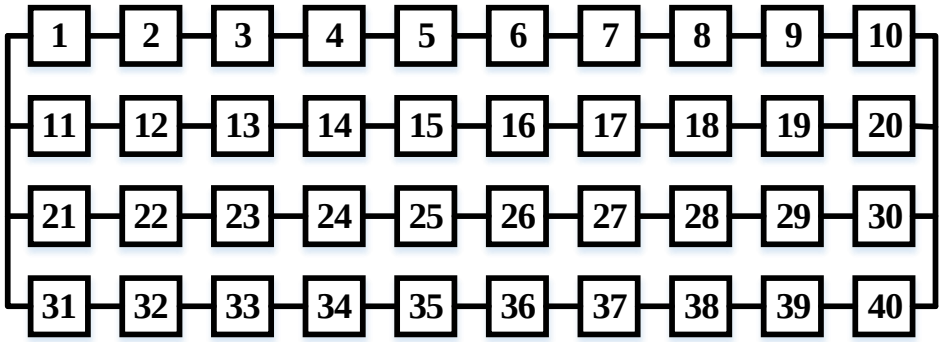

Figure 2.5: 4×10 LSS-SP array configuration

2.3.3 Proposed Adaptive GA Based Technique for Module Arrangement

To address the problem of minimizing the MML in SP PV array, *GA* is used find an optimum method of modules with the expectation that if the array output power can be maximized, the MML will be minimized. Therefore, in this optimization problem, the fitness function of *GA* is defined as the array output power, P_{Array}^{mpp} that is to be maximized. The expression of the fitness function, FF as follows.

$$FF = P_{Array}^{mpp} \tag{2.8}$$

The total procedure is divided into three steps: Selection, Crossover, and Mutation. Initially, a random number of setups are generated. For generosity, it is considered N numbers of setups are generated. By setup, it is mean a matrix of r×c consisting of a fixed number of modules. Where ‘r’ is the number of rows, and ‘c' is the number of columns. Each setup is a sample in the solution space of the optimization problem. The objective of the problem is to find out the best sample with maximum fitness value. The process is illustrated with a flowchart shown in Figure 2.6.

As in the flowchart in Figure 2.6, it is started with the phase of selection. In the selection phase, parent samples are selected through some criterion function. In this case, the criterion function is the average of the fitness values of the samples generated randomly. If any sample has a fitness greater or equal to the average of the fitness values of the samples, it is selected as a parent of the current generation. Initially, the average value of the fitness function of the samples is termed as global best, BG. Usually; this process reduces the population size to less than N.

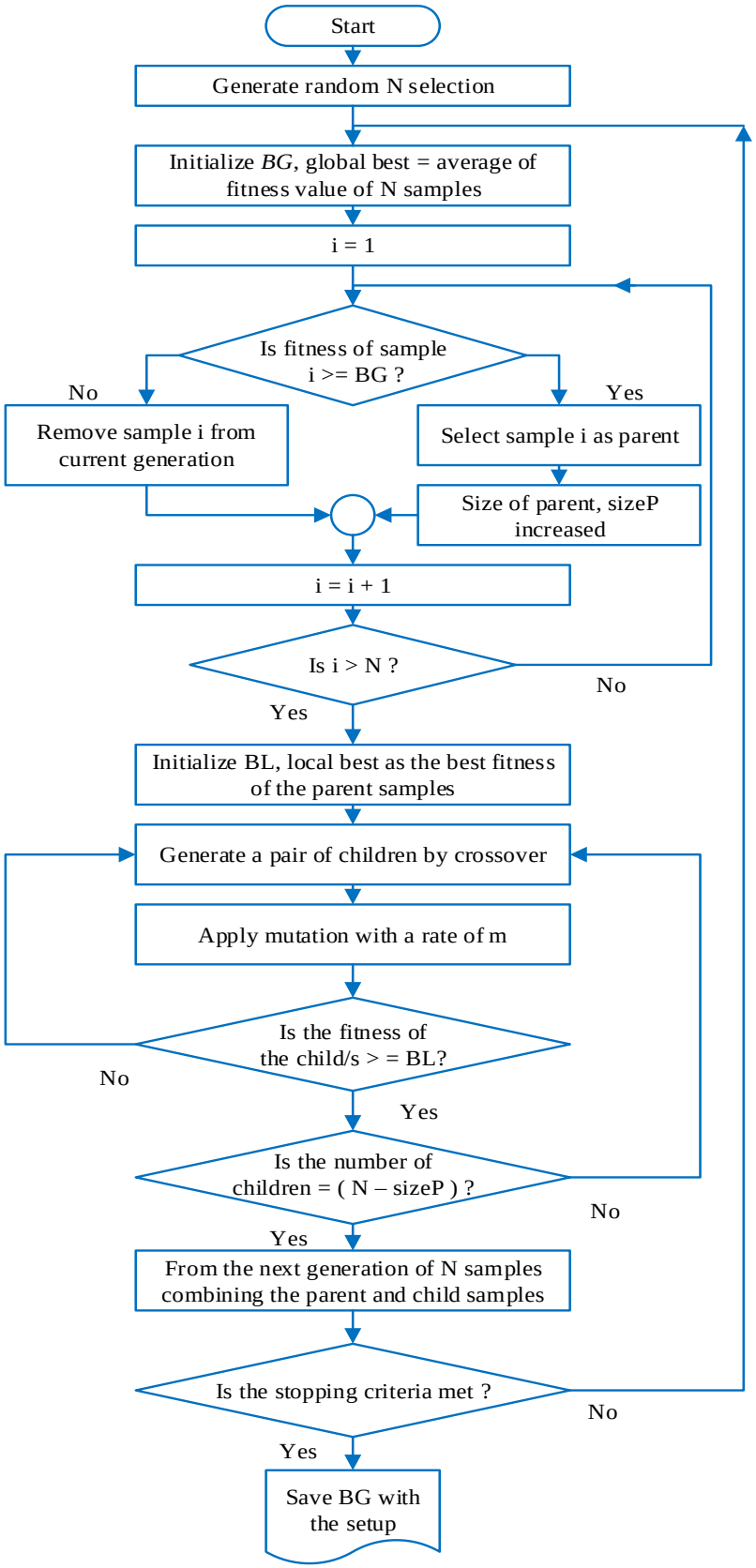

Figure 2.6: Flowchart of Genetic Algorithm based PV modules arrangement technique

Now, in the following phase known as a crossover, it crosses the parent samples and generated new samples. However, the newly created samples are included in the current generation if they excel in fitness value compared to the best fitness value of the parent samples. The best fitness value of the current parent samples is termed as local best, *'BL.'* The process is terminated when the population size is increased to N again. While selecting a pair of parents for the crossover, Roulette wheel selection is used [78]. If FF_i is the fitness of an individual sample, 'I' in the population, its probability of being selected is as follows:

$$P_i = \frac{FF_i}{\sum_{j=1}^{N} FF_j} \tag{2.9}$$

Where 'N' denotes as the number of individuals in the population, while any candidate solution with a higher fitness will make less likely to be eliminated, there is still a chance that they may be. Again, with this type of selection, there is a chance some weaker solutions may survive the selection process, which serves as an advantage. These retain some feeble properties of weak solutions that could prove useful in the following steps.

For the crossover phase, the order one crossover technique is used in this work because of its simplicity and faster operation. Figure 2.7 and Figure 2.8 show the order one (OX) crossover technique and partially matched (PMX) crossover technique between two parents. However, in the previous work [31], PMX crossover technique was used, which requires more simulation time to execute the optimal arrangement of PV modules of a particular array compared to OX crossover technique. To the best of the author knows, this is the first-time OX crossover technique has been applied to this type of *GA* based optimal process of module arrangement for series-parallel PV array configuration. Therefore, this is called as an adaptive GA based module arrangement technique. During the crossover process, after generating every child sample, a small mutation at a rate of 'm' is introduced. This threshold is tuned during simulations. Finally, the procedure stops whenever the global best, 'BG' is stabilized for a predefined number of iterations. Otherwise, the current population is again reassessed using the selection procedure and passed through the crossover and mutation phases until the stopping criterion is met. The *GA* process takes a data set of PV modules with a determined row-column dimension and returns an optimal arrangement of modules position in the array as output.

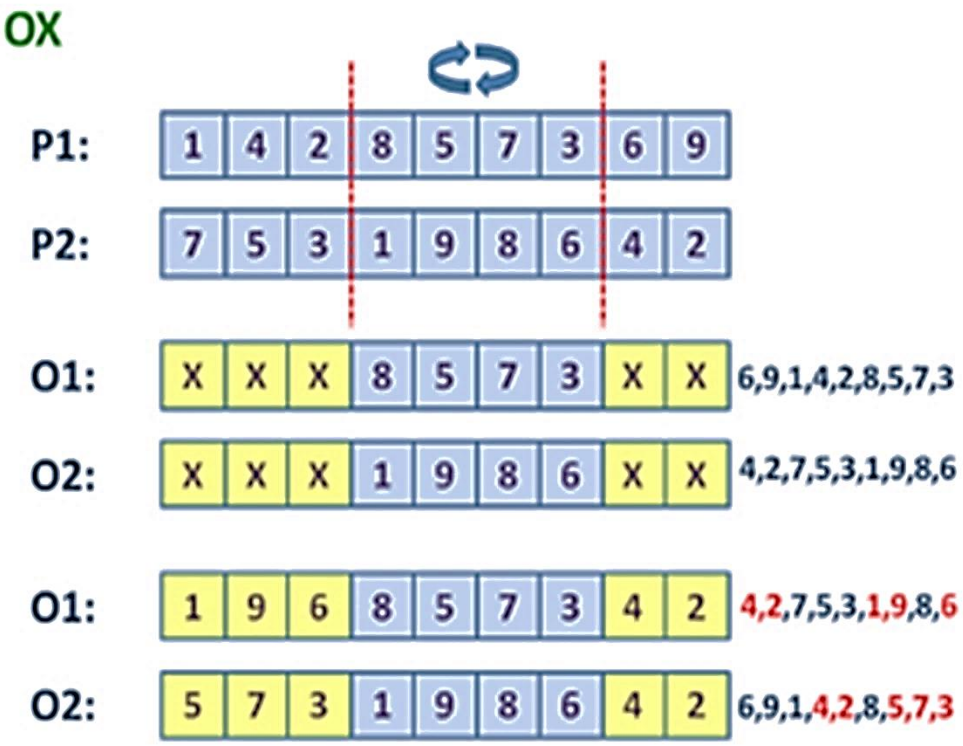

Figure 2.7: Order one crossover technique

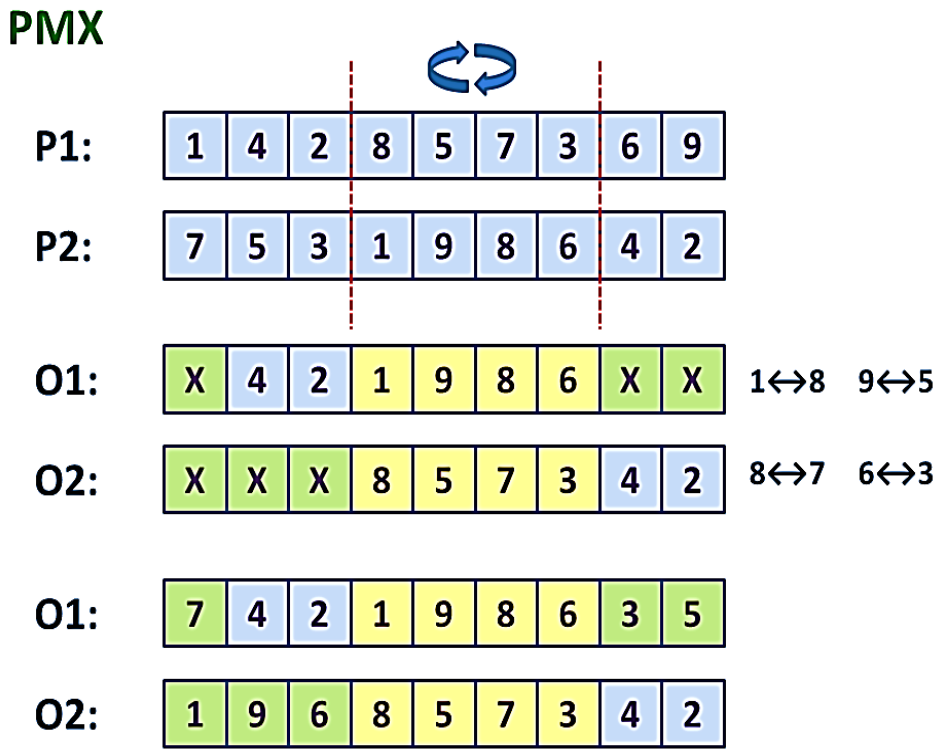

Figure 2.8: Partially matched crossover technique

2.3.4 Testing of the Proposed GA based Technique

In this section, a comparative analysis is performed between the proposed adaptive GA based module arrangement technique and previously used GA based technique in [31], with respect to MML minimization. As mentioned earlier OX crossover technique is first time introduced in this work for GA based module arrangement technique. Therefore, this technique is called as an adaptive GA based module arrangement technique. In [31], GA was performed using PMX crossover technique and simulation-based investigation was made for 3×6, 4×10, 5×13 and 5×18 array using 95 W PV modules. In [31], four datasets contain 18, 40, 65, and 90 modules, which are arranged by 3×6, 4×10, 5×13, and 5×18 array dimensions respectively. The PV modules are chosen in the datasets by maintaining the standard performance deviation of the module parameter, P_{mpp} (± 3%), V_{mpp} (± 10%), I_{mpp} (± 10%). In order to test the proposed GA based module arrangement technique and to make a comparison with the previous work, the similar datasets are used here by maintain all the standard conditions. In the previous work for the dataset of 4×10 array, the summation of modules power was 3796 W and in this work the same power is used. The four datasets of 3×6, 4×10, 5×13, and 5×18 arrays are shown in Figure 2.9 (a), (b), (c) and (d) respectively. Where, each figure is showing the deviation of modules parameters Vmpp and Impp for the corresponding datasets.

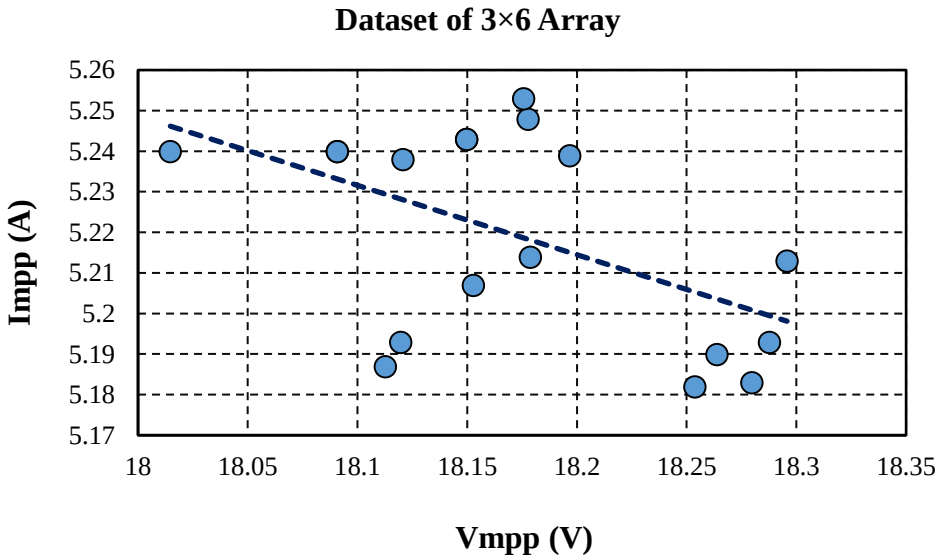

Figure 2.9 (a): Correlation between Vmpp and Impp of 95 W modules in 3×6 array

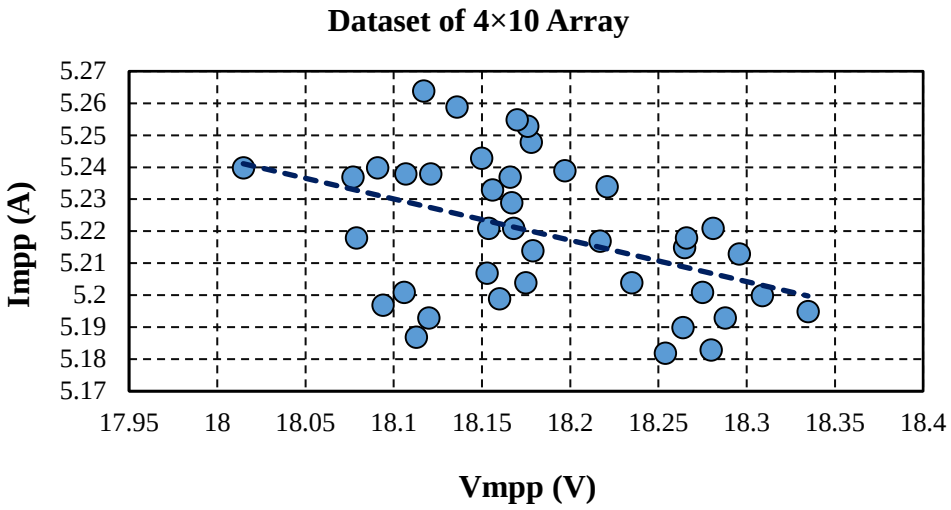

Figure 2.9 (b): Correlation between Vmpp and Impp of 95 W modules in 4×10 array

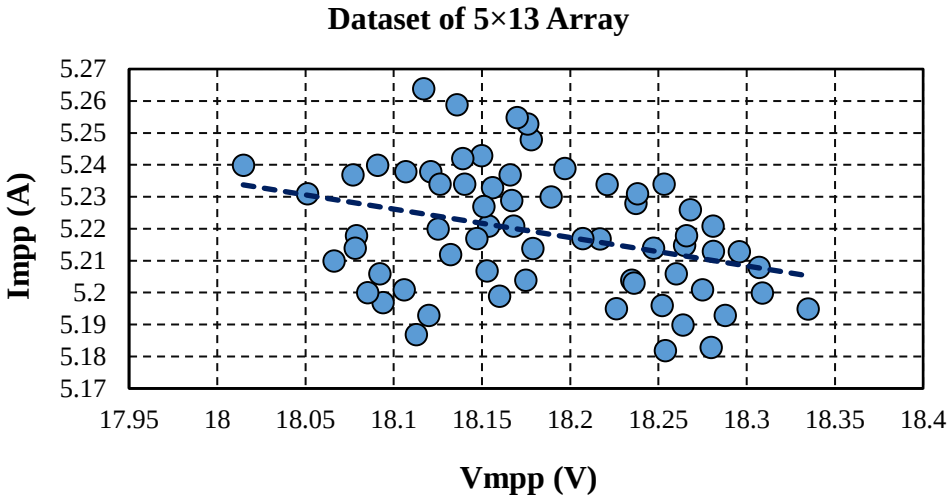

Figure 2.9 (c): Correlation between Vmpp and Impp of 95 W modules in 5×13 array

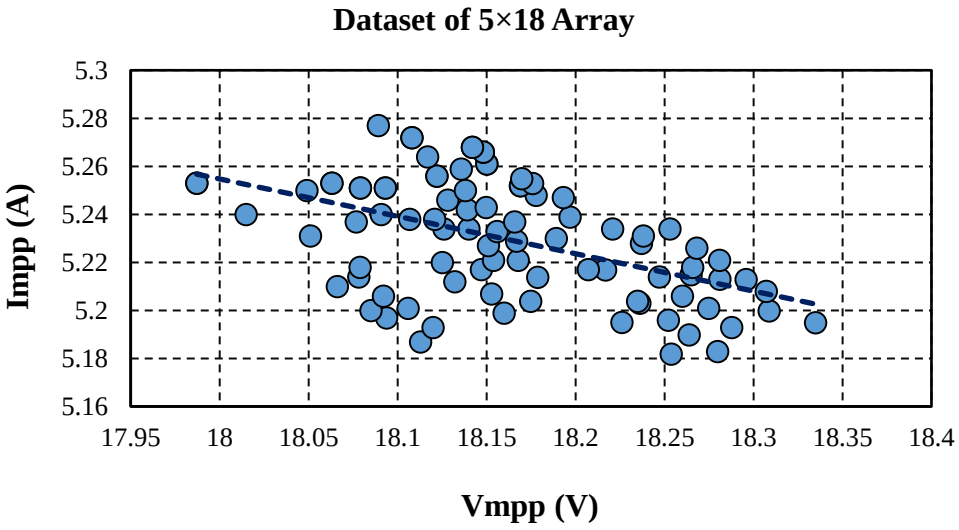

Figure 2.9 (d): Correlation between Vmpp and Impp of 95 W modules in 5×18 array

Table 2.2: Comparison of Array Power and %MML obtained by Proposed and Previous GA based Module Arrangement Technique

Array size	Proposed technique		Previous technique [31]	
	Parray_OX (W)	MML_OX(%)	Parray_PMX (W)	MML_PMX (%)
3×6	1695.795	0.669	1689.801	1.02
4×10	3779.044	0.448	3767.968	0.74
5×13	6138.312	0.477	6122.130	0.74
5×18	8507.228	0.476	8494.065	0.63
Avg.	5030.095	0.518	5018.491	0.783

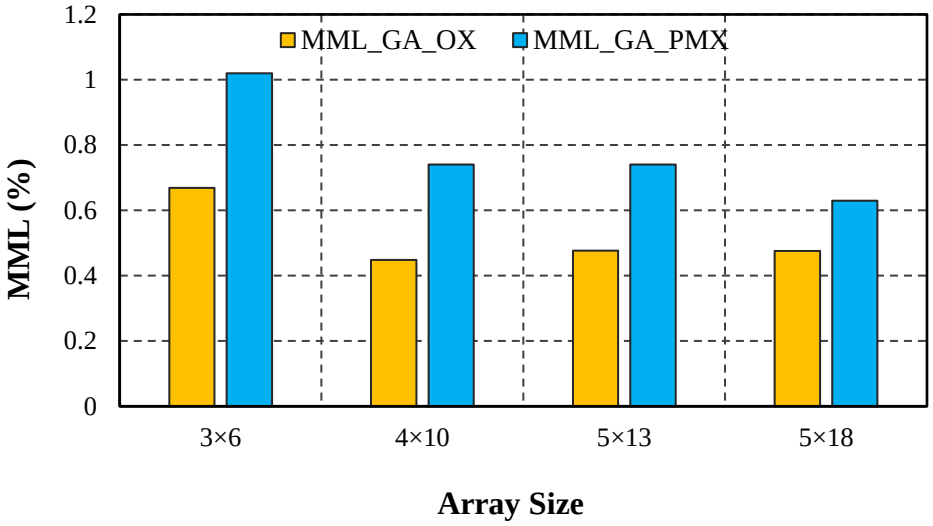

Figure 2.10: Comparison of MML obtained by Proposed and Previous GA based Module Arrangement Techniques

The array output power and MML% are tabulated in Table 2.2 for 3×6, 4×10, 5×13, and 5×18 arrays, where the summation of modules power are 1707.21 W, 3796.06 W, 6167.77 W and 8547.92W respectively. For the proposed work the array output power and mismatch losses are denoted as Parray_OX and MML_OX. Whereas for the previous work the array output power and mismatch losses are denoted as Parray_PMX and MML_PMX respectively. The Parray_OX of 3×6, 4×10, 5×13, and 5×18 arrays are 16.95.795 W, 3779.044 W, 6138.312W and 8507.228 W respectively and the corresponding MML_OX (%) are 0.669, 0.448, 0.477 and 0.476 respectively. However, the Parray_PMX of 3×6, 4×10, 5×13, and 5×18 arrays are 16.89.801 W, 3767.968 W, 6122.131 W and 8494.065 W respectively. And the corresponding MML_PMX (%) are 1.02, 0.74, 0.74 and 0.63 respectively. Figure 2.10 summarizes that the proposed GA based technique can minimizes MML 0.265% (average) more than the previous work.

2.4 Simulation Result Analysis of New PV Arrays

2.4.1 Case Study on 400 W PV Array

In this section, seven different methods (*Ra*_method, *Vm*_method, *Voc*_method, *Pm*_method, *Isc*_method, *Im*_method, and *GA*_method) are applied on a 400 W PV array with 40 modules of 10 W each for arranging the modules accordingly to get maximum array output power. Figure 2.11 shows the optimal arrangement of modules is obtained for LSS-SP (2×20) array arrangements using conventional techniques (a-f) and proposed *GA* technique (g). The same methods are also performed for 1×40, 2×20, 4×10, 5×8, 40×1, 20×2, 10×4, and 8×5 array configurations and simulation results of array output power are calculated using a mathematical model described in section 3. The array output power is depicted in Table 2.3 for four different LSS-SP array arrangments (1×40, 2×20, 4×10, 5×8). The results show that power generation by arranging module using *GA* based method is the maximum for all array arrangements, and the maximum array power is 403.785W for 5×8 array arrangement. An interesting observation is that for 1×40 array arrangement, the array power remains the same for all techniques because of the array voltage, and the array current remains same arrangement. 4×10 and 5×8 array arrangements are generating different output power for different methods, and the result shows that the current based methods (*Im* and *Isc*) are producing more energy than voltage-based methods (*Vm* and *Voc*).

Table 2.4 shows the array output power for four different LPB-SP array arrangements (40×1, 20×2, 10×4, and 8×5). Here 8×5 array output power is 402.827 W, which is the maximum power generated by using *GA* based method. The array power remains the same for 40×1 array arrangement. Though the power generation by *Pm* based technique is higher than voltage-based methods (*Vm, Voc*) but it is lower than the current based methods (*Im, Isc*) both for LSS-SP and LPB-SP array arrangements. By comparing Table 2.2 and Table 2.3, LSS-SP arrays output powers are always higher than LPB-SP arrays for the corresponding module arrangement techniques. However, the lowest array output power 383.643 W is obtained for the 40×1 array arrangement.

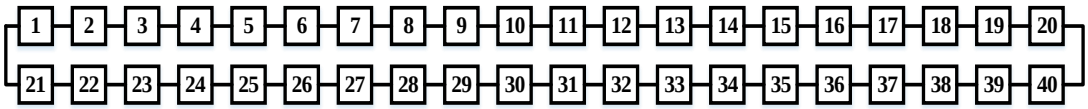

(a) Ra_method

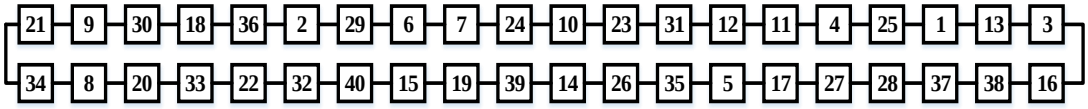

(b) Im_method

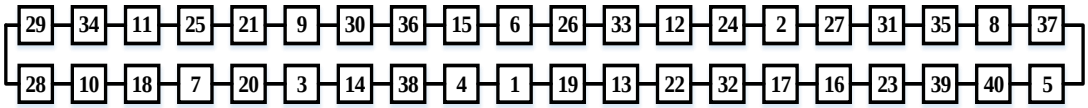

(c) Isc_method

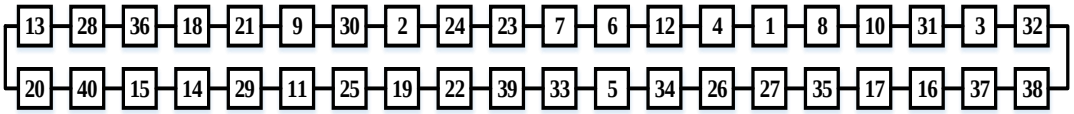

(d) Pm_method

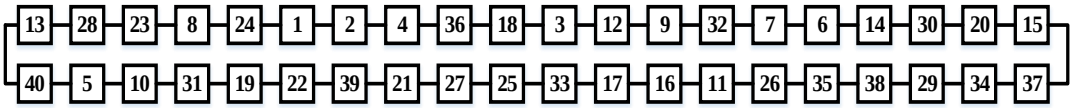

(e) Vm_method

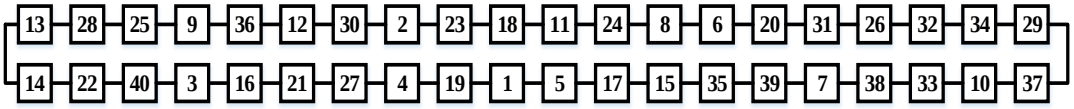

(f) Voc_method

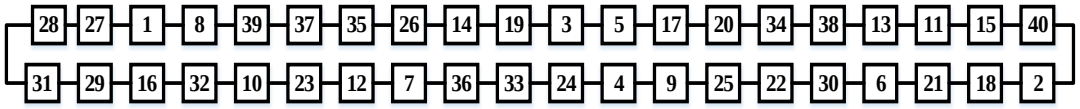

(g) GA_method

Figure 2.11: 2×20 array modules are arranged by (a) *Ra*, (b) *Im*, (c) *Isc*, (d) *Pm*, (e)*Vm*, (f) *Voc* and (g) GA methods

Table 2.3: Array output power for 400 W LSS-SP array configurations

Array Size	**Array output power (W) by using different techniques for 400 W LSS-SP arrays**						
	Ra_method	Vm_method	Voc_method	Pm_method	Isc_method	Im_method	GA_method
1×40	398.125	398.125	398.125	398.125	398.125	398.125	398.125
2×20	396.659	396.499	398.072	397.711	398.341	401.544	402.067
4×10	395.028	395.132	396.728	397.978	400.086	402.693	403.059
5×8	394.340	394.476	396.086	397.630	400.228	403.754	403.785

Table 2.4: Array output power for 400 W LPB-SP array configurations

Array Size	**Array output power (W) by using different techniques for 400 W LPB-SP arrays**						
	Ra_method	Vm_method	Voc_method	Pm_method	Isc_method	Im_method	GA_method
40×1	383.643	383.643	383.643	383.643	383.643	383.643	383.643
20×2	392.090	383.978	383.978	385.219	394.482	394.657	398.356
10×4	391.648	391.166	393.361	393.845	397.598	400.556	402.729
8×5	392.807	392.503	395.221	395.821	399.553	401.379	402.827

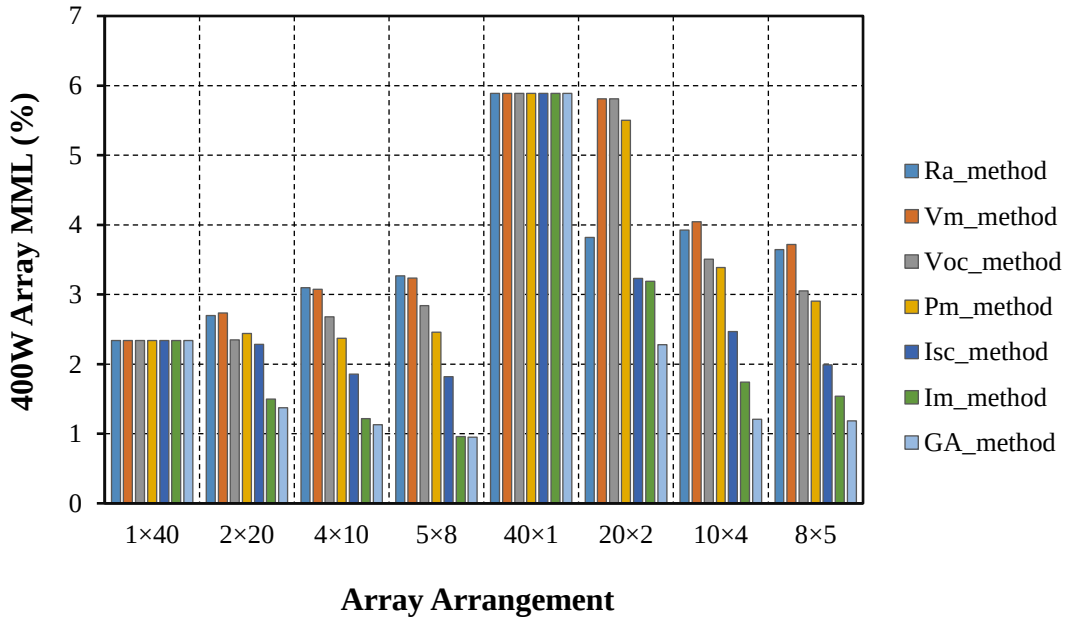

Figure 2.12. MML for LSS-SP and LPB-SP array configurations of 400 W array

Figure 2.12 shows the %MML in the 400 W array both for LSS-SP (1×40, 2×20, 4×10, 5×8) and LPB-SP (40×1, 20×2, 10×4, 8×5) array arrangements are obtained by using different module arrangement methods. In one hand, minimum %MML are achieved by *GA* based method both for LSS-SP and LPB-SP array arrangements and the minimum values are 0.94% and 1.18% for 5×8 and 8×5 arrays, respectively. On the other hand, *Vm* based method gives higher %MML for 20×2, 10×4, 8×5, and 2×20 array arrangements. For 4×10 and 5×8 array arrangements, the random process gives even more %MML than the *Vm* based approach. However, for 1×40 and 40×1 array arrangement the %MML are unchanged for all the methods, and the maximum MML obtained is 5.89% in 40×1 array arrangement. Though the %MML obtained by all techniques are following a similar pattern for LPB-SP (20×2, 10×4, and 8×5) array arrangements as shown in Figure 2.10, the values of %MML for LPB-SP array arrangements are always higher than LSS-SP array arrangements for each method.

2.4.2 Case Study on 3400 W PV Array

A 3400 W PV array is made by using 40 modules of 85 W rating using the datasets from Table 2.1. The array is arranged in 1×40, 2×20, 4×10, 5×8, 40×1, 20×2, 10×4, and 8×5 array arrangements by using all seven module arrangement methods. The corresponding array power is calculated and tabulated in Table 2.5 and Table 2.6. The results are similar like 400 W array because *GA* based process is again performed better by generating higher array power than all other purposes. While *Vm* based method shows poor performances by generating lower output power for almost all array arrangements. The highest output power, 3427.43 W is obtained by 5×8 array arrangement using *GA* based method and the lowest output power, 3400.94 W is received by *Vm* based technique for the same array. For 8×5 array arrangement by *GA* based technique output power is 3425.13 W, which is the maximum and by *Vm* based technique output is 3401.62 W, which is the minimum. By comparing Table 2.4 and Table 2.5 results show that *GA* based technique is superior for both LSS-SP and LPB-SP array arrangements. However, LSS-SP arrangements are generating more output power than LPB-SP array arrangements.

Table 2.5: Array output power for 3400 W LSS-SP array configurations

Array Size	Array output power (W) by using different techniques for 3400 W LSS-SP arrays						
	Ra_method	Vm_method	Voc_method	Pm_method	Isc_method	Im_method	GA_method
1×40	3415.950	3415.950	3415.950	3415.950	3415.950	3415.950	3415.950
2×20	3405.038	3405.528	3409.419	3412.540	3418.861	3422.724	3424.072
4×10	3402.887	3401.572	3405.725	3412.003	3419.048	3425.178	3426.417
5×8	3403.273	3400.943	3405.158	3408.437	3414.527	3426.038	3427.430

Table 2.6: Array output power for 3400 W LPB-SP array configurations

Array Size	Array output power (W) by using different techniques for 3400 W LPB-SP arrays						
	Ra_method	Vm_method	Voc_method	Pm_method	Isc_method	Im_method	GA_method
40×1	3407.484	3407.484	3407.484	3407.484	3407.484	3407.484	3407.484
20×2	3410.415	3405.485	3410.201	3406.900	3409.463	3414.522	3426.913
10×4	3407.268	3403.179	3406.017	3411.639	3412.906	3424.642	3425.935
8×5	3405.368	3401.627	3406.7	3408.674	3415.815	3425.138	3426.92

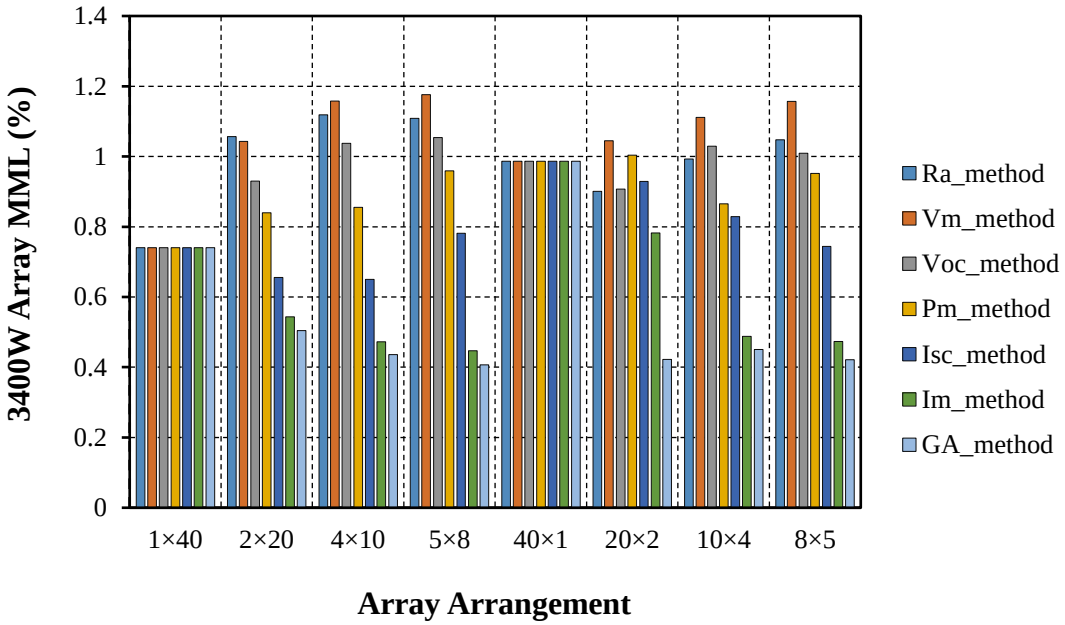

Figure 2.13: MML for LSS-SP and LPB-SP array configurations of 3400 W array

The %MML in 3400 W PV array for LSS-SP arrays (1×40, 2×20, 4×10, 5×8) and LPB-SP arrays (40×1, 20×2, 10×4, 8×5) are illustrated in Figure 2.13. Where the *GA* based module arrangement method is performed as the best method for both LSS-SP and LPB-SP array arrangements. The minimum MML is 0.41% and 0.42% obtained by the *GA* method for 5×8 and 8×5 array, respectively. The *Vm* based process shows higher %MML for both LSS-SP and LPB-SP array arrangements. The highest values are 1.176% and 1.156% for 5×8 and 8×5 array arrangements respectively obtained by *Vm* based method.

2.4.3 Case Study on 9880 W PV Array

In this section, module arrangement methods are investigated on a 9880 W PV array. A 9880 W array is developed by using 40 modules of 247 W using datasets from Table 2.1. At first, 9880 W array is arranged in LSS-SP arrangements (1×40, 2×20, 4×10, 5×8) and LPB-SP array arrangements (40×1, 20×2, 10×4, 8×5) by using all module arrangement techniques. After that, the array output power is calculated by simulation and tabulated in Table 2.7 and Table 2.8. For 1×40 and 40×1 array arrangement the output power is 9769.91 W and 9609.63 W, respectively. Table 2.6 shows that the *GA* based method has a significant role in generating maximum output power for 2×20, 4×10, and 5×8 array arrangements. While *Vm* based approach produces the lowest output power for the same array arrangements. In this case, the highest array output power is 9818.371 W obtained by the *GA* based method for 4×10 array arrangement. The lowest array output power is 9660.148 W obtained by *Vm* based technique for 5×8 array arrangement.

Table 2.7: Array output power for 9880 W LSS-SP array configurations

Array Size	Array output power (W) by using different techniques for the 9880 W LSS-SP array						
	Ra_method	Vm_method	Voc_method	Pm_method	Isc_method	Im_method	GA_method
1×40	9769.912	9769.912	9769.912	9769.912	9769.912	9769.912	9769.912
2×20	9709.074	9695.554	9742.637	9712.042	9758.631	9786.046	9810.914
4×10	9685.239	9678.068	9740.016	9691.434	9732.185	9766.97	9818.371
5×8	9682.299	9660.148	9723.505	9696.234	9709.943	9769.702	9816.904

Table 2.8: Array output power for 9880 W LPB-SP array configurations

Array Size	Array output power (W) by using different techniques for the 9880 W LPB-SP array						
	Ra_method	Vm_method	Voc_method	Pm_method	Isc_method	Im_method	GA_method
40×1	9609.63	9609.63	9609.63	9609.63	9609.63	9609.63	9609.63
20×2	9717.518	9609.245	9622.994	9608.048	9718.273	9743.883	9814.136
10×4	9706.703	9629.607	9636.243	9656.269	9712.061	9771.7	9822.291
8×5	9688.570	9638.369	9692.488	9644.886	9715.177	9773.501	9815.887

Table 2.8 shows that maximum output power is achieved by *the GA* based method for 20×2, 10×4 and 8×5 array arrangements and minimum output powers are obtained by *Vm* based approach for the same array arrangements. The highest potential is 9822.291 W in 10×4 arrays while the lowest power is 9609.245 W for the 20×2 array. By comparing Table 2.7 and Table 2.8, it is found that the *GA* based method is generating higher power than other methods for both LSS-SP and LPB-SP arrays.

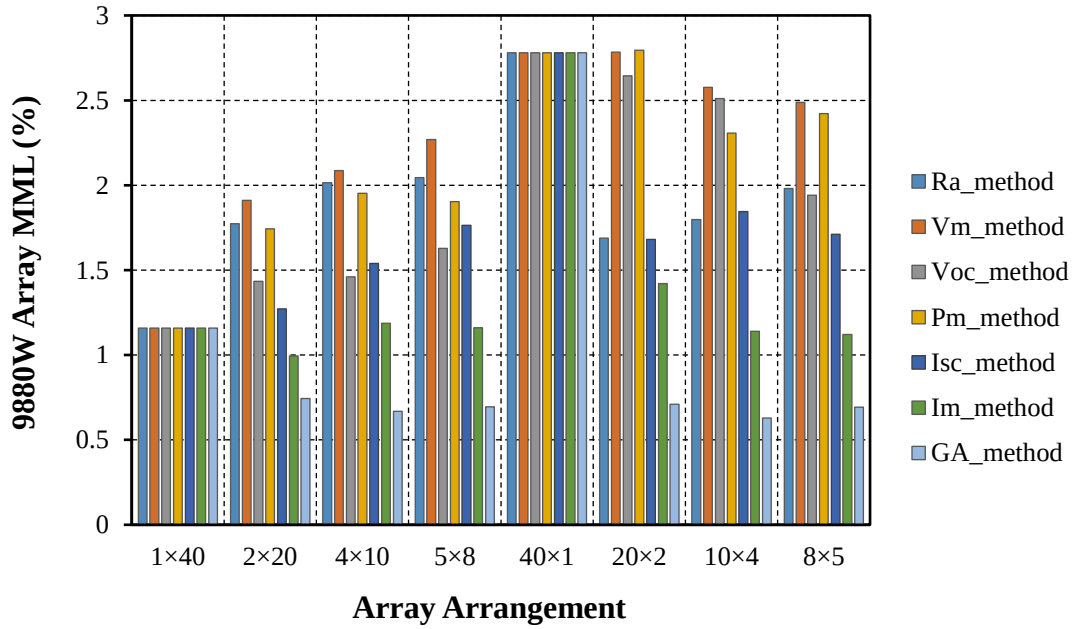

Figure 2.14: MML for LSS-SP and LPB-SP array configurations of 9880 W array

For both LSS-SP and LPB-SP array arrangements of 9880 W array, the %MML are illustrated in Figure 2.14. Where %MML is always higher for *Vm* based method, and the higher value is 2.78 % for 20×2 array arrangements. The lowest value is 0.628 % for 10x4 array obtained by *GA* based method. The lower values of MML are 0.66

% and 0.69 % acquired for 4×10 and 8×5 array arrangements respectively by *GA* based technique. Figure 2.12 shows that the highest MML is 2.8% achieved by the *Pm* based technique for 20×2 arrays. However, the LSS-SP array arrangements are performed better than LPB-SP array arrangements for *GA* based method to lower %MML. The current based methods (*Im* and *Isc*) are also performed better for both LSS-SP (2×20, 4×10, 5×8) and LPB-SP (20×2, 10×4, 8×5) array arrangements with lower %MML than the random (*Ra*) and the power-based method (*Pm*).

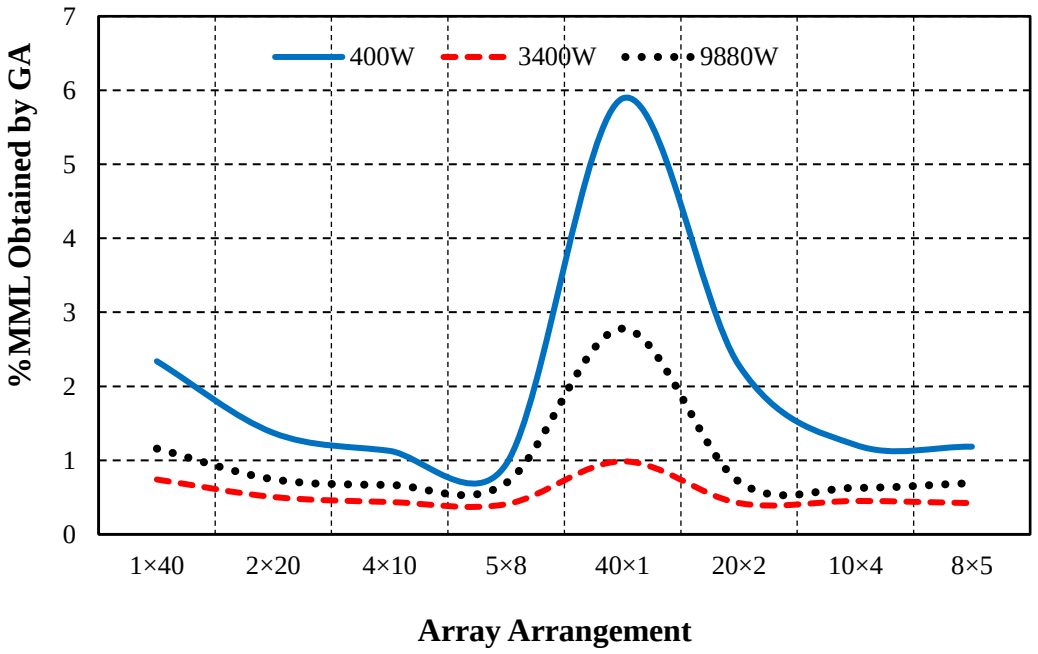

Figure 2.15: MML obtained by *GA* based method for different configurations of 400 W, 3400 W, and 9880 W array

2.4.4 Comparative Analysis of MML in New PV Arrays

Figure 2.15 shows the %MML obtained by *GA* based method for different array configurations (1×40, 2×20, 4×10, 5×8, 40×1, 20×2, 10×4, 8×5) of 400 W, 3400 W, and 9880 W arrays. The results show that each array configurations influence the %MML, and it follows a similar trend for three different PV power systems. In LSS-SP configurations (1×40, 2×20, 4×10, 5×8) the highest %MML is found for the most extended LSS-SP array (1×40), and the %MML is gradually decreasing with the decreasing number of series modules in the array. Hence, the lowest %MML is obtained for a 5×8 array. On the other hand, in LPB-SP array configurations (40×1, 20×2, 10×4, 8×5) the highest %MML is found for the most extended LPB-SP array (40×1), and the %MML is decreasing with decreasing the parallel branches in the

array. An interesting observation is located between the %MML and the correlation coefficient of Vm and Im of the corresponding datasets. The correlation coefficient of 400 W, 98800 W, and 3400 W arrays are positive (+0.148), negative (-0.567) and negative (-0.435), respectively. The maximum %MML found in 400 W arrays at positive correlation and the minimum is in 3400 W arrays at negative correlation.

Finally, the simulation results show that *GA* based method is performed better than *Im* based process for higher output power and lower %MML, while *Im* is better than *Pm* and *Vm* for all three different power ratted arrays (400 W, 3400 W, and 9880 W). Another important observation is that LSS-SP configurations are generating higher power than LPB-SP array configurations. Therefore, these research results will help to take the correct decision about the selection of array size (LSS-SP and LPB-SP) and module rearrangement techniques (*GA, Im, Pm, Vm*) for future research on this field. The PV system configurations (LSS-SP and LPB-SP) are used based on the load voltage and current. For high voltage PV system such as water pumping, grid tie system, LSS-SP is suitable, and for the low voltage PV system, such as battery charging for electric vehicles, LPB-SP is suitable. For both, the cases *GA* and *Im* based module arrangement techniques can perform better to maximize the array output power.

2.5 Experimental Work at New Condition of 400 W Array

In order to validate the simulation results, experimental investigations are carried out using the 400 W array for LSS-SP (4×10, 5×8) and LPB-SP (10×4, 8×5) configurations. The experimental setup and the corresponding results are presented in this section.

2.5.1 Experimental Setup of 400W Array

A 400 W PV array system is composed of 40 poly-crystalline PV modules of 10 W each are placed on the structures with a fixed tilt angle of 23.5°. The array consists of four parallel PV strings of ten PV modules in series. All the PV modules are south facing and are mounted on a rooftop, the geographical location of latitude is 23°43'N and longitude is 90°25'E, shown in Figure 2.16. Where direct sunlight is available during the daytime. The PV modules are collected from ESPL with flash test dataset, and their electrical characteristics are already shown in Table 2.1.

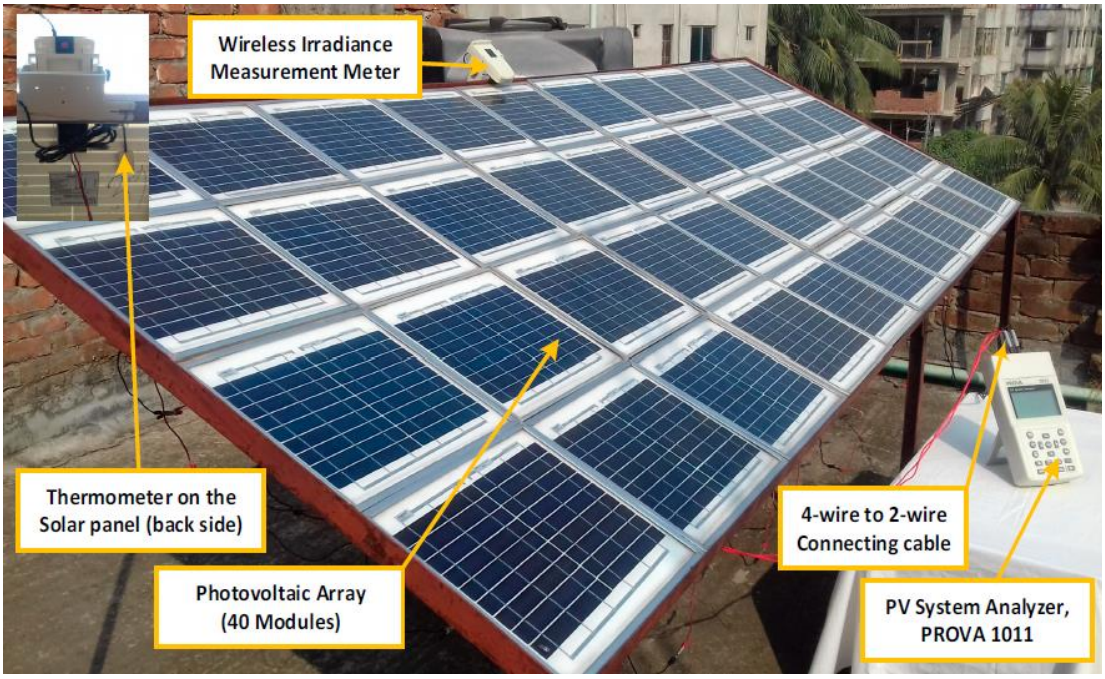

Figure 2.16: Experimental setup of 400 W array at new condition for comparing maximum array output power using different methods of modules arrangement

The current-voltage and power-voltage characteristics curves for the 400 W array modules with LSS-SP and LPB-SP configurations are measured and recorded in different atmospheric conditions. To determine the *I-V* and *P-V* characteristics, irradiance and temperature corrections are performed according to IEC 60904-1 standard. The *I-V* and *P-V* characteristics measurements are performed using the photovoltaic system analyzer (PVSA), PROVA 1011 from the TES Electrical Electronic Corp. The PVSA device measures the electrical characteristics curves of PV module as well as of string or array. It also regulates and calculates Efficiency, Temperature, Irradiance, series resistance of the PV system at outdoor operating condition (OPC). The PVSA device can convert *I-V* and *P-V* curves under OPC to data STC based upon IEC standard. The International Electrotechnical Commission (IEC) is the world's leading organization for the preparation and publication of International Standards for all electrical and electronic related technologies. For instance, the requirements for I-V measurement of photovoltaic devices are laid down in IEC 60904-1.

Figure 2.17 shows the PVSA device, PROVA 1011, a remote solar detector (RSD) 1012 with a thermometer. The analyzer device and RSD rare connected by Bluetooth wireless communication. The RSD device is fully moisture-proof. The maximum power rating of the PVSA device is 12000 W, and accuracy for the *I-V* curve

measurement is ±1%. Table 2.9 shows the technical specifications of the analyzer, Irradiance sensor, and temperature sensor. The four-wire to two-wire connecting cables are used to eliminate the systematic errors in voltage measurement, and the measuring interval is 0.02-2 seconds for a single measure. The PVSA device waits and tests the PV system automatically until appropriate sunlight irradiance is detected.

Table 2.9: Specifications of the analyzer, irradiance sensor, and temperature sensor.

Measurement	Range	Resolution	Accuracy
DC Voltage	1 ~ 1000 V	0.01V / 0.1V	±1%
DC Current	0.1 ~ 12 A	1mA / 10mA	±1%
Irradiance	0 ~ 2000 W/m^2	1 W/m^2	± 3 %
Temperature	-22 ~ 85 °C	0.1°C	± 1 %

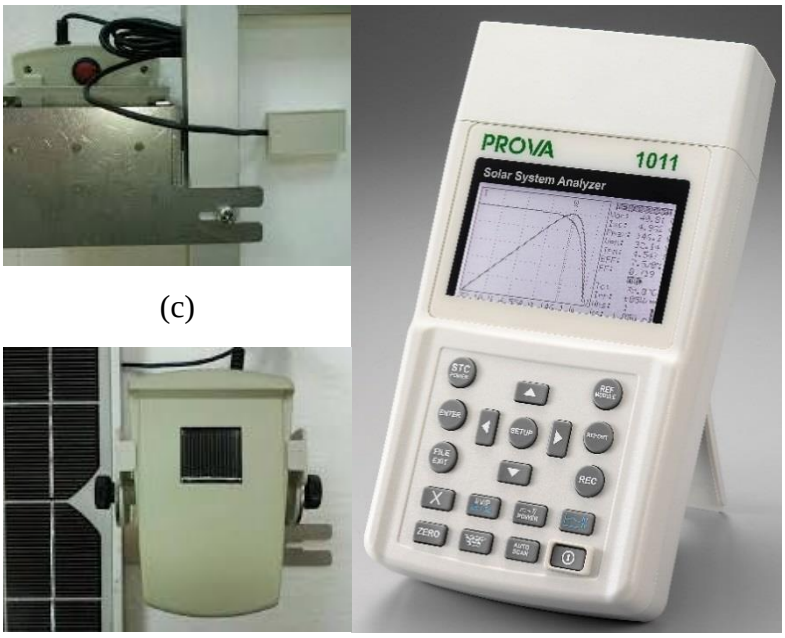

(c)

(b) (a)

Figure 2.17: PV system analyzer: (a) PROVA 1011, (b) Remote Solar Detector and (c) Thermometer

2.5.2 Experimental Measurement Procedure

The experimental data measurements of the PV array configurations are carried out in real atmospheric weather conditions throughout the middle of a sunny day and clear sky. By maintaining standard test conditions at outdoor, are described in [79], a

single test for I-V characteristics measurement of the PV array is carried out by less than 30 seconds using the PVSA device, PROVA 1011. As stated by IEC 60904-1 standards, photovoltaic I-V characteristic curve measurement can be performed in natural outdoor sunlight during one percent variation of global solar radiation. The incident solar radiation should be at least 800 W/m^2 [75]. Therefore, in this work, the experimental data recorded within the radiation range between 800 W/m^2 and 900 W/m^2 considering small temperature variations. However, the irradiance values are corrected considering 1000 W/m^2 as reference irradiance. Consequently, the second procedure of irradiance correction is used in this work, among the three correction procedures proposed in IEC 60891. The irradiance correction procedure [79] is as follows:

$$I_{ref} = I_m \left(1 + \alpha_{rel} \times \left(T_{ref} - T_m\right)\right) \times \frac{G_{ref}}{G_m} \tag{2.10}$$

$$V_{ref} = V_m + V_{OCm}\left(\beta_{rel}\left(T_{ref} - T_m\right) + \delta \times \ln\left(\frac{G_{ref}}{G_m}\right)\right) - R_s\left(I_{ref} - I_m\right) - k \times I_{ref}\left(T_{ref} - T_m\right) \tag{2.11}$$

$$P_{ref} = \frac{P_m \times \left(\frac{G_{ref}}{G_m}\right)}{\left(1 + \gamma\left(T_{ref} - T_m\right)\right) \times \left(1 + \delta \times \ln\left(\frac{G_{ref}}{G_m}\right)\right)} \tag{2.12}$$

Where ‘ref’ and ‘m’ subscripts refer the reference and measured values respectively. ‘I’ is array current; ‘V’ is array voltage; ‘V*oc*’ is open circuit voltage; ‘G’ is irradiance; ‘α_{ref}’ and ‘β_{ref}’ are relative temperature coefficient of current and voltage; ‘δ’ is irradiance correction factor (=0.06); ‘R_s’ is internal series resistance; ‘k’ is curve correction factor; ‘γ’ is power temperature coefficient; ‘P’ is array power. The PVSA device is intelligent to measure and store the values of array current, array voltage, array power, and irradiance under fast-changing weather conditions. Hence, the reference power in (2.12) represent the corrected maximum power measured at STC. It is the value considered for the performance comparison of array configurations under the same irradiance and temperature conditions.

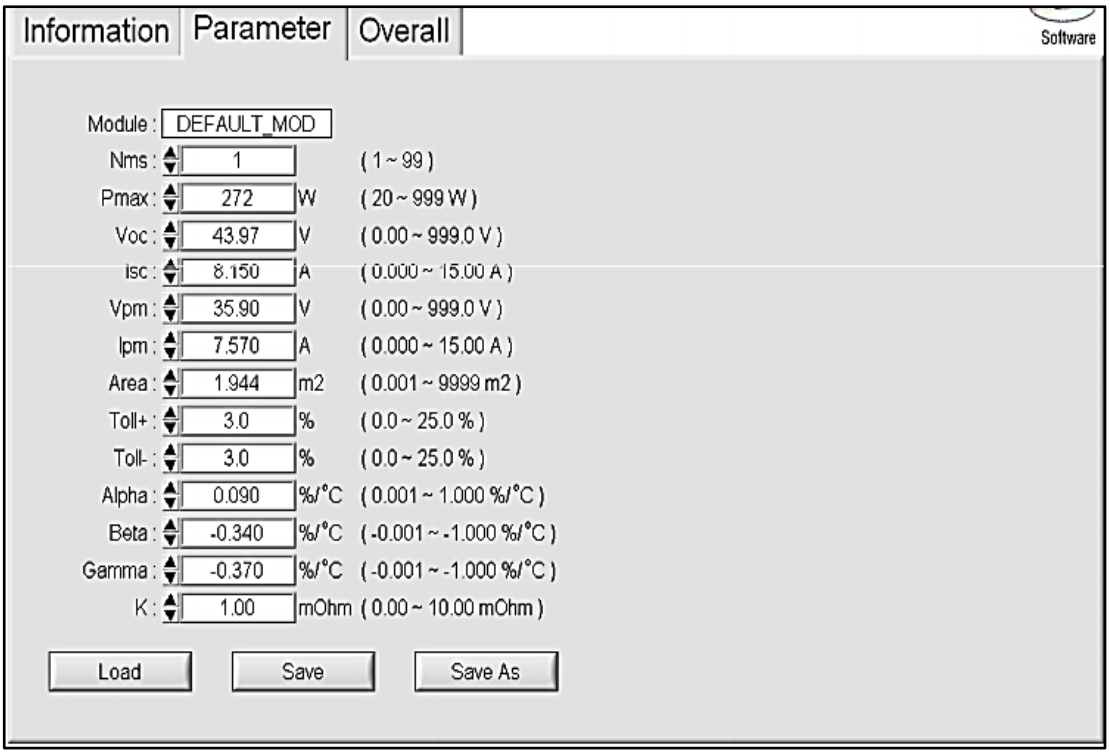

Figure 2.18: Reference parameters value used in the PV system analyzer, PROVA 1011

Figure 2.18 shows different reference parameters value, which have been used in the PVSA device (PROVA-1011), in order to make the correction to convert from OPC to STC data. In addition, Air Mass (AM) can be calculated with the following equations:

$$G_G = 1.1 \times G_D \tag{2.13}$$

$$G_D = 1.353 \times 0.7^{AM^{0.678}} \tag{2.14}$$

Where, 'G_D' is direct beam intensity (kW/m^2); 'G_G' is estimate of global irradiance (kW/m^2). For example, AM = 1.5 has been calculated when, G_D = 0.846 and G_G = 0.9306.

Changing the light intensity incident on a solar module changes all PV parameters, including the short-circuit current, the open-circuit voltage, the FF, the efficiency and the impact of series and shunt resistances. The light intensity on a solar module is called the number of suns, where 1 sun corresponds to standard illumination at AM1.5, or 1 kW/m2.

The objective of the experimental investigation is to record and compare the array output power obtained under different module arrangement methods applied to

the LSS-SP (4×10, 5×8) and LPB-SP (10×4, 8×5) array configurations. The simulation result shows that the *GA* based arrangement method and *Im* based arrangement methods are outperforming than other PV array modules arrangement methods. The random arrangement method is usually used as a conventional PV array module arrangement method. Therefore, these three PV array module arrangement methods are experimentally compared using a 400 W PV array at uniform irradiance condition. Hence shading effects are not considered in this work. All experiments are performed under real operating conditions, and the measured OPC data is processed before being compared using equation (2.12). Before each experimental test, the front side of all the PV modules are cleaned, and the module positions are rearranged according to the arrangement results obtained by simulation.

2.5.3 Experimental Results

In Table 2.10, the experimental array output power is obtained for four different array configurations (4×10, 5×8, 10×4, and 8×5) using three techniques. Maximum output power was obtained using GA based arrangement for all these array configurations, and the highest power of 392.559 W is obtained in 5×8 configuration. Besides, the *Im* based technique also performed well by generating higher output power than *Ra*_method. However, the output power is lower than that obtained using the GA method. Hence, the *%RE* is calculated with respect to the most conventional Ra_method of module arrangement. Therefore, *%RE* by *Im* based method, (*%RE_Im)*, and *%RE* by *GA* based method (%*RE_GA)* are calculated for both *Im* and *GA* based techniques, comparing with random based arrangement technique as follows.

$$\%RE\_Im = \frac{P\_Im\ - P\_Ra}{P\_Ra} \times 100 \tag{2.15}$$

$$\%RE\_GA = \frac{P\_GA\ - P\_Ra}{P\_Ra} \times 100 \tag{2.16}$$

Where *P_Ra*, *P_Im*, and *P_GA* are denoted as PV array output power measured by arranging modules using the random method, *Im* method, and *GA* method, respectively. The calculated values of *%RE_Im* and *%RE_GA* are tabulated in Table 2.11 for both LSS-SP (4×10, 5×8) and LPB-SP (10×4, 8×5) configurations. The minimum and maximum value of *%RE_Im* are 2.62 % and 3.249 %, respectively. On the other hand, by *the GA* method, the minimum and maximum amount of *%RE_GA*

are 3.267 % and 4.159 %, respectively. In both cases, the maximum values are obtained by LSS-SP (5×8) configuration. The result shows that average *%RE* obtained by LSS-SP configuration is higher than LPB-SP configurations for both *Im* and *GA* based techniques. The average *%RE* obtained by *Im* method is 2.88 %, and by *GA* method is 3.60 %. Therefore, the *GA* based technique is performed better than *Im* based technique for both LSS-SP and LPB-SP configurations.

Table 2.10: Array output power obtained by experimental work

Array Configuration	Array Size	400 W Array Output Power Obtained by Experimental Work (W)		
		Ra_method	Im_method	GA_method
LSS-SP	4×10	378.201	388.110	390.559
	5×8	377.06	389.312	392.743
LPB-SP	10x4	375.421	386.502	388.648
	8x5	376.733	386.919	389.781

Table 2.11: Comparison of recoverable energy between *Im* based method and *GA* based method

Array Configuration	Array Size	Recoverable Energy Obtained by Experimental Work	
		%RE_Im	%RE_GA
LSS-SP	4 × 10	2.620	3.267
	5 × 8	3.249	4.159
LPB-SP	10 × 4	2.951	3.523
	8 × 5	2.703	3.463

The %MML obtained by the experimental work for 400 W array is shown in Figure 2.19. The experimental %MML for LSS-SP (4×10, 5×8) and LPB-SP (10×4, 8×5) configurations are calculated by using (2.7). Where the value of modules power is used 407.63 W, as used in the simulation and the array output power is applied from Table 2.9 for each array configuration. The experimental results show that the minimum %MML are obtained by *GA* based method both for LSS-SP and LPB-SP configurations, which is similar to simulation results.

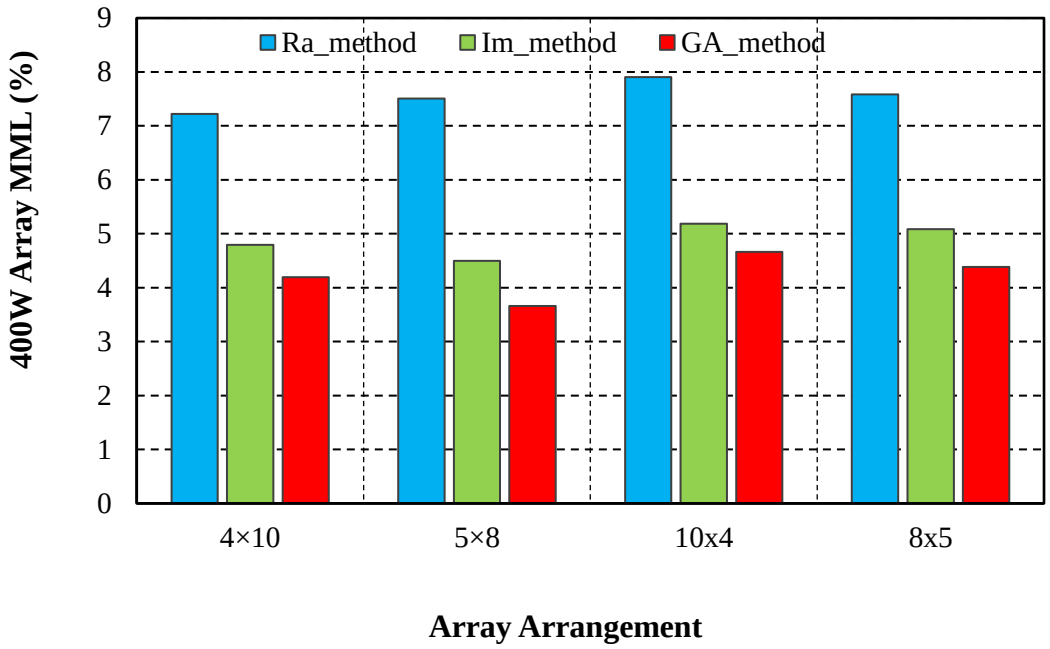

Figure 2.19: MML obtained by an experiment using three different techniques for 400 array configurations

2.5.4 Summary on MML Minimization of New PV arrays

In this work, a new technique of module sorting of PV arrays using adaptive *GA* is experimentally validated both for LSS-SP (4×10, 5×8) and LPB-SP (10×4, 8×5) configurations in minimizing MML. The performance of the proposed *GA* technique regarding total output power and %MML are compared with other conventional module sorting techniques. The traditional current-based methods (Im, Isc) show better performance than the voltage-based methods (Vm, Voc); however, the proposed technique outperforms the conventional ones in every array configuration. Simulation results show that GA and Im based techniques are outperformed for both LSS-SP and LPB-SP array configurations in 400 W, 3400 W, and 9880 W arrays at new condition. The experimental analysis also shows similar results. Finally, it is observed that the percentage of recoverable energy (*%RE*) obtained by arrangement using the *GA* based method is higher than *Im* based method for both LSS-SP and LPB-SP array configurations. A maximum *%RE* of 4.159 % is recorded for 5×8 LSS-SP array configuration by applying the *GA* based MML reduction method.

2.6 MML Investigation in Aged PV Arrays

Power degradation due to non-uniform aging is a common phenomenon in large PV array systems. Aging increases *I-V* mismatch in the array modules that results

in MML in the array. Therefore, it is essential to minimize MML to increase the array output power. In order to mitigate the MML due to non-uniform aging, genetic algorithm (GA) based and short circuit current (SCC) based module rearrangement techniques are investigated in this work to obtain an optimal arrangement that yields maximum output power from the aged arrays. Besides, the performance of these two techniques is compared with randomly module arrangement technique (RA) to find the effectiveness of the rearrangement techniques on the aged PV arrays considering the four different power ratings (400 W, 1.6 kW, 3.2 kW, and 10 kW).

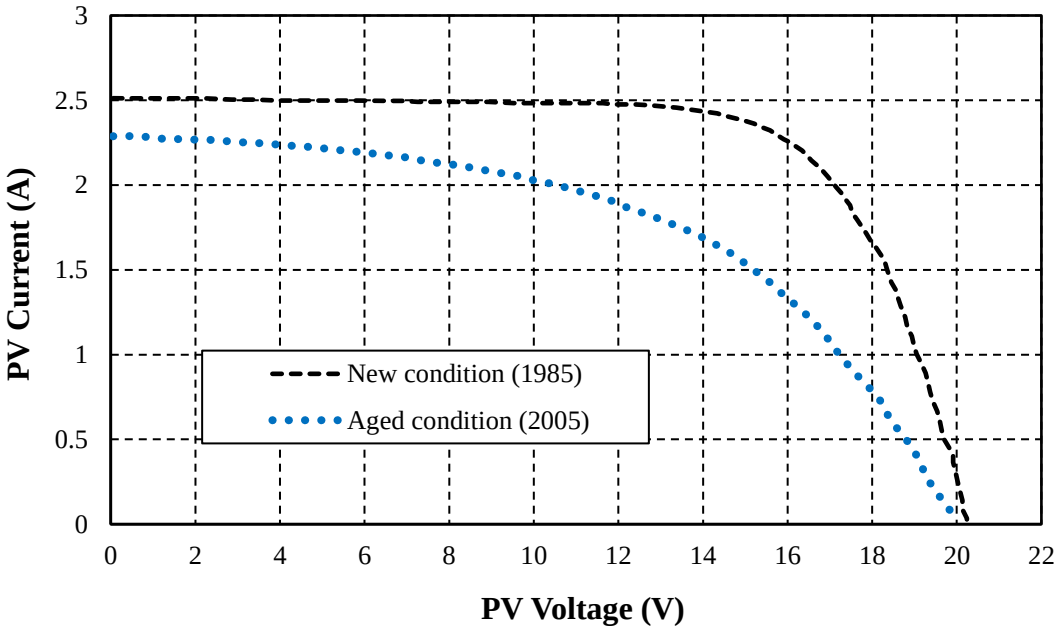

Figure 2.20: Electrical characteristics of a PV module, which have been tested at new and aged condition in 1985 and 2005, respectively.

2.6.1 Mismatch Loss in Aged PV Array

The aging of PV panels causes the change of the slope of the *I-V* curve due to the variation of series and shunt resistances close to open circuit voltage and short circuit current respectively, as shown in Figure 2.20. Therefore, the fill factor decreases and consequently reduces the peak power point of the PV module [80]. Aging of the PV module is a continuous process, but it is not uniform in nature[81]. In an array, the non-uniform aging of PV modules increases mismatch in the *I-V* curves . This *I-V* mismatch is the critical factor of MML in a vast PV array [82]. The aging speed of modules is non-uniform, and power loss is averagely 0.8% per year. The power degradation of PV modules can vary from 0.5% to 1% per year due to different

aging effects . A closed-loop relation exists among MML and non-uniform aging of PV modules in an array. Therefore, it is beneficial to investigate the MML reduction methods for old PV array to maximize power [83].

2.6.2 Mathematical Model of MML for Aged PV Array

An aged PV module generates lower power than its rated power. In a one-year-old PV module, the average degradation rate of open circuit voltage and short circuit current are 2% and 10%, respectively [32]. Hence, the power degradation in an aged module has a close relationship with the short circuit current. The non-uniformly aged modules are compared using maximum short circuit current, considering the same open circuit voltage; where the power degradation of an old PV module due to its non-uniformly aged cells is explained by using the bucket effect. In this paper, it is considered that in an array, all the PV modules are non-uniformly aged and are not bypassed by diodes.

In an aged PV module, the cell-units may be aged differently, but, in this chapter, it is considered that within a PV module, all cell-units are uniformly aged. Therefore, an aged PV module can be represented by a single maximum short circuit current of any cell-unit considering the same open circuit voltage of all cell-units.

In order to derive the expressions for voltage and current of an aged PV string, let us consider, *'α'* numbers of series-connected PV modules with the string terminal voltage, V_{String}, and the current, I_{String}; they can be expressed by module terminal voltage, $V_{Module,P}$ and current, $I_{Module,P}$ of the *P-th* PV module as,

$$I_{String} = I_{Module,1} = I_{Module,2} = \cdots = I_{Module,\alpha} \tag{2.17}$$

$$V_{String} = V_{Module,1} + V_{Module,2} + \cdots + V_{Module,\alpha} \tag{2.18}$$

However, the string current is limited at the lower value of the maximum short circuit current, $I_{Module,P}^{max}$ of the *P-th* PV module because of the bucket effect [43] and can be expressed as follows,

$I_{String} \leq \min \{I_{Module,P}^{max} : 1 \leq P \leq \alpha, and\ the\ Pth\ module$ is not by passed$\}$.

Now, to find the expressions of the array terminal voltage, V_{Array}, and the array output current, I_{Array} of an aged PV array considering, 'β' number of parallel

connected strings. Hence, for the *Q-th* PV string, the terminal voltage and current are $V_{String,Q}$, and $I_{String,Q}$, respectively. The expressions are as follows.

$$I_{Array} = I_{String,1} + I_{String,2} + \cdots + I_{String,\beta} \tag{2.19}$$

$$V_{Array} = V_{String,1} = V_{String,2} = \cdots = V_{String,\beta} \tag{2.20}$$

Now, consider an ($\alpha \times \beta$) array with SP arrangement, where, in a string *'α'* number of PV modules are connected in series, and *'β'* number of strings are connected in parallel. The maximum output power of an aged array, P_{Array}^{max} can be written as,

$$P_{Array}^{max} = \sum_{Q=1}^{\beta} min \{ P_{Q,P}^{max} : 1 \le P \le \alpha, \; and\ the\ (Q,P)th \text{ module is non by passed} \} \tag{2.21}$$

Where, $P_{Q,P}^{max}$ is denoted as the maximum output power from the non-bypassed module at position (*Q, P*) (*P-th* module in the *Q-th* string) of the PV array. If '*q*' number of modules generate current then (α-*q*) modules are bypassed by a diode in the *Q-th* PV string, the maximum power $P_{Q,P}^{max}$ can be expressed as:

$$P_{Q,P}^{max} = qV_{Module}^{mpp} I_Q^q \tag{2.22}$$

Where, V_{Module}^{mpp} is the maximum voltage generated by a PV module and I_Q^q is the *q-th* highest short circuit current generated within the following set:

$$\{I_{Module,Q,1}, I_{Module,Q,2}, \ldots, I_{Module,Q,\alpha}\}.$$

Now the summation of all modules power, P_{Module}^{Sum}, and percentage of MML of the ($\alpha \times \beta$) SP-PV array can be expressed as:

$$P_{Module}^{Sum} = \sum_{I=1}^{\alpha\beta} P_{Module,I} \tag{2.23}$$

$$MML\% = \frac{P_{Module}^{Sum} - P_{Array}^{max}}{P_{Module}^{Sum}} \times 100 \tag{2.24}$$

In an aged PV array, P_{Array}^{max} is always lower than P_{Module}^{Sum} due to *I-V* mismatch in aged PV modules. Therefore, to minimize MML by maximizing P_{Array}^{max}, module rearrangement techniques are investigated in this work.

2.7 Module Rearrangement Techniques for Aged PV Array

As mentioned earlier, this paper investigates two techniques for the rearrangement of aged PV arrays to minimize the MML by maximizing the array output power, which are presented in the subsequent subsections.

2.7.1 SCC based Rearrangement Technique

In this technique, the aged modules in an array are rearranged according to the short circuit current of the modules. Where all the modules positions are determined by the value of the aged module short circuit current (I_{SC}). Let us consider a 4×10 size SP-PV array configuration consists of 40 modules, as shown in Figure 2.21.

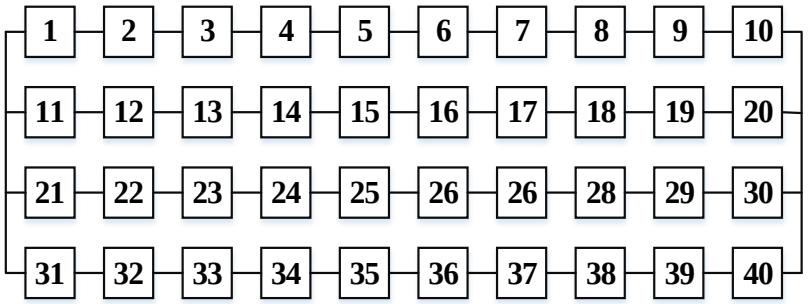

Figure 2.21: 4×10 SP-PV array modules are rearranged by SCC based technique

The I_{SC} of the aged modules are measured from the pre-collected dataset and sorted in ascending order.

$$I_{SC,min} \leq \cdots \leq I_{SC,max} \tag{2.25}$$

The sorting has been completed from minimum values to maximum values of I_{SC}; as a consequence, module 1 carries the lowest value ($I_{SC,min}$) and module number 40 has the highest value ($I_{SC,max}$). Consequently, current increases gradually from the first row to the last row. Hence, array current increases, and that also increases array output power.

2.7.2 GA based Rearrangement Technique

In the area of computational optimization problems, GA has proven to be effective other than any other nature-inspired evolutionary algorithms. The diversity and combination created to solve the rearrangement problem utilizing the mechanism of crossover and mutation, GA becomes evidentially effective to find the optimal

solution [31]. For an ($\alpha \times \beta$) PV array, the total possible number of combinations, X can be calculated as:

$$X = \binom{\alpha\beta}{\beta}\binom{(\alpha-1)\beta}{\beta}\binom{(\alpha-2)\beta}{\beta}\ldots\binom{2\beta}{\beta}\binom{\beta}{\beta}/\alpha! \quad (2.26)$$

With the increase of α and β values in equation (3.10), the number of 'X' goes significantly high, and the computational capability gets inadequate, as depicted in [41]. On the other hand, because of finding the global maxima in each iteration of mutation and crossover, GA based optimization outperforms the greater dimensionality problem. Therefore, the GA based rearrangement technique is adopted in this work to find out an optimal arrangement of PV modules in an array with maximum output power. Hence, the array output power is used as the fitness function of GA, to be maximized. The fitness function, FF, can be calculated as equation 2.8.

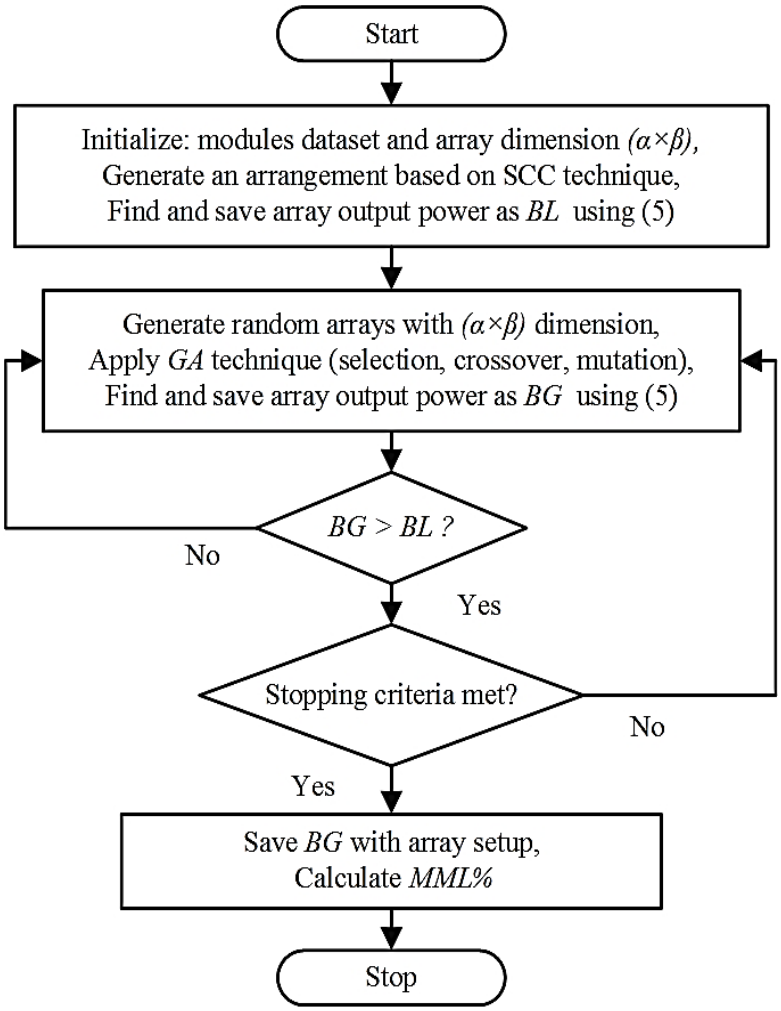

Figure 2.22: Flowchart of GA based rearrangement technique for Aged PV array

The procedure of the GA based module rearrangement technique is shown in the flow chart of Figure 2.22. At the initialization stage, the tested datasets of the aged modules are applied as input and set the array dimensions ($\alpha \times \beta$). After that, the modules are rearranged according to the SCC based technique, and the output power is calculated using (3.5). This value is saved as local best (*BL*), to obtain higher output power than SCC based technique. In the next step, N number of ($\alpha \times \beta$) random array samples are generated and calculated their fitness function, and the maximum fitness value is saved as global best (*BG)*. Then the Roulette wheel selection is used to select a pair of parents for crossover. A simple and faster order one crossover technique has been used to generate children, and after the mutation process, the *FF* is calculated for each child. If the *FF* value exceeds the previous *BG* than the new value replaces it, this process is repeated until the obtained *BG* is higher than the *BL* and also is continued until a constant maximum *BG* is achieved and the maximum *FF* with the module setup arrangement is stored. Finally, the MML% is calculated for the highest value of *FF*.

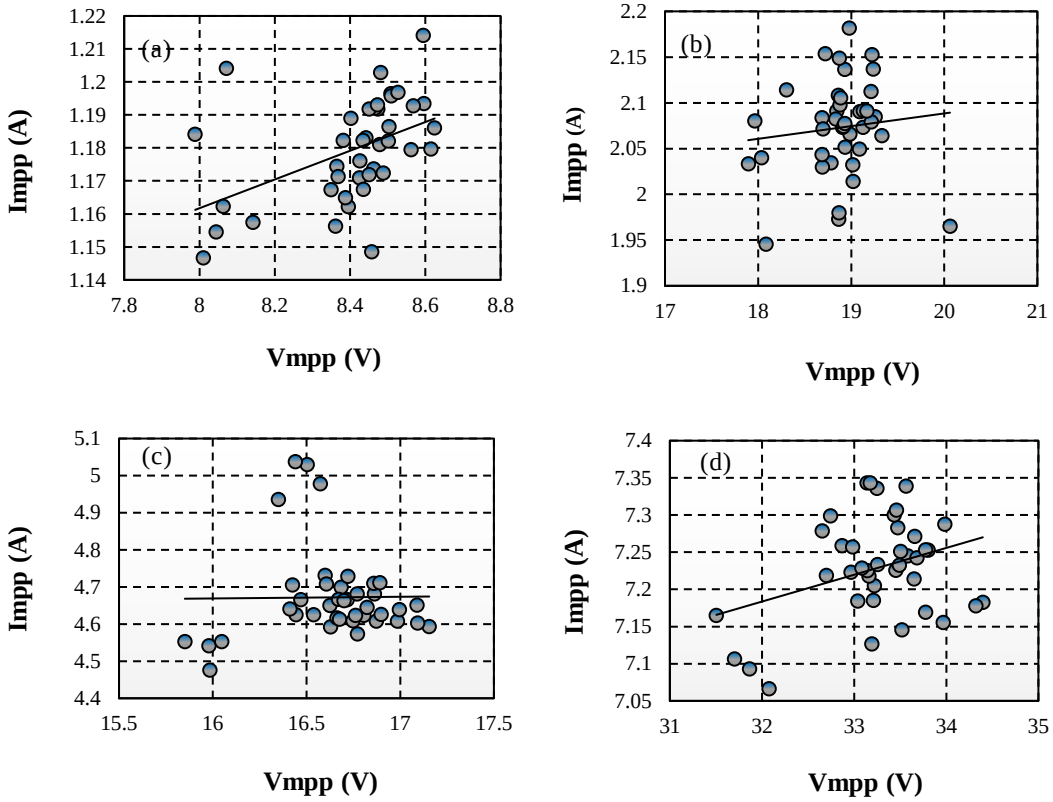

Figure 2.23: Correlation between Vmpp and Impp of aged PV modules datasets:

(a)10 W, (b) 40 W, (c) 80 W and (d) 250 W

2.8 Simulation Work on Aged PV Array

Simulation is performed to investigate the module rearrangement techniques to reduce MML% for aged PV arrays and the performances of the proposed methods (SCC and GA) are determined in respect of the RA method, in terms of array maximum power and reduction of MML%. Four datasets of aged PV arrays (400 W, 1.6 kW, 3.2 kW, and 10 kW) are used here, to make a valid comparison. Each array consists of 40 PV modules (polycrystalline), aged two years. The panels are tested from a commercial manufacturer organization, Electro Solar Power Limited using IEC60904-1 standard (1.0 kW/m^2, 25 °C, AM 1.5G) [84]. The correlation between the parameters maximum power point voltage, (*Vmpp*) and maximum power point current (*Impp*) of the tasted PV modules datasets (10 W, 40 W, 80 W, and 250 W) are shown in Figure 2.23.

The simulation is performed by a high configuration computer (with Intel Core i7 processor) using the NetBeans IDE 8.0.2 software. It makes the simulation very faster. For GA based PV modules rearrangement technique, a single simulation took a maximum of 10 minutes to determine the optimal arrangement with maximum output power. Here, the MML% is calculated using the mathematical model, described in section 3.2. In this chapter, for each array, six dimensions (2×20, 4×10, 5×8, 20×2, 10×4, and 8×5) are considered. For each array dimension, three rearrangement techniques (RA, SCC, and GA) are applied separately to find out the corresponding array output power *Po_RA, Po_SCC, and Po_GA,* respectively. In order to perform a real comparison between the proposed techniques (SCC and GA), the %RE is calculated with the corresponding values obtained by RA technique. The %RE both for SCC based technique (%RE$_{SCC}$) and GA based technique (%RE$_{GA}$) is calculated as follows.

$$\%RE_{SSC} = \frac{Po\_SCC - Po\_RA}{Po\_RA} \times 100 \tag{2.28}$$

$$\%RE_{GA} = \frac{Po\_GA - Po\_RA}{Po\_RA} \times 100 \tag{2.29}$$

2.8.1 Analysis of Simulation Results

The array output power and %RE are tabulated in Table 2.12, for four arrays (400 W, 1.6 kW, 3.2 kW, and 10 kW) with six dimensions (2×20, 4×10, 5×8, 20×2, 10×4 and 8×5). For 400W PV array with 10×4 size, there are parallel ten strings, each

of which has four modules. The corresponding array connection diagram with modules position are shown in Figure 2.24 (a), (b), and (c), respectively, for RA, SCC, and GA techniques. In this case, *Po_RA* is 347.31W, *Po_SCC*, and *Po_GA* are 382.01 W and 390.12 W, respectively. The output power is increased by 2.05% using SCC based technique and by 4.22% using GA based technique, compared to RA method. For 400 W array, the highest output power is 390.28 W, obtained by GA for 8×5 array dimension.

Table 2.12: Aged PV Arrays Output Power Obtained by Simulation

Rated array power (W)	Array size	Array output power obtained by three different techniques			Recoverable energy	
		Po_RA (W)	*Po_SCC (W)*	*Po_GA (W)*	RE_{SCC} *(%)*	RE_{GA} *(%)*
400	2×20	380.89	383.63	390.21	0.71	2.44
	4×10	377.13	380.88	390.02	0.99	3.41
	5×8	377.79	382.96	389.93	1.36	3.21
	20×2	374.97	378.21	388.19	0.86	3.52
	10×4	374.31	382.01	390.12	2.05	4.22
	8×5	374.16	379.98	390.28	1.55	4.30
1.6k	2×20	1456.08	1475.5	1516.94	1.33	4.18
	4×10	1451.16	1504.76	1530.97	3.69	5.49
	5×8	1455.89	1500.81	1542.55	3.08	5.95
	20×2	1469.49	1507.00	1526.43	2.55	3.87
	10×4	1454.93	1499.16	1539.17	3.03	5.79
	8×5	1447.29	1517.62	1526.36	4.85	5.46
3.2k	2×20	2972.48	2987.18	3030.87	0.49	1.96
	4×10	2961.27	2999.53	3048.47	1.29	2.94
	5×8	2959.98	3016.78	3037.84	1.91	2.63
	20×2	2942.98	2964.05	3057.72	0.71	3.89
	10×4	2940.47	3027.42	3047.23	2.95	3.63
	8×5	2943.81	3009.11	3042.42	2.21	3.35
10k	2×20	9318.31	9368.65	9486.88	0.54	1.81
	4×10	9233.64	9362.38	9490.99	1.39	2.78
	5×8	9208.88	9382.43	9490.28	1.88	3.06
	20×2	9094.49	9148.94	9472.47	0.59	4.16
	10×4	9119.77	9354.79	9497.11	2.57	4.14
	8×5	9155.43	9394.22	9495.16	2.60	3.71

For the 1.6 kW PV array, the maximum output power is obtained by the GA based technique for all array dimensions. The highest power of 1542.55 W is generated by the 5×8 array dimension, while energy increased by 5.95%, the 3.2 kW array, the highest power of 3057.72 W is generated by 20×2 array and for the 10 kW array, the maximum power is 9497.11 W, obtained by 10×4 array also using the GA based method. Undoubtedly, the GA based module rearrangement technique generates higher output power for all above-sized PV arrays.

Table 2.12 also provides the $\%RE_{SSC}$ and $\%RE_{GA}$ information for all the inspected PV arrays. Here in all the occasions, $\%RE_{GA}$ is higher than $\%RE_{SSC}$. For small scale PV array of 400 W, $\%RE_{GA}$ is 2.44% to 4.3%, and for the 1.6 kW array, it is 4.18% to 5.95%. For medium scale PV array of 3.2 kW, $\%RE_{GA}$ is 1.96% to 3.89%, while for large scale PV array of 10 kW, the energy improvement is 1.81% to 4.16%. It has been observed that $\%RE_{GA}$ of the small-scale array (5.95% for 1.6 kW) is comparatively higher than large scale array (4.16% for 10 kW). While, the maximum value of $\%RE_{SSC,}$ obtained from a small array (4.85% for 1.6 kW) is also higher than the vast array (2.6% for 10 kW). However, the output power improvement by GA based technique is consistently higher than the SCC based method for each PV array dimension.

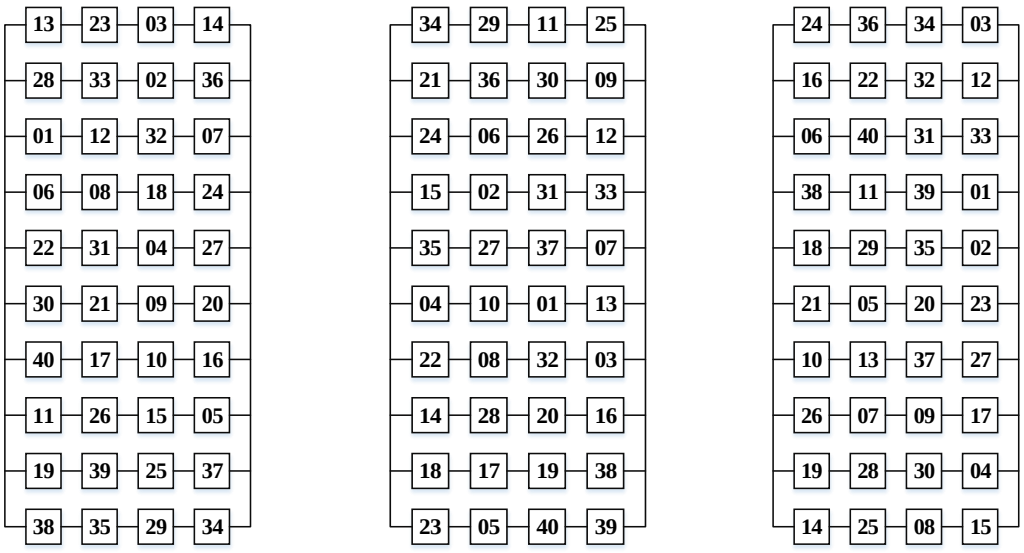

(a) RA (b) SCC (c) GA

Figure 2.24: PV modules are rearranged by three different techniques (a) RA (b) SCC (c) GA for the 400 W array with 10×4 dimension

Table 2.13: MML Obtained by Simulation for Aged PV Arrays

Rated array power (W)	Array size	MML in PV arrays for three techniques		
		MML_{RA} (%)	MML_{SCC} (%)	MML_{GA} (%)
400	2×20	3.983	3.293	1.63
	4×10	4.931	3.986	1.682
	5×8	4.765	3.462	1.705
	20×2	5.476	4.659	2.143
	10×4	5.642	3.701	1.657
	8×5	5.680	4.213	1.616
	Avg.	5.079	3.885	1.738
1.6k	2×20	6.986	5.746	3.098
	4×10	7.300	3.876	2.202
	5×8	6.998	4.129	1.462
	20×2	6.130	3.733	2.492
	10×4	7.059	4.234	1.678
	8×5	7.547	3.055	2.497
	Avg.	7.003	4.128	2.238
3.2k	2×20	4.426	3.953	2.549
	4×10	4.786	3.556	1.983
	5×8	4.828	3.002	2.325
	20×2	5.374	4.697	1.685
	10×4	5.455	2.660	2.023
	8×5	5.348	3.248	2.177
	Avg.	5.036	3.519	2.123
10k	2×20	3.033	2.509	1.279
	4×10	3.914	2.575	1.236
	5×8	4.172	2.366	1.244
	20×2	5.362	4.796	1.429
	10×4	5.099	2.653	1.173
	8×5	4.728	2.243	1.193
	Avg.	4.385	2.857	1.259

The MML for RA based technique (MML_{RA}), SCC based technique (MML_{SCC}) and GA based technique (MML_{GA}), are summarized in Table 2.13 for four arrays (400 W, 1.6 kW, 3.2 kW, and 10 kW); where the losses obtained by the GA based technique are consistently lower than both the RA and SCC based methods for all arrays. However, the losses caused by the SCC based rearrangement technique are regularly lower than RA technique. The minimum value of MML_{GA} is 1.173%, obtained by 10×4 dimension for the 10-kW array, while the amount of MML_{SCC} and MML_{RA} are 2.653% and 5.099% respectively. The average value of losses for four arrays are also calculated and tabulated in Table 3.2. Where the maximum average value is 7.003% for 1.6 kW

array obtained by RA method. While by the SCC and GA methods, the average values are 4.128% and 2.238% obtained for the same array. Hence, SCC and GA based rearrangement methods can reduce the maximum of 2.9% and 4.8% (average) losses respectively compared to RA method for the 1.6 kW aged array.

2.9 Comparative Analysis of MML in New and Aged PV Arrays

2.9.1 Case Study on 400 W PV Array

In this section a comparative analysis is made to investigate MML minimization by RA, SSC and GA based module rearrangement techniques using 400 W at three different aging condition. The aging times are 0-year, 2-years and 7-years where, 0-year means at new condition of 10 W PV modules in 400 W array. As mentioned earlier 0-year and 2-years aged modules are collected from ESPL. On the other hand, 7-years aged datasets are generated by adding the degradation factors of aged datasets from the work in [82]. The datasets of three different aging conditions are illustrate in Figure 2.25. Where it is clearly shown that with increasing the aging period the degradation of modules voltage and current are also increased.

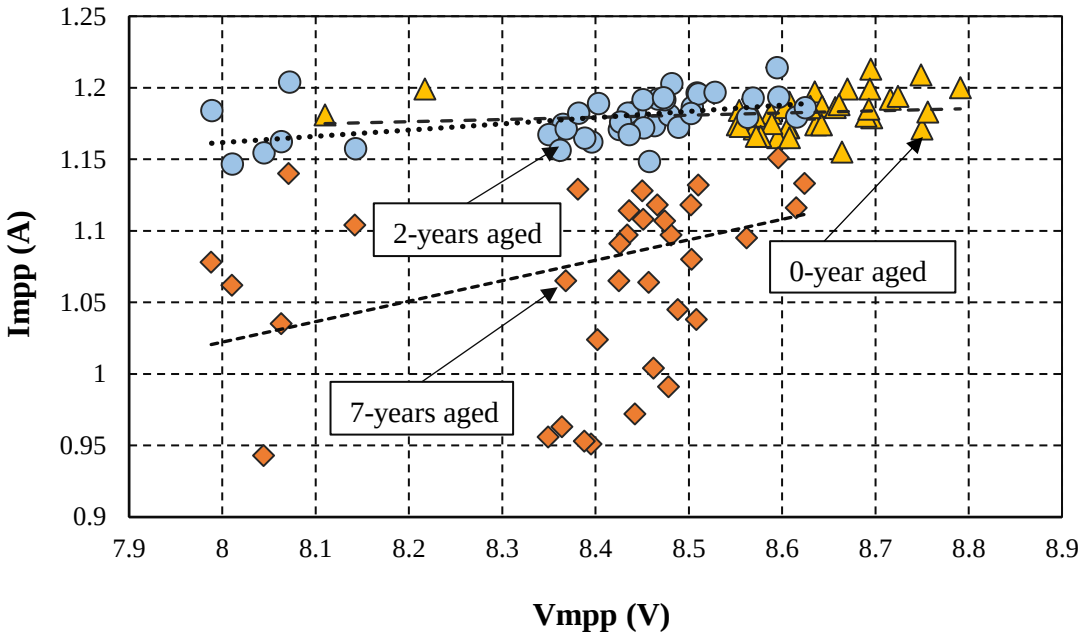

Figure 2.25: Dataset of 400 W array modules at three different aging condition: a) 0-year, b) 2-years and c) 7-years aged.

The array output power and % RE are tabulated in Table 3.3, for different dimensions of 400 W array at three different aging conditions. The array dimensions are (2×20, 4×10, 5×8, 20×2, 10×4 and 8×5) same for each aging conditions. The

average values of output power and %RE for each rearrangement methods are also tabulated in Table 2.14. At new condition the average output power is 402.137 W. While at 2 years and 7 years aged conditions the average output power is 389.791 W and 351.328 W respectively. Therefore, the average output power is higher at new condition of PV modules than aging conditions (2 and 7 years). The $\%RE_{SCC}$ is lower than $\%RE_{GA}$ for each array dimensions both at new and aged conditions. At new condition the average values of $\%RE_{SCC}$ and $\%RE_{GA}$ are 1.173% and 2.128% respectively. At 2 years of aged condition the values of %RE by SCC and GA methods are 1.259% and 3.522%, but at 7 years of aged condition the values are 10.58% and 11.701% respectively. Though the output powers are decreasing with aging of PV modules but the %RE are increasing. Figure 2.26 illustrate that for each array dimensions the %RE are considerably higher at 7 years of aging condition with respect to new and 2 years of aging.

Table 2.14: Output Power of 400 W Array Obtained by Simulation at different aging

PV modules aging period	Array size	400 W Array output power obtained by three different techniques			Recoverable energy	
		Po_RA (W)	*Po_SCC (W)*	*Po_GA (W)*	RE_{SCC} *(%)*	RE_{GA} *(%)*
0 year	2×20	396.659	398.341	402.067	0.424	1.363
	4×10	395.028	400.086	403.059	1.280	2.033
	5×8	394.340	400.228	403.785	1.493	2.395
	20×2	392.090	394.482	398.356	0.610	1.598
	10×4	391.648	397.598	402.729	1.519	2.829
	8×5	392.807	399.553	402.827	1.717	2.550
	Avg	393.762	398.381	**402.137**	1.173	**2.128**
2 years	2×20	380.89	383.63	390.21	0.719	2.446
	4×10	377.13	380.88	390.02	0.994	3.417
	5×8	377.79	382.96	389.93	1.368	3.213
	20×2	374.97	378.21	388.19	0.864	3.525
	10×4	374.31	382.01	390.12	2.057	4.223
	8×5	374.16	379.98	390.28	1.555	4.308
	Avg	376.541	381.278	**389.791**	1.259	**3.522**
7 years	2×20	314.288	342.738	346.928	8.301	9.408
	4×10	310.933	346.753	350.809	11.520	12.824
	5×8	309.923	348.447	352.687	12.430	13.798
	20×2	327.559	350.909	354.293	7.128	8.161
	10×4	314.372	349.783	355.580	11.264	13.108
	8×5	310.681	351.206	353.671	13.043	13.837
	Avg	314.626	347.806	**351.328**	10.580	**11.701**

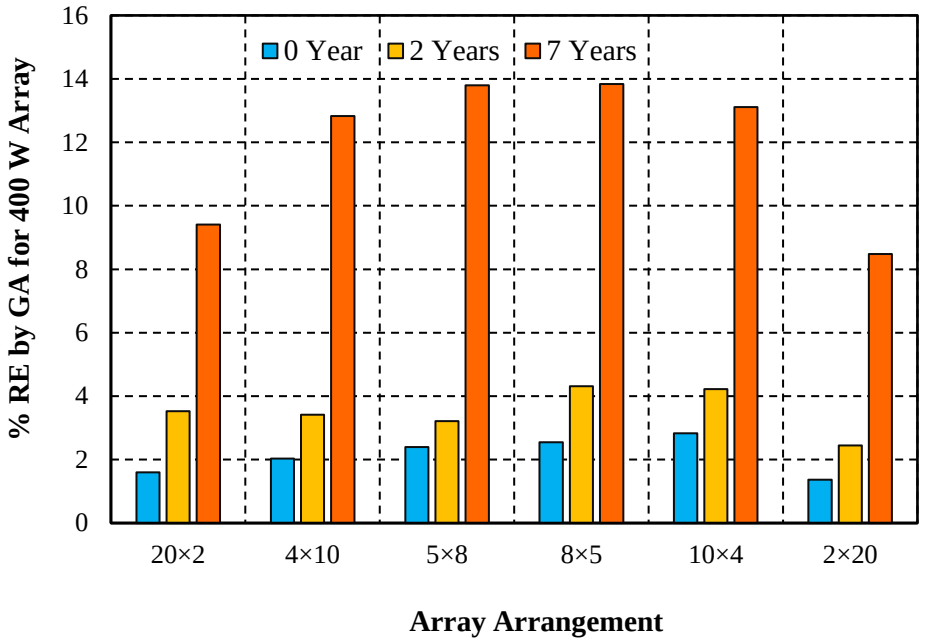

Figure 2.26: Comparison of %RE of 400 W array obtained at three different aging condition

Table 2.15: MML Obtained by Simulation for 400 W Array at Three Different Aging Conditions

PV modules aging period	Array size	MML in 400 W PV array for three techniques		
		MML_{RA} (%)	MML_{SCC} (%)	MML_{GA} (%)
0 year	2×20	2.697	2.284	1.370
	4×10	3.097	1.856	1.127
	5×8	3.266	1.821	0.949
	20×2	3.818	3.231	2.281
	10×4	3.926	2.467	1.208
	8×5	3.642	1.987	1.184
	Avg.	**3.408**	**2.274**	**1.353**
2 years	2×20	3.983	3.293	1.630
	4×10	4.931	3.986	1.682
	5×8	4.765	3.462	1.705
	20×2	5.476	4.659	2.143
	10×4	5.642	3.701	1.657
	8×5	5.680	4.213	1.616
	Avg.	**5.079**	**3.885**	**1.738**
7 years	2×20	13.534	5.707	4.555
	4×10	14.457	4.603	3.487
	5×8	14.735	4.137	2.970
	20×2	9.883	3.459	2.528
	10×4	13.517	3.769	2.174
	8×5	14.527	3.378	2.700
	Avg.	**13.441**	**4.313**	**3.344**

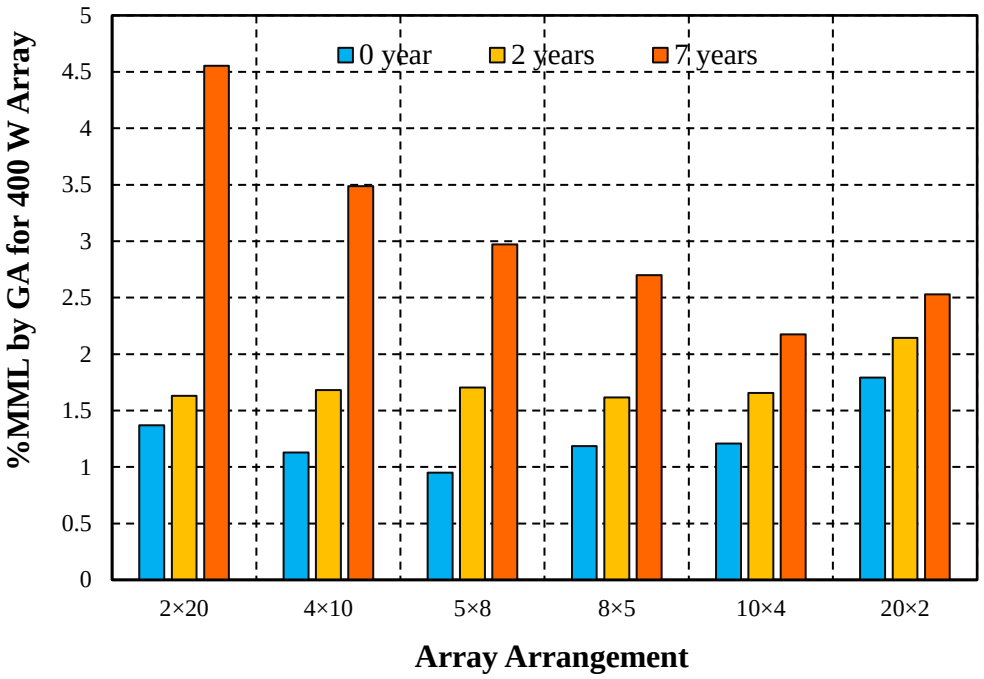

Figure 2.27: Comparison of %MML of 400 W array obtained at three different aging condition

The MML for RA based technique SCC based technique and GA based technique, are summarized in Table 3.2 for 400W array with three different aging conditions. The average value of losses is also calculated and tabulated in Table 2.15. At new condition the average value of MML_{GA} is 1.353%, while the amount of MML_{SCC} and MML_{RA} are 2.247% and 3.408% respectively. At 2 years of aged condition the average value of MML_{GA} is 1.738%, while the amount of MML_{SCC} and MML_{RA} are 3.885% and 5.079% respectively. At 7 years of aged condition the average value of MML_{GA} is 3.344%, while the amount of MML_{SCC} and MML_{RA} are 4.313% and 13.441% respectively. Where the average losses obtained by the GA based technique are consistently lower than both the RA and SCC based methods for each aging conditions. However, the average losses caused by the SCC based rearrangement technique are regularly lower than RA technique. Figure 2.27 illustrate the %MML obtained by GA based method using 400W array at three different aging conditions. Though for each array dimensions (2×20, 4×10, 5×8, 20×2, 10×4 and 8×5) %MML is increased with aging time period, but the values are depending on the array dimensions. At 7 years of aged condition the lowest %MML is (2.174%) obtained by 10×4 array while the highest %MML is (4.555%) obtained by 2×20 array dimension.

2.9.2 Case Study on 10 kW PV Array

In this subsection a comparative analysis is made to investigate MML minimization by RA, SSC and GA based module rearrangement techniques using 10 kW at three different aging condition. The aging times of 10 kW array modules are 0-year, 2-years and 7-years where, 0-year means at new condition of PV modules. Figure 2.28 shows the relation between Vmpp and Impp of the datasets at three different aging conditions. At new condition the modules are converged towards it trendline. While at 2-years aged condition the modules are scattered from it trendline and four modules are degraded more as a result they are located far away from the ideal location. At 7 years of aging condition the PV modules are scattered more from the trendline. It is clearly shown that with increasing the aging period the degradation of modules Vmpp and Impp are increased. The degradation rate of Vmpp is lower than the degradation rate of Impp.

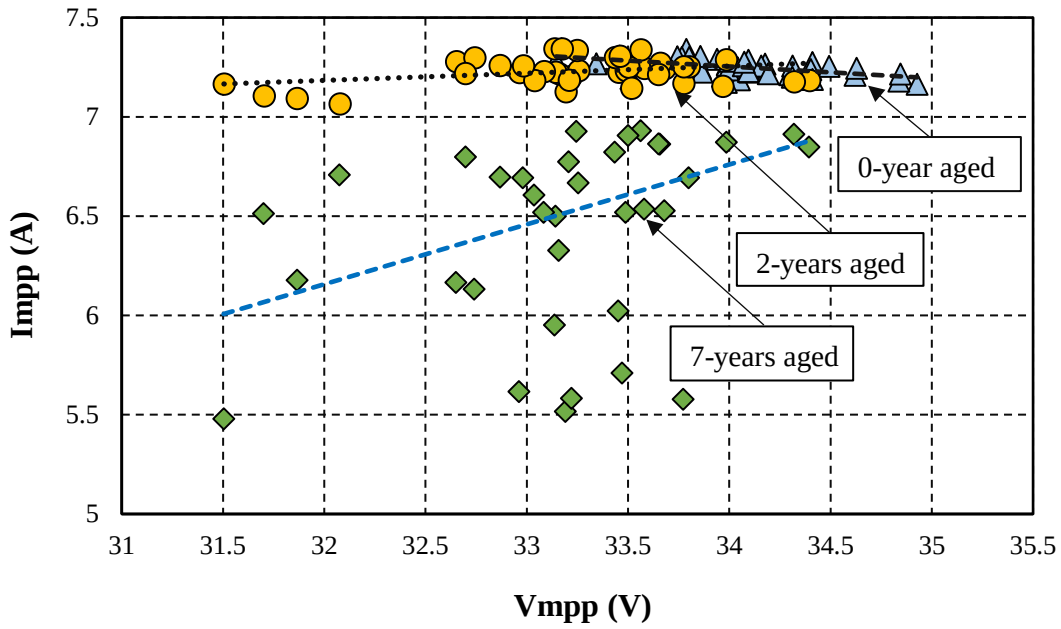

Figure 2.28: Dataset of 10 kW array modules at three different aging condition: a) 0-year, b) 2-years and c) 7-years aged.

The array output power and % RE are tabulated in Table 2.16, for different dimensions of 10 kW array at three different aging conditions. The array dimensions are (2×20, 4×10, 5×8, 20×2, 10×4 and 8×5) same for each aging conditions. The average values of output power and %RE for each rearrangement methods are also tabulated in Table 2.16. At new condition the average output power is 9816.41W obtained by GA based rearrangement. While by RA and SCC based methods the

average output powers are 9698.23W and 9724.37W respectively. At 2 years and 7 years aged conditions the average output power is 9488.81 W and 8353.38 W respectively generated by GA based rearrangement. Though the average output power obtained by SSC method is higher than RA based method but it is lower than GA based method both at 2-years and 7-years aged conditions. Therefore, at each aged condition GA performed better than SCC method with respect to array output power. On the other hand, at new condition the average values of $\%RE_{SCC}$ and $\%RE_{GA}$ are 0.269% and 1.218% respectively. At 2 years of aged condition the values of %RE by SCC and GA methods are 1.600% and 3.275 %, but at 7 years of aged condition the values are 12.748% and 14.192 % respectively. Though the output powers are decreasing with aging of PV modules but the %RE are increasing. Figure 2.29 illustrate that for each array dimensions the %RE are considerably higher at 7 years of aging condition with respect to new and 2 years of aging.

Table 2.16: Output Power of 10 kW Array Obtained by Simulation at different aging

PV modules aging period	Array size	10kW Array output power obtained by three different techniques			Recoverable energy	
		Po_RA (W)	*Po_SCC (W)*	*Po_GA (W)*	RE_{SCC} *(%)*	RE_{GA} *(%)*
0 year	2×20	9709.074	9758.63	9810.91	0.510	1.048
	4×10	9685.23	9732.18	9818.37	0.484	1.374
	5×8	9682.29	9709.94	9816.90	0.285	1.390
	20×2	9717.51	9718.27	9814.13	0.007	0.994
	10×4	9706.70	9712.06	9822.29	0.055	1.190
	8×5	9688.57	9715.17	9815.88	0.274	1.314
	Avg	9698.23	9724.37	**9816.41**	**0.269**	**1.218**
2 years	2×20	9318.31	9368.65	9486.88	0.540	1.809
	4×10	9233.64	9362.38	9490.99	1.394	2.787
	5×8	9208.88	9382.43	9490.28	1.884	3.055
	20×2	9094.49	9148.94	9472.47	0.598	4.156
	10×4	9119.77	9354.79	9497.11	2.577	4.137
	8×5	9155.43	9394.22	9495.16	2.608	3.710
	Avg	9188.42	9335.23	**9488.81**	**1.600**	**3.275**
7 years	2×20	7209.62	8002.13	8220.75	10.992	14.024
	4×10	7179.94	8226.71	8323.04	14.579	15.920
	5×8	7168.42	8269.21	8333.06	15.356	16.246
	20×2	7751.95	8320.89	8417.38	7.339	8.584
	10×4	7343.47	8356.21	8431.36	13.790	14.814
	8×5	7263.96	8312.66	8394.71	14.436	15.566
	Avg.	7319.56	8247.97	**8353.38**	**12.748**	**14.192**

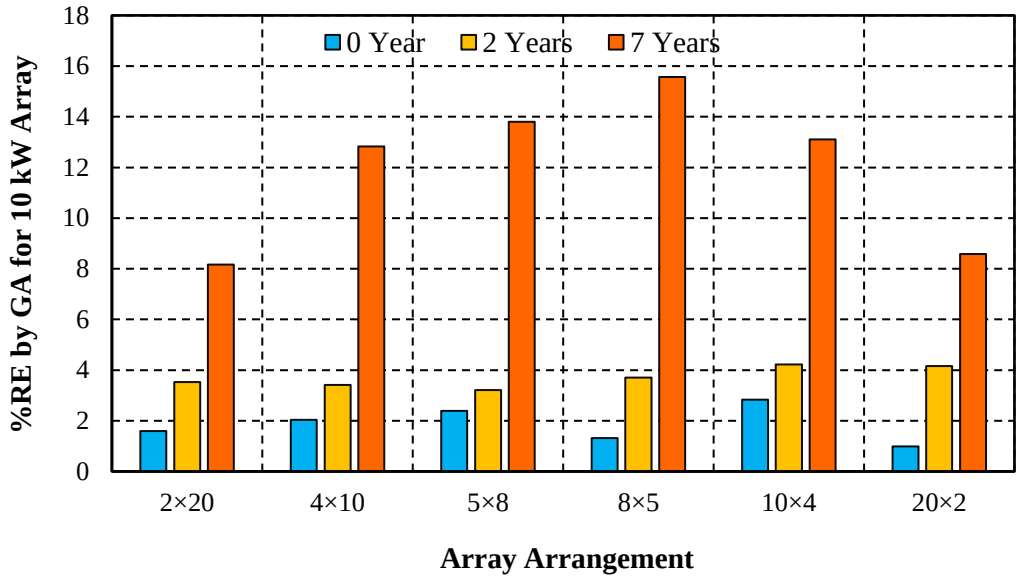

Figure 2.29: Comparison of %RE of 10 kW array obtained at three different aging condition

Table 2.17: MML Obtained by Simulation for 10 kW Array at Three Different Aging Conditions

PV modules aging period	Array size	MML in 10 kW PV array for three techniques		
		MML_{RA} (%)	MML_{SCC} (%)	MML_{GA} (%)
0 year	2×20	1.772	1.271	0.742
	4×10	2.013	1.538	0.666
	5×8	2.0433	1.763	0.681
	20×2	1.687	1.679	0.709
	10×4	1.796	1.742	0.627
	8×5	1.979	1.710	0.691
	Avg.	1.882	**1.617**	**0.686**
2 years	2×20	2.994	2.470	1.239
	4×10	3.875	2.535	1.196
	5×8	4.133	2.326	1.204
	20×2	5.324	4.757	1.389
	10×4	5.061	2.614	1.132
	8×5	4.689	2.204	1.153
	Avg.	4.346	**2.818**	**1.219**
7 years	2×20	16.447	7.262	4.729
	4×10	16.791	4.659	3.543
	5×8	16.924	4.167	3.427
	20×2	10.162	3.568	2.450
	10×4	14.895	3.159	2.288
	8×5	15.817	3.663	2.713
	Avg.	15.173	**4.413**	**3.192**

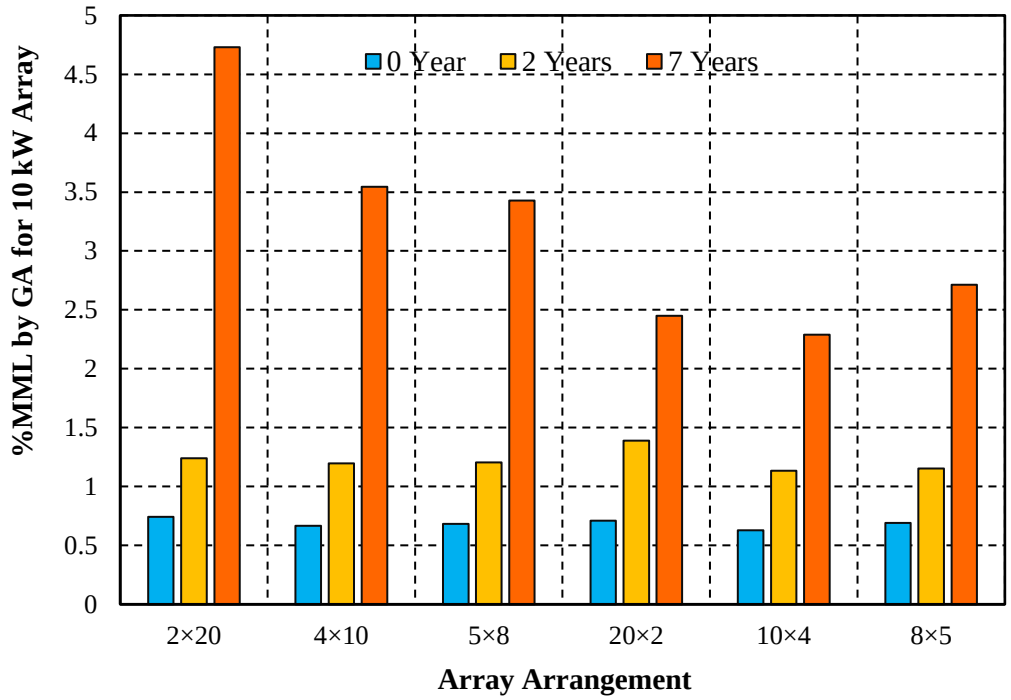

Figure 2.30: Comparison of %MML of 10 kW array obtained at three different aging condition

The MML for RA based technique, SCC based technique and GA based technique, are summarized in Table 2.17 for 10 kW array with three different aging conditions. The average value of losses is also calculated and tabulated in Table 2.16. At new condition the average value of MML_{GA} is 0.686%, while the amount of MML_{SCC} and MML_{RA} are 1.617% and 1.882% respectively. At 2 years of aged condition the average value of MML_{GA} is 1.219%, while the amount of MML_{SCC} and MML_{RA} are 2.818% and 4.346% respectively. At 7 years of aged condition the average value of MML_{GA} is 3.192%, while the amount of MML_{SCC} and MML_{RA} are 4.413% and 15.173% respectively. Where the average losses obtained by the GA based technique are consistently lower than both the RA and SCC based methods for each aging conditions. However, the average losses caused by the SCC based rearrangement technique are regularly lower than RA technique. Figure 2.30 illustrate the %MML obtained by GA based method using 10 kW array at three different aging conditions. Though for each array dimensions (2×20, 4×10, 5×8, 20×2, 10×4 and 8×5) %MML is increased with aging time period, but the values are depending on the array dimensions. At 7 years of aged condition the lowest %MML is (2.288%) obtained by 10×4 array while the highest %MML is (4.729%) obtained by 2×20 array dimension.

2.10 Experimental Work on 400 W Aged PV Array

The experiments are carried to validate the simulation results. The implementation of the proposed rearrangement techniques (GA, SCC, and RA) has been carried out in the following way. Firstly, the position of the PV modules is determined for a specific array dimension for each of the rearrangement techniques by simulation. Then, the array has been constructed practically by connecting the modules according to the simulation result. The output characteristics of the PV array are measured using the PV system analyzer (PVSA). Finally, the numerical data of output characteristics of the PV arrays are extracted from the analyzer using the software of PVSA. The same procedure is adopted for GA, SCC, and RA techniques.

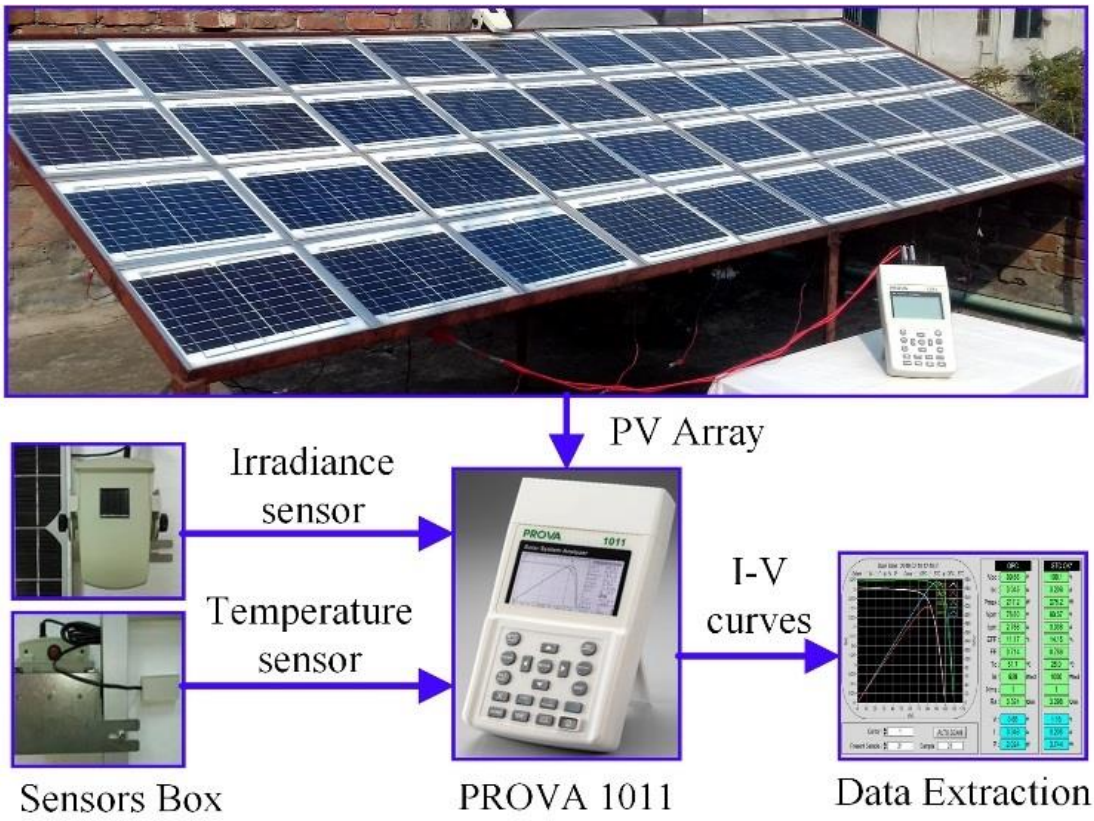

Figure 2.31: Experimental Setup of a 400 W PV array of two years aged

2.10.1 Experimental Setup of Aged PV Array

A 400 W PV array is mounted on a rooftop. The geographical location of latitude is 23°43'N and longitude is 90°25'E, where direct sunlight is available during the daytime. The PV array consists of 40 modules (polycrystalline) of two years aged.

The electrical characteristics of a single PV module and the array used in the experimental work are reported in Table 2.18. The experimental setup is shown in Figure 2.31. Here, the output characteristics (*I-V* and *P-V* curves) of the PV array are extracted using a PVSA (PROVA-1011). An irradiance sensor and temperature sensors are integrated with the measuring device, PROVA-1011 by Bluetooth communication to accomplish the measurement. PROVA-1011 can measure and store the output characteristics of the PV array in real meteorological conditions during the middle of a sunny day and clear sky. Modules rearrangement process takes 10 minutes while a single test by PROVA-1011 takes about a minute, maintaining standard test conditions at outdoor. According to IEC 60904-1 standards, during *I-V* curve measurement at outdoor, the irradiance should be at least 800 W/m^2. Hence, the experimental data are recorded within the irradiance ranges (800 to 950) W/m^2.

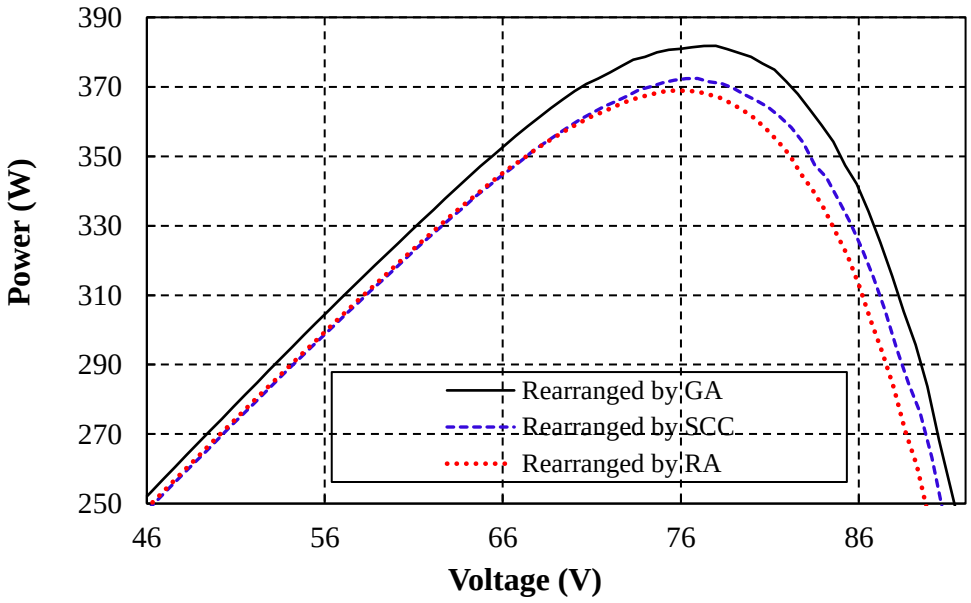

Figure 2.32: *P-V* characteristics curves obtained by experimental work using three different techniques (a) RA (b) SCC and (c) GA for 4×10 array dimension

2.10.2 Analysis of Experimental Results

The comparative analysis is made using a 400 W array with four (4×10, 5×8, 10×4, and 8×5) different SP-PV array dimensions. In a 4×10 SP-PV array, there are 4 PV strings and 10 PV modules in each string. The array output characteristic (*P-V*) curves are measured by the PROVA-1011 and illustrated in Figure 2.32 for three rearrangement techniques. Here, the array output (peak) power 381.8 W and 372.4 W are obtained by GA and SCC based rearrangement techniques, respectively, while

368.9 W is achieved by the RA based method. Hence, the output power improvements are 3.49% and 0.95% obtained by GA and SCC based methods, respectively. The GA based module rearrangement technique significantly improves output power. The similar analysis is also repeated for 5×8, 10×4, and 8×5 array dimensions. The output power in three methods and corresponding %RE are quantified and summarized in Table 2.19. As can be noted, the output power enhancement is achieved by the GA based rearrangement is higher in all the cases. The maximum value of $\%RE_{GA}$ is 4.67% for the 8×5 array. For the same array, $\%RE_{SCC}$ is only 1.69%. Generally speaking, the GA based rearrangement technique shows robustness to maximize the output power for any array dimensions.

Table 2.18: Electrical Features of the PV Module and Array for the Experimental Work

Specifications	Voc (V)	Isc (A)	Vmpp (V)	Impp (A)	Pmpp (W)
PV Module	10.39	1.31	8.41	1.18	9.92
PV Array (4×10)	103.83	5.24	84.04	4.72	396.67

Table 2.19: Array Output Power and Recoverable Energy Obtained by Experimental Work for 400W Aged PV Array

Array Size	Array output power obtained by three different techniques			Recoverable Energy	
	Po_RA (W)	Po_SCC (W)	Po_GA (W)	RE_{SCC} (%)	RE_{GA} (%)
4×10	368.90	372.40	381.80	0.95	3.49
5×8	367.06	373.31	378.74	1.70	3.18
10×4	365.42	374.50	380.64	2.48	4.16
8×5	364.73	370.91	381.78	1.69	4.67

Table 2.20: Comparison of Average Recoverable Energy between Simulation and Experimental Works using 400W Aged PV Array

Rearrangement methods	Average Recoverable Energy (%)		ΔRE_{AVG} (%)
	Simulation	Experimental	
SCC based	1.487	1.705	0.21
GA based	3.785	3.875	0.09

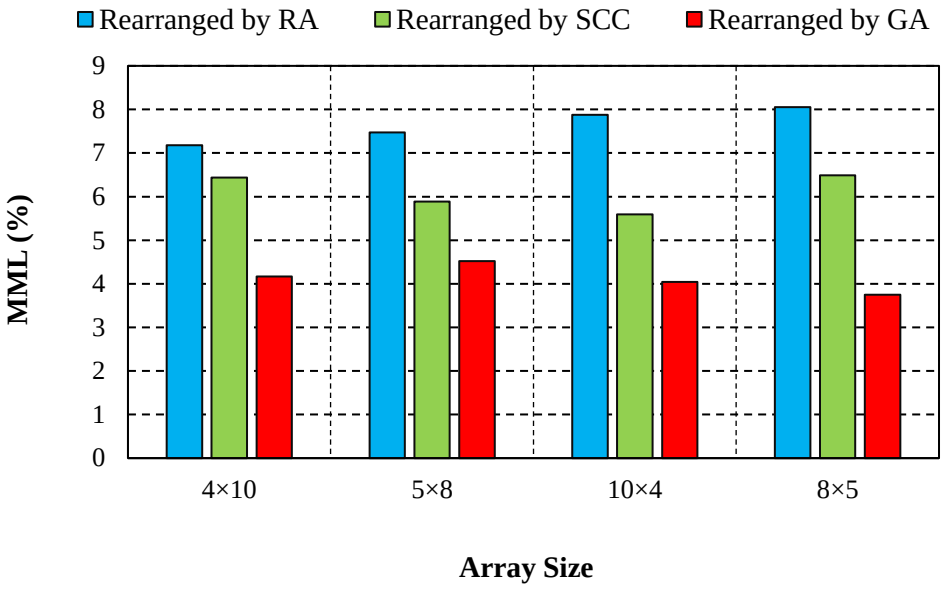

Figure 2.33: Comparison of MML obtained by experimental work using three different methods (a) RA (b) SCC (c) GA for the 400 W array

Figure 2.33 summarizes the MML% values of the four array dimensions obtained by RA, SCC, and GA in the inspected PV array. It shows that GA based rearrangement provides lower losses compared with the other two rearrangement approaches. Also, it can be noticed that SCC based rearrangement performs batter in minimizing MML% than RA. Furthermore, by comparing the array dimensions, the minimum value of MML_{GA} is 3.75% obtained in the 8×5 array, while for the SCC technique, the minimum MML_{SSC} is 5.59% in a 10×4 array. The above experimental results show the superiority of GA based method over others, and the similar results obtained from the simulation presented earlier.

The average values of $\%RE_{SCC}$ and $\%RE_{GA}$ for 4×10, 5×8, 10×4, and 8×5 arrays from both simulation and experimental works are summarized in Table 2.20. The mismatch of %RE (ΔRE_{AVG}) between the experimental and simulation works is calculated using equation (2.30).

$$\Delta RE_{AVG} = \left|\%RE_{Simulation} - \%RE_{Experimental}\right| \tag{2.30}$$

The ΔRE_{AVG} for SCC and GA based techniques are 0.21% and 0.09%, respectively which validate the effectiveness of the work.

2.10.3 Summary on MML Minimization of Aged PV Arrays

In this chapter, both SSC and GA based rearrangement techniques of aged PV modules are compared with a random arrangement technique in terms of array output power and mismatch losses. Simulation results show that GA and SCC based techniques reduce a maximum of 4.8% and 2.9% (average) losses, respectively compared to RA technique using a 1.6 kW two years aged array. The experimental investigation shows that the GA and SCC based techniques yield a maximum percentage of recoverable energy (%RE) of 4.67% and 1.69%, respectively for two years aged 8×5 array. Additionally, the simulation shows that the GA based rearrangement technique for MML% reduction shows superiority for both small and large-size aged PV arrays with different dimensions. To the best of the authors' knowledge, this is the first time that the influences of rearrangement techniques to minimize MML% in real aged SP-PV array configurations are compared experimentally. The GA based optimal rearrangement technique presented in this chapter can be applied to offline aged PV arrays of any size or dimension.

CHAPTER 3

MML Minimization in Aged PV Arrays Using Optimal Configuration

In the previous chapter 2, MML reduction techniques are investigated for both new and aged PV array using different size of series-parallel (SP) configuration. Where, the results show that MML minimization for differently aged PV arrays is beneficial for energy maximization. However, to extract maximum power by minimizing MML, different standard and hybrid PV array configurations had gain popularity at non-uniform irradiance condition not for aging. Therefore, in chapter 3, both indoor and outdoor experimental investigations are carried out for MML minimization in aged PV arrays using different array configurations. At first, MML minimization is investigated at indoor condition for 4×6 PV array modules of two years aged using four standard array configurations. After that, different standard and hybrid array configurations are investigated at outdoor weather condition using a nonuniformly aged 4×10 PV array.

3.1 Experimental Investigation at Indoor Test Condition

In order to extract the maximum power from the 4×6 aged PV array, the significance of four different standard array configurations is experimentally investigated in the laboratory. In addition, three different module rearrangement techniques are also investigated for each array configurations. Therefore, a 14.4 W PV array is used in this chapter. Where, the PV array contains 24 PV aged modules of 0.6 W are connected in a 4×6 array arrangement. These 24 PV modules are two years of aged and collected from a solar lantern manufacturing company. After that, these modules are tested by a PV System Analyzer to get their datasets with electrical characteristics. Hence, these datasets are used to rearrange the PV modules according to the rearrangement techniques. Finally, the significance of four standard PV array configurations (SP, TCT, BL, and HC) is investigated experimentally applying all these three rearrangement techniques for the 4×6 aged PV array and their output powers are compared accordingly. The step by step procedures is described in the following sub-sections.

3.1.1 Dataset of 4×6 Array Modules

In this chapter, 24 polycrystalline PV modules of two years aged are tested by a PV System Analyzer. Where, the PV modules are tested at STC (25°C, 1000 W/m2, AM 1.5G) according to the IEC 60904-1 standard [74]. The verified data have been tabulated in Table 3.1; which contains the value of electrical characteristics of Voc, Isc, Pm, Vm and Im for each PV modules. According to the datasets some modules power is highly degraded, where the current is decreased significantly with respect to the voltage.

Table 3.1: A Dataset of Two Years Aged 24 PV Modules

PV No	Electrical Characteristics of Two Years Aged PV Modules				
	Voc *(V)*	*Isc* *(A)*	*Vm* *(V)*	*Im* *(A)*	*Pm* *(W)*
1	2.92	0.08	2.394	0.073	0.175
2	2.80	0.14	2.296	0.128	0.294
3	2.81	0.23	2.304	0.211	0.486
4	2.85	0.25	2.337	0.230	0.538
5	2.89	0.25	2.369	0.230	0.545
6	2.75	0.27	2.255	0.248	0.559
7	2.78	0.27	2.279	0.248	0.565
. . .	. . .	. . .	. . .	. . .	. . .
23	2.97	0.28	2.435	0.257	0.626
24	3.00	0.28	2.460	0.257	0.632

3.1.2 Conventional PV Array Configurations

The well-known PV array configurations are SP, TCT, BL, and HC are mostly used for the new PV array arrangement purpose. In this chapter, these PV array configurations are used to analyze the rearrangement techniques for aged PV array with respect to output power. The connection diagram is shown in Figure 3.1 (a), (b), (c) and (d) of SP, TCT, BL, and HC array configurations, respectively.

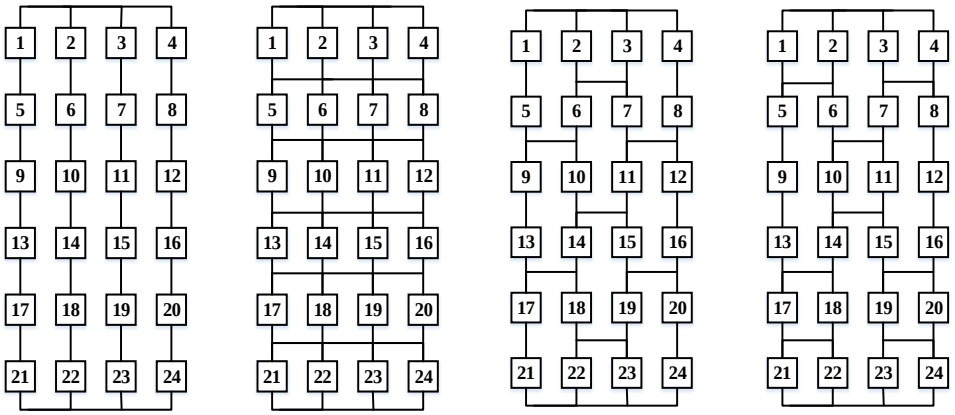

(a) (b) (c) (d)

Figure 3.1: 4x6 Array configurations: (a) SP; (b) TCT; (c) BL; (d) HC

3.1.3 PV Module Rearrangement Techniques

The work in [28, 85], developed the current based and voltage based module rearrangement techniques for different PV array configurations. In this chapter, aged PV array modules are rearranged by using three different techniques: i) Random method; ii) Im based method; iii) Vm based method. In order to explain the methods, let consider, 24 PV modules are connected in a 4×6 (column × row) array, and their positions are numbered by 1, 2, and 3 up to 24. Figure 3.2(a) shows the modules position are determined by a Random method which is a conventional technique of module arrangement usually used for the newly installed PV array and remain unchanged until any severe damage or fault occurs in the array.

1	2	3	4
5	10	11	12
6	13	14	15
7	16	17	18
8	19	20	21
9	22	23	24

(a)

1	12	13	24
2	11	14	23
3	10	15	22
4	9	16	21
5	8	17	20
6	7	18	19

(b)

1	19	7	13
24	6	18	12
2	20	8	14
23	5	17	11
3	21	9	15
22	4	16	10

(c)

Figure 3.2: 4×6 PV array rearrangement techniques (a) Random method;

(b) Im based method; (c) Vm based method

Figure 3.2(b) shows the modules position determined by Im based method. In this method, all 24 modules are sorted in ascending order by their MPP current Im. Hence, the module in position 1 contains the lowest current and the module in position 24 contain the highest current. According to this technique, the current will increase from the first column to the fourth column, actually here increase the parallel brunch currents means array currents increases; thus, output power also increases. Figure 3.2(c) shows the module positions are determined by Vm based method. In this method, the sorting of 24 modules has been done from lower values to higher values of Vm; as a result, module position1 contains the lowest value of Vm while module position 24 is the highest one. In this technique, the parallel connected modules are operated almost in the same average voltages, thus reduces mismatch voltage loss and output power increases accordingly.

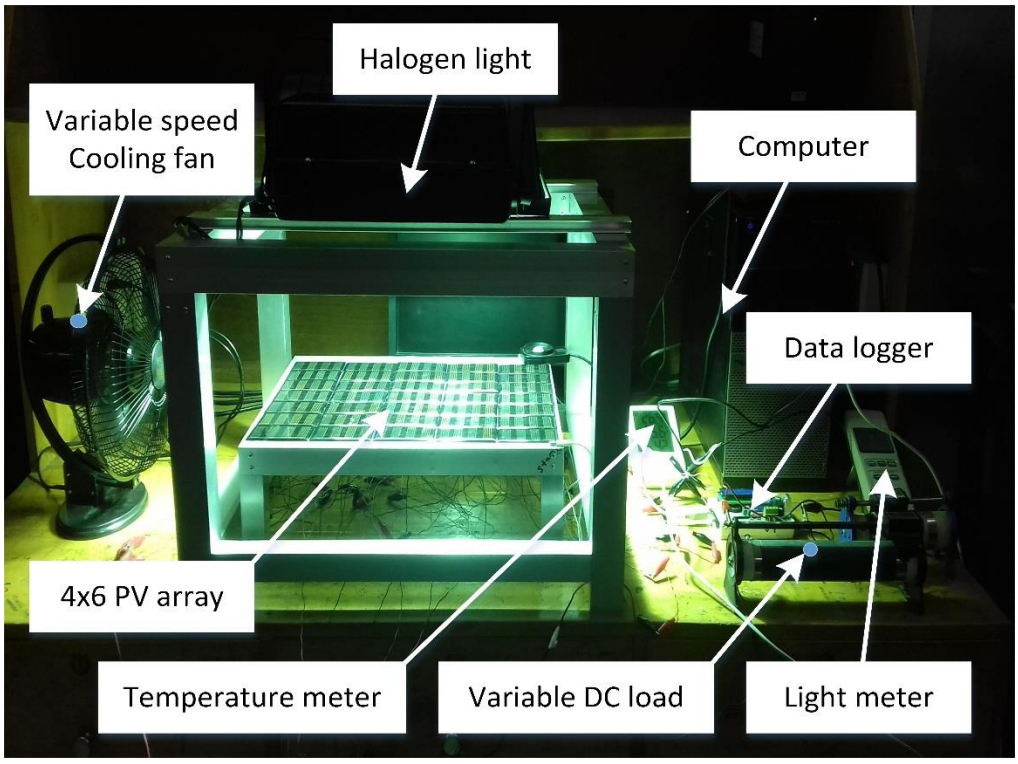

Figure 3.3 (a): Experimental setup during the measurement of the output power of a 4×6 PV array for SP, TCT, BL, and HC configurations.

3.1.4 Experimental Procedure

In this section, the experimental procedure is described for the measurement of *I-V* and *P-V* characteristics of 4×6 aged PV array configurations at indoor test condition. The experimental setup during the test and after the test are shown in Figure 3.3 (a) and Figure 3.3 (b) respectively. The PV array modules are placed on an

aluminum frame, with electrical isolation using double sided Sellotape and a 1000W halogen bulb is mounted parallel to the PV modules using another aluminum frame. The measurement of light is done by a light meter LX-1102, and temperature are measured by using TA298. The input light intensity for the modules is fixed in 350 lux, which is almost one third on the full sun irradiance (1000 Wm^{-2}) since the distance between the light source and modules remain constant. The laboratory room temperature is 25ºC has been maintained using an air conditioner. All practical data measurements of the PV array configurations are carried out according to the standard test conditions are described in [79].

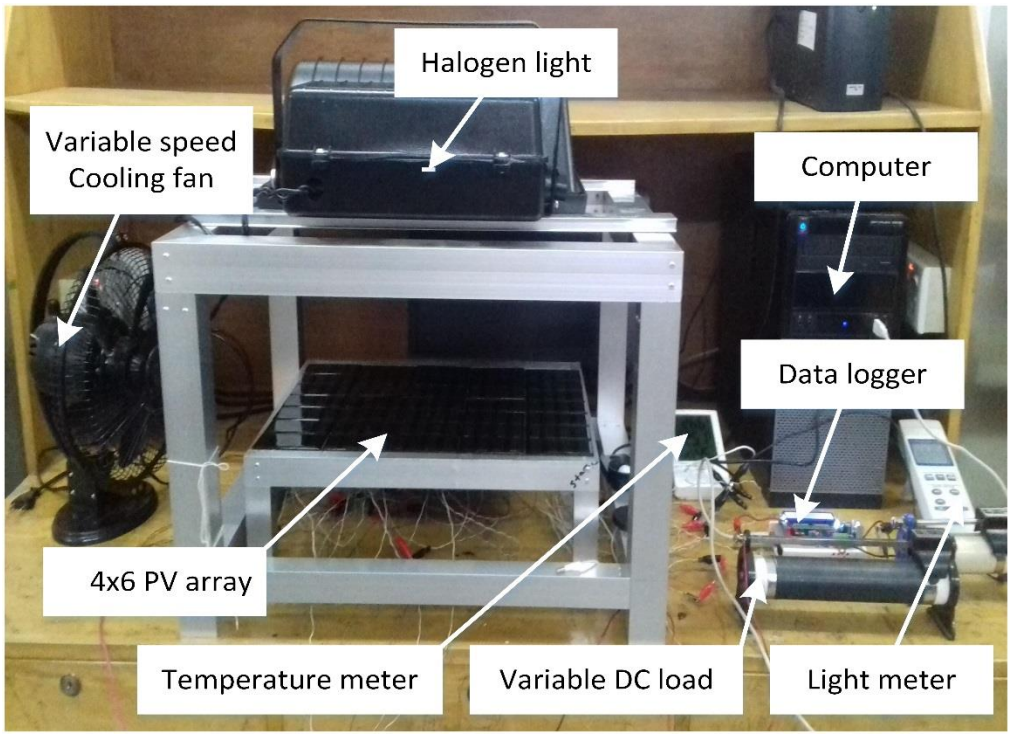

Figure 3.3(b): Experimental setup after the measurement of the output power of a 4×6 PV array for SP, TCT, BL, and HC configurations.

A single test for *I-V* characteristics measurement of the PV array is carried out by less than a minute, and real-time electrical data of output current and its corresponding voltage are recorded in a memory card of the data logger. During a single test, the PV module temperature has been increased maximum 1ºC, and a variable speed cooling fan is used to reduce the temperature of the PV modules. After completion of each test five minutes interval is required to get the module temperature 25ºC using the cooling fan. In addition, a single test is repeated five times for each

array configuration to get more accurate *I-V* curves. After a daylong experimental investigation, the output array power for all four array configurations has been tested and recorded using all three techniques.

3.1.5 Experimental Results at Indoor

Table 3.2 shows that the 4x6 array electrical characteristics mean array voltage, array current, and, array power is obtained by using the random module arrangement technique for four array configurations. The maximum output power, 5.214 W is generated by HC configuration, and the minimum power 4.377 W is generated by SP configuration. Though the array voltage is higher in SP configuration because of the lower array current its output power becomes lower. However, the current is dominating the output power. Hence, in TCT, BL, and HC, the array voltages are the same, but the currents are different. The highest current is generating by HC. Therefore, the highest power is also obtained by HC configuration.

Table 3.2: Array Output Obtained by Random Based Method

Array Configurations	**Array Outputs Obtained by Random Method**		
	Voltage (V)	***Current (A)***	***Power (W)***
SP	11.948	0.366	4.377
TCT	11.457	0.433	4.960
BL	11.457	0.448	5.130
HC	11.457	0.455	5.214

Table 3.3: Array Output Obtained by Im Based Method

Array Configurations	**Array Outputs Obtained by Im Based Method**		
	Voltage (V)	***Current (A)***	***Power (W)***
SP	10.911	0.455	4.966
TCT	10.911	0.525	5.733
BL	10.911	0.533	5.814
HC	11.457	0.511	5.850

Table 3.4: Array Output Obtained by Vm Based Method

Array Configurations	**Array Outputs Obtained by Vm Based Method**		
	Voltage (V)	***Current (A)***	***Power (W)***
SP	10.366	0.437	4.526
TCT	10.366	0.522	5.408
BL	10.366	0.537	5.561
HC	10.911	0.503	5.561

The Im based module rearrangement technique is also applied in 4x6 arrays for SP, TCT, BL and HC configurations. The output results are presented in Table 3.3. The maximum output power is 5.85W, and the minimum power is 4.966 W obtained by HC and SP configurations respectively. For SP, TCT, and BL the output voltages are same, but the currents are not, they are dominating the power outputs. Therefore, the higher power 5.814 W is obtained at BL configuration because of the higher output current. However, HC configuration is generating the highest output power for its higher output voltages.

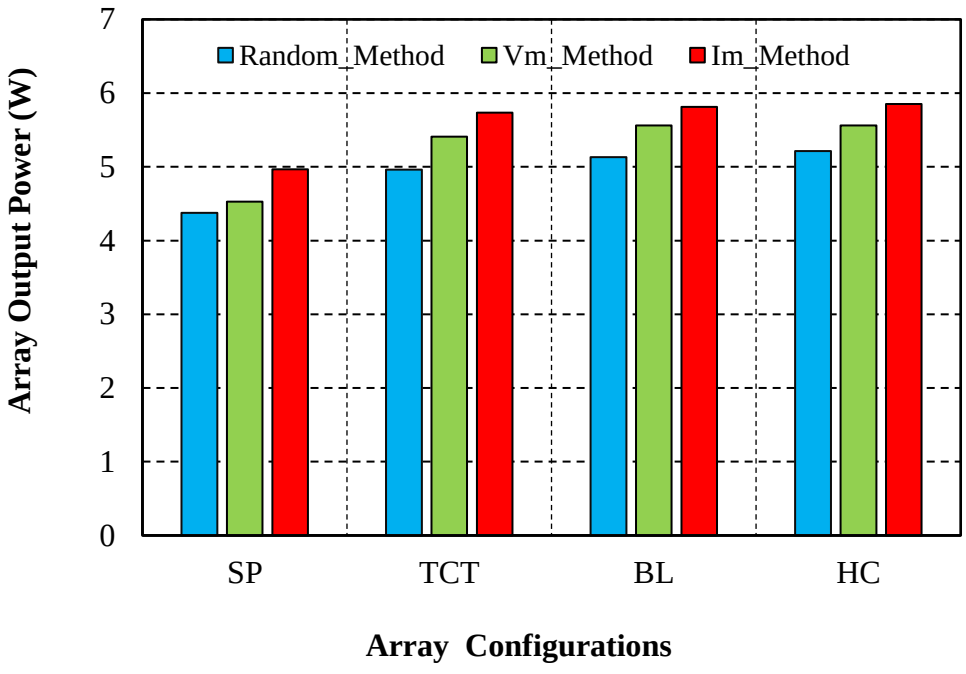

Figure 3.4: Comparison of power outputs between SP, TCT, BL and HC configurations

Table 3.4 shows the output results, which are obtained by using Vm based module arrangement technique. It can be seen the lower output is 4.526 W obtained by SP array configurations and the higher output power 5.611 W obtained by both BL and HC configuration. The comparative analysis is illustrated in figure 3.4. The HC configuration is performed better than SP, TCT, and BL with respect to output power. Another significance of HC configuration is that its output voltage is higher both in Im and Vm based techniques. Finally, the current based technique is performed better than the voltage-based technique for all four array configurations.

3.1.6 Summary on Indoor Test

In this chapter, a comparative analysis of aged PV module rearrangement techniques is analyzed for SP, TCT, BL, and HC configurations to extract the maximum array output power. One of the main contributions of the paper illustrates that the Im based technique is performed better for all array configurations with respect to array output power. Additionally, it is observed that TCT, BL, and HC configurations are outperformed than SP configuration. Besides, BL performed better than TCT configuration. Finally, HC configuration is recommended as the best configuration among the standard array configurations for the aged PV array.

3.2 Experimental Investigation at Outdoor Test Condition

In order to extract higher output power from a PV array with modules at mismatch condition, array configurations can play an important role. In the previous section 3.1, the conventional array configurations such as series-parallel (SP), total cross tied (TCT), bridge-linked (BL), honey-combed (HC), ladder-diagram (LD) have been investigated experimentally in indoor weather condition, for a 4x6 aged PV array. Therefore, to validate the indoor test the standard array configurations are tested again in the outdoor real weather condition is one of the objectives of this section. According to the literature, hybrid array configurations are investigated for PV array at shading condition not for aging. Therefore, investigation of different hybrid array configurations for an aged PV array and compared them with standard array configurations is another objective of this chapter 3. Moreover, some novel PV array configurations are proposed and their performance are compared with conventional array configurations using an artificial nonuniformly aged 4×10 PV array.

3.2.1 Conventional and Proposed Array Configurations

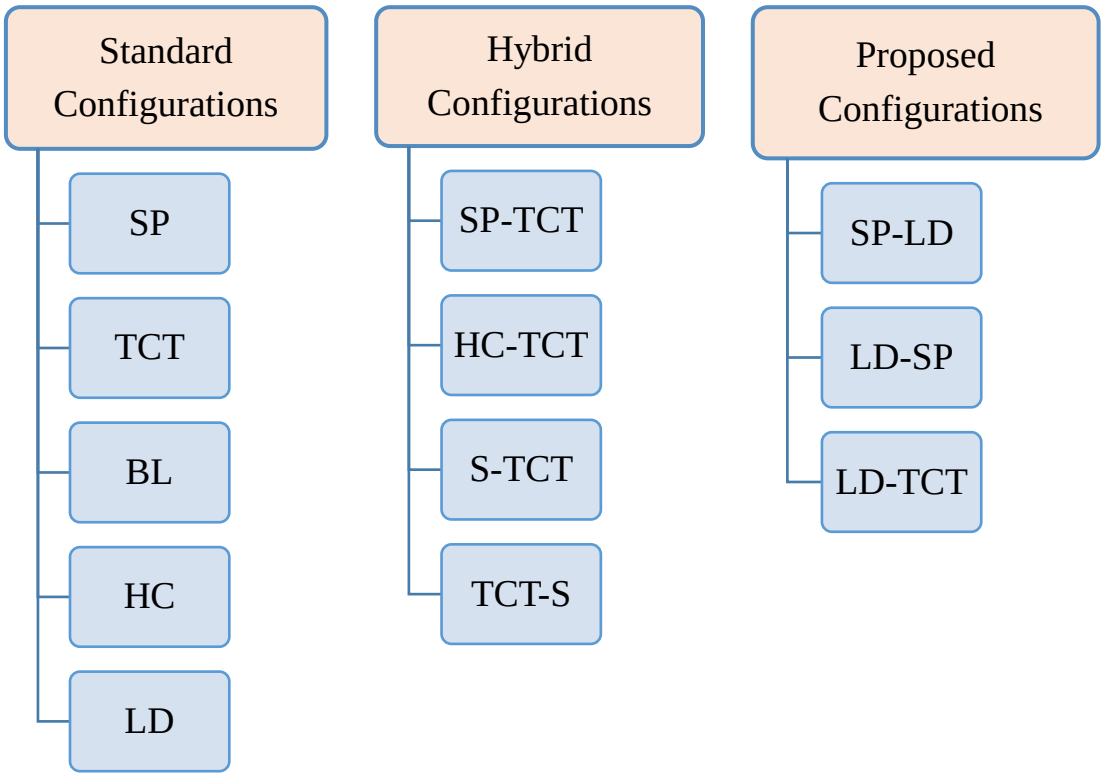

Fig. 3.5. Standard, hybrid and proposed configurations of PV array modules

Figure 3.5 shows standard, hybrid and proposed array configurations, which are investigated in this chapter. The standard (conventional) array configurations are: (a) SP (series-parallel), (b) TCT (total-cross-tied), (c) BL (bridge-linked), (d) HC (honey-combed) and (e) LD (ladder-diagram). The hybrid array configurations are: (f) SP-TCT (series-parallel and total-cross-tied), (g) HC-TCT (honey-combed and total-cross-tied), (h) S-TCT (series and total-cross-tied) and (i) TCT-S (total-cross-tied and series). The proposed array configurations are: (j) SP-LD (series-parallel and ladder-diagram), (k) LD-SP (ladder-diagram and series-parallel) and (l) LD-TCT (ladder-diagram and total-cross-tied). The connection diagram of the above-mentioned PV array configurations is shown in Figure 3.6 (a)-(l).

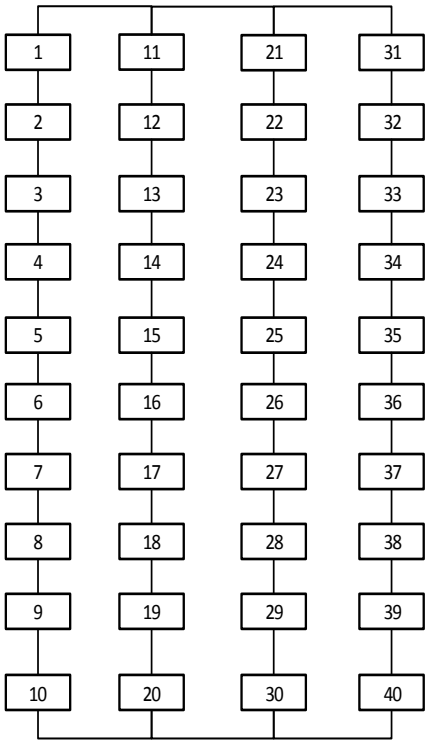

(a) SP configuration

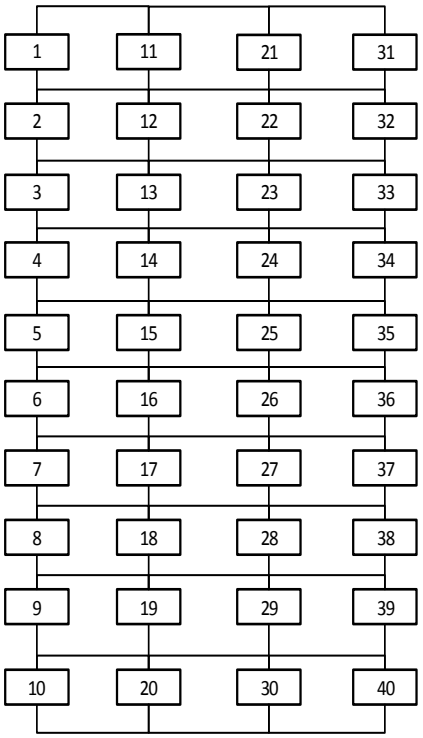

(b) TCT configuration

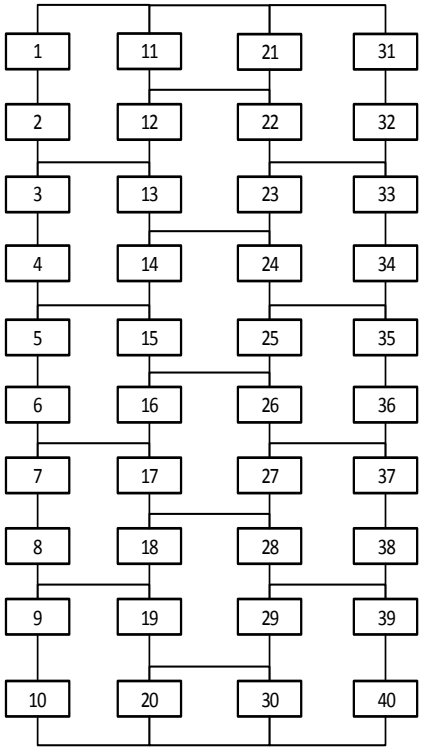

(c) BL configuration

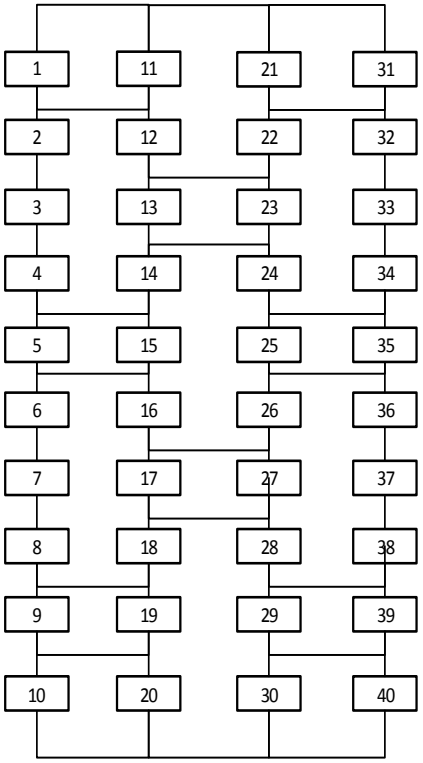

(d) HC configuration

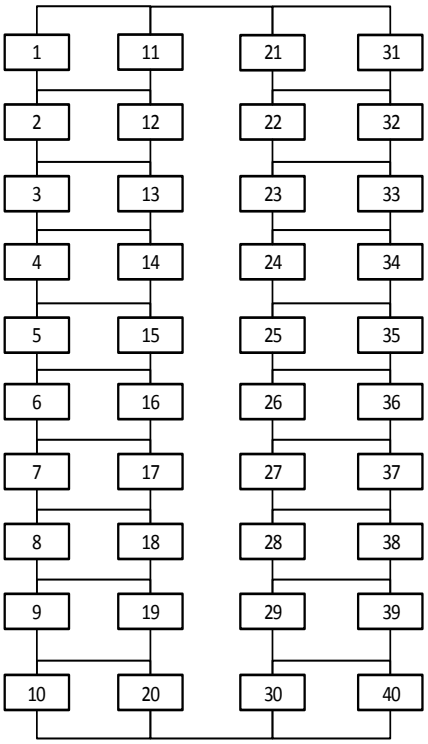

(e) LD configuration

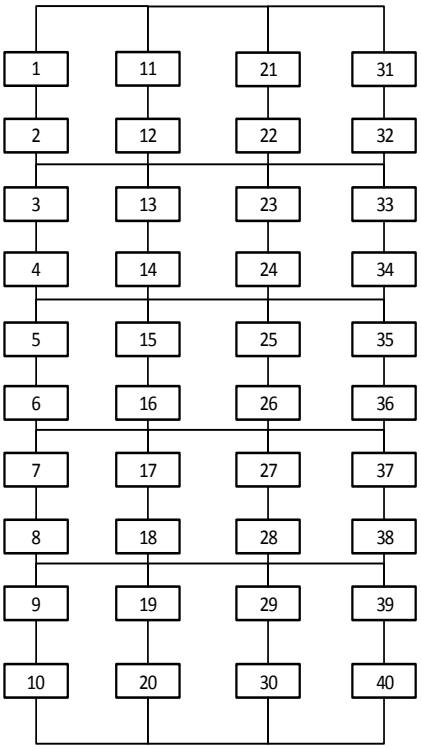

(f) SP-TCT configuration

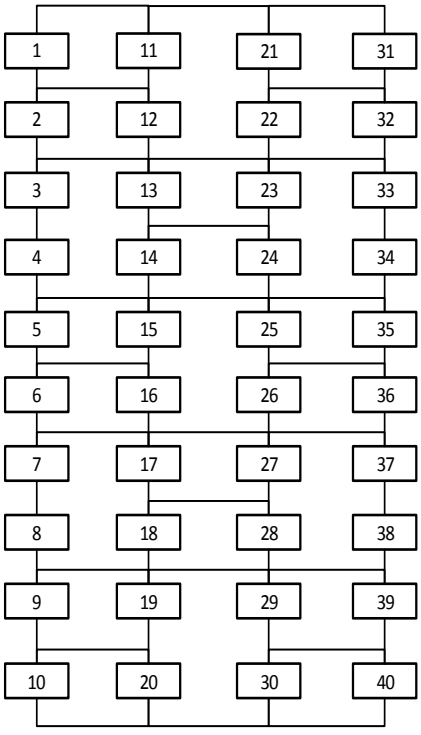

(g) HC-TCT configuration

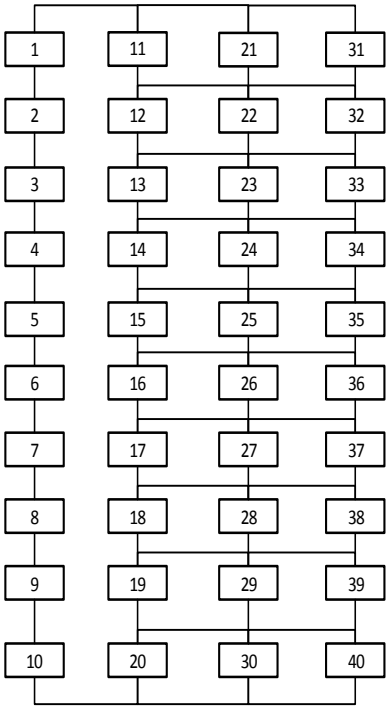

(h) S-TCT configuration

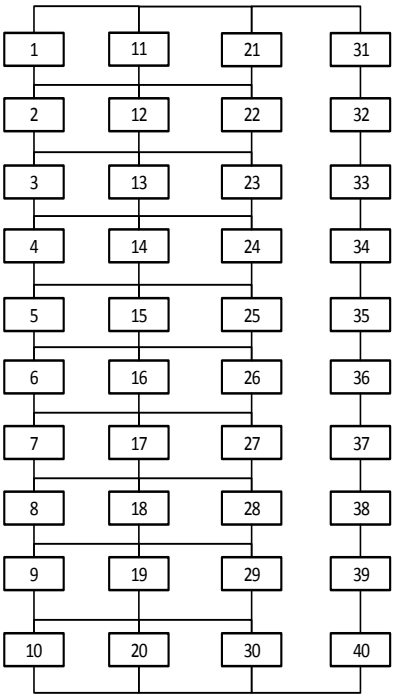

(i) TCT-S configuration

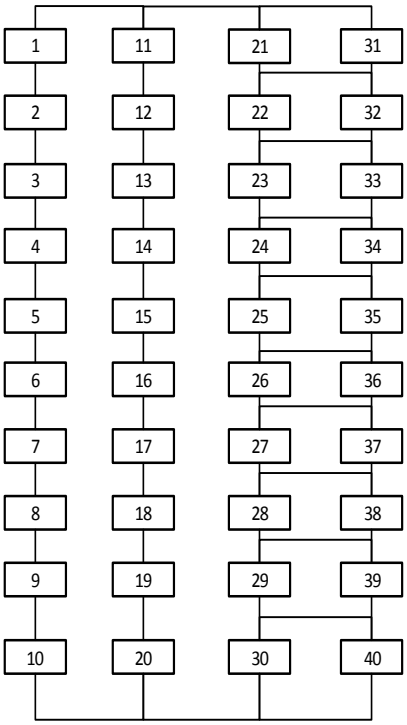

(j) SP-LD configuration

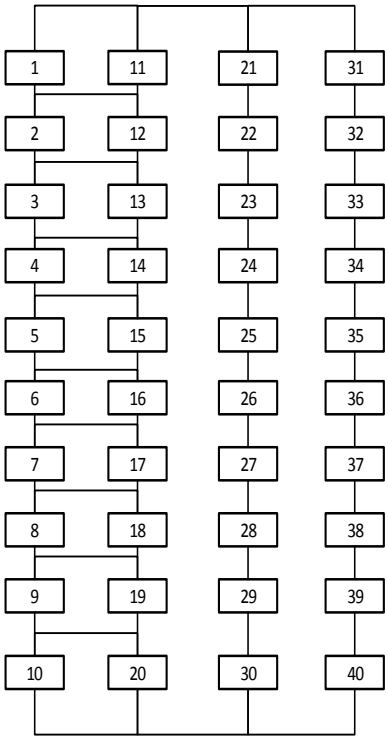

(k) LD-SP configuration

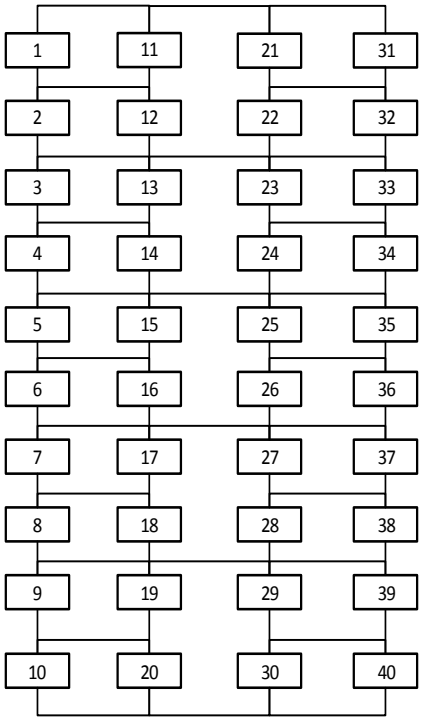

(l) LD-TCT configuration

Fig. 3.6. Different configurations of PV modules in a 4×10 array: (a) SP, (b) TCT, (c) BL, (d) HC, (e) LD, (f) SP-TCT, (g) HC-TCT, (h) S-TCT, (i) TCT-S, (j) SP-LD, (k) LD-SP, and (l) LD-TCT.

3.2.2 Dataset of 4×10 Array Modules

In this subsection, 40 polycrystalline PV modules are used to investigate MML% in non-uniformly aged PV array using twelve (12) configurations. The non-uniform aging condition of PV modules is made by covering the surface of the modules using different size of plastic films [41]. The PV modules are tested, and corresponding electrical characteristics are measured using PV System Analyzer (PROVA-1011) by maintaining the IEC 60904-1 standard. The tested data are converter at STC (25°C, 1000 W/m2, AM 1.5G) using the PVSA software and tabulated in Table 3.5. The electrical characteristics (*Vmpp, Impp,* and *Pmpp*) of each PV modules are shown in the table. It has been seen from Figure 3.7 that, the (*Vmpp, Impp)* for the individual modules are scattered from the ideal location (average value). Mostly aged modules are located far away from the ideal location.

Table 3.5: Electrical Characteristics of Non-uniformly Aged PV Modules

SI no	Module model no	Vmpp (V)	Impp (A)	Pmpp (W)	SI no	Module model no	Vmpp (V)	Impp (A)	Pmpp (W)
1	1612E020001	8.364	0.963	8.058	21	1612E020025	8.457	1.064	8.999
2	1612E020002	8.349	0.956	7.985	22	1612E020026	8.434	1.097	9.260
3	1612E020003	8.044	0.943	7.589	23	1612E020027	8.010	1.062	8.509
4	1612E020004	8.442	0.972	8.206	24	1612E020028	8.426	1.091	9.199
5	1612E020005	8.508	1.038	8.833	25	1612E020029	8.562	1.095	9.376
6	1612E020006	8.395	0.951	7.986	26	1612E020030	8.502	1.118	9.511
7	1612E020007	8.388	0.953	8.001	27	1612E020031	8.450	1.128	9.536
8	1612E020008	8.402	1.024	8.608	28	1612E020032	8.071	1.140	9.208
9	1612E020009	8.462	1.004	8.503	29	1612E020033	8.615	1.116	9.618
10	1612E020010	8.478	0.991	8.403	30	1612E020034	8.451	1.108	9.369
11	1612E020011	8.488	1.045	8.877	31	1612E020035	8.436	1.114	9.403
12	1612E020012	8.368	1.065	8.918	32	1612E020036	8.381	1.129	9.467
13	1612E020013	7.988	1.078	8.616	33	1612E020037	8.142	1.104	8.994
14	1612E020014	8.063	1.035	8.350	34	1612E020038	8.624	1.133	9.774
15	1612E020017	8.503	1.080	9.192	35	1612E020039	8.596	1.151	9.896
16	1612E020019	8.481	1.097	9.307	36	1612E020040	8.361	1.156	9.668
17	1612E020020	8.474	1.107	9.383	37	1612E020041	8.568	1.192	10.220
18	1612E020021	8.425	1.065	8.976	38	1612E020042	8.594	1.214	10.434
19	1612E020022	8.510	1.132	9.637	39	1612E020044	8.527	1.196	10.206
20	1612E020023	8.466	1.118	9.467	40	1612E020046	8.472	1.193	10.108

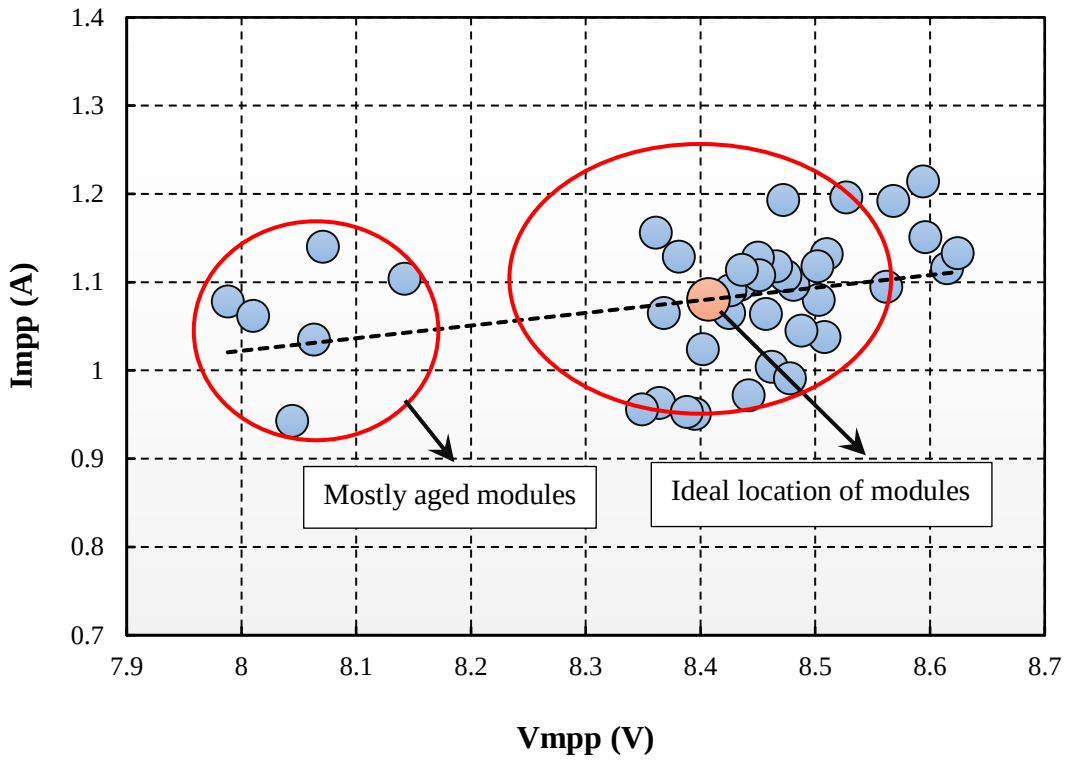

Figure 3.7: Correlation between *Vmpp* and *Impp* of non-uniformly aged forty Polycrystalline PV modules

3.2.3 Modules Arrangement Technique for Outdoor Test

At outdoor test condition, the artificially aged PV modules are arranged according to the short circuit current (SCC) of the PV modules. All module positions are determined by the value of the module short circuit current (I_{SC}). Let us consider a 4×10 size total-cross-tied (TCT) array configuration consists of 40 modules, as shown in Figure 3.8. The I_{SC} of the modules are measured from the pre-collected dataset and are sorted in ascending order as follows,

$$I_{SC,min} \leq \cdots \leq I_{SC,max} \tag{5.1}$$

The sorting has been done from lower values to higher values of I_{SC}; as a result, module 1 contains the lowest value ($I_{SC,min}$) while module number 40 has the highest value ($I_{SC,max}$). Consequently, current increases gradually from the first row to the last row. Hence, array current increases, and that also increases array power.

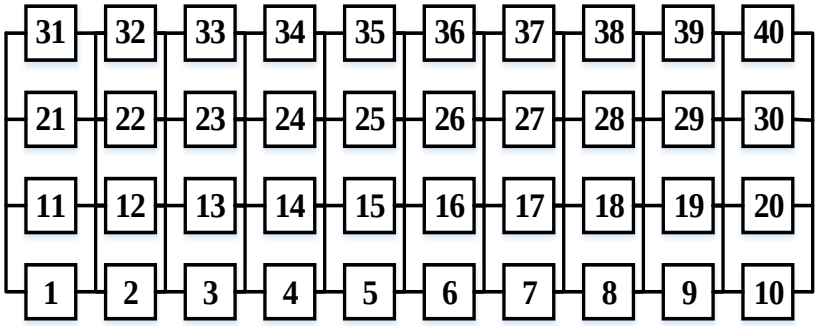

Figure 3.8: 4×10 TCT array modules are rearranged by SCC technique

3.2.4 Experimental Work at Outdoor

The experiments are carried out to investigate the performance of all 12 array configurations using a 4×10 PV array. The PV array consists of 40 polycrystalline PV modules. Here, each PV modules are considered as non-uniformly aged. The PV modules setup is placed on a rooftop; where the geographical location of latitude is 23°43'N and longitude is 90°25'E. The experimental setup is shown with front view and back view in Figure 3.9, and Figure 3.10 respectively. The PV system analyzer PROVA-1011 is used to measure the output characteristics of the PV array. The experiment is done on sunny weather with a clear sky. The experimental data are obtained by maintaining IEC 60904-1 standard, within (800- 900) W/m^2. According to IEC 60891 standards [75].

Figure 3.9: Experimental setup of the non-uniformly aged PV array (front view)

Fig. 3.10: Experimental setup of the non-uniformly aged PV array (back view)

In general, a photovoltaic panel is a current source and its output current as well the output power is directly proportional with the input irradiance level. On the other hand, its output voltage is inversely proportional to the temperature and remain constant during the small variation of irradiance level. However, in an aged PV module the average degradation rate of open circuit voltage and short circuit current are 2% and 10% respectively. Hence, the power degradation in an aged module has close relationship with the short circuit current. In chapter 3 the non-uniform aging of PV modules is compared using maximum short circuit current, considering constant open circuit voltage. Therefore, nonuniform aging of PV module is equivalent to a module with nonuniform shadow condition. In plastic films are used to cover the surface of the modules to make nonuniform aging condition. Therefore, in this work different size of EVA papers are used to cover the surface of the modules to make different aging condition.

3.2.5 Experimental Results at Outdoor

Table 5.2 shows the output voltage, current, and power of the 4×10 array obtained by using twelve array configurations. Among the standard array configurations (SP, TCT, BL, HC, and LD) the maximum output power is 342.18 W obtained by HC configurations, and the minimum power is 298.36 W obtained by SP configuration. Among the hybrid array configurations (HC-TCT, LD-TCT, TCT-S, S-TCT, SP-LD, LD-SP, and SP-TCT), the highest output power is 345.91 W generated by LD-SP configuration. Figure 3.10 shows that SP-LD and LD-SP configurations are

outperforming with respect output power. Figure 3.12 summarizes the MML% values of all twelve array configurations. Where SP configuration shows poor performance with 17.96% losses while LD-SP configuration shows only 4.88% losses. The experimental results show the superiority of LD-SP configuration over others for its minimum MML% by generating maximum output power. The percentage of recoverable energy (%RE) is calculated for each configuration with respect to the most commonly used SP configuration. The values of %RE are also tabulated in Table 3.6. The maximum %RE is 15.94% achieved by LD-SP configuration.

Table 3.6: Array Output Power and MML% Obtained by Experimental Work for Different Array Configurations

SI No	Array Configurations	Voltage (V)	Current (A)	Parray (W)	MML (%)	RE (%)
1	SP	72.54	4.113	298.36	17.96	0.00
2	TCT	73.12	4.088	298.91	17.81	0.18
3	BL	81.36	3.708	301.68	17.05	1.11
4	S-TCT	75.45	4.205	317.29	12.75	6.34
5	LD-TCT	74.77	4.366	326.46	10.23	9.41
6	HC-TCT	75.04	4.388	329.26	9.46	10.35
7	LD	76.39	4.336	331.24	8.92	11.02
8	TCT-S	75.73	4.457	337.56	7.18	13.13
9	SP-TCT	76.32	4.435	338.46	6.93	13.44
10	HC	78.18	4.377	342.18	5.91	14.68
11	SP-LD	78.6	4.396	345.53	4.99	15.80
12	LD-SP	78.74	4.393	345.91	4.88	15.94

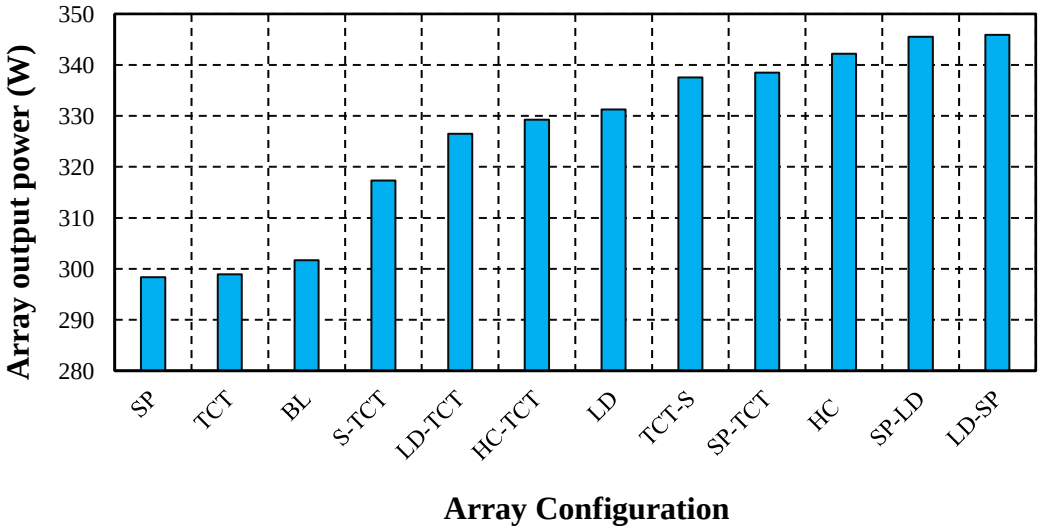

Figure 3.11: Comparison of power outputs among different array configurations

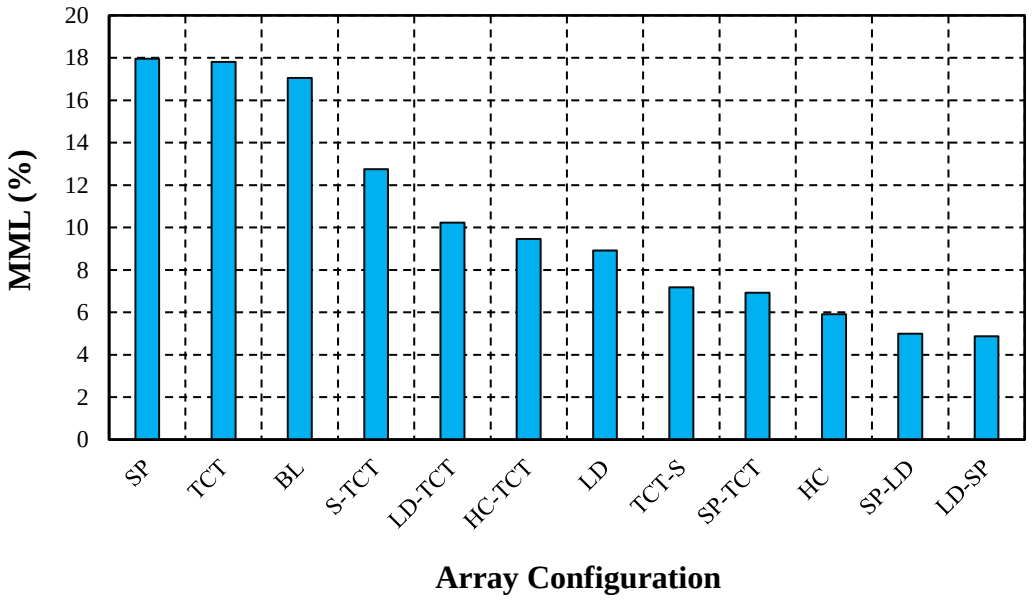

Figure 3.12: Comparison of the value of MML% among different array configurations for 4×10 array

3.2.6 Summary on Outdoor Test

In this chapter, a comparative analysis of different array configurations is analyzed to extract the maximum array output power from nonuniformly aged PV array. It has been observed that hybrid array configurations performed better than standard array configurations with respect to array output power. The hybrid array configuration can also reduce mismatch loss more effectively than conventional interconnection topologies for non-uniformly aged PV array. In this work, a 400W PV array has been used to investigate twelve different array configurations. Experimental result shows that the maximum %RE is 15.94% for LD-SP configuration.

It should be noticed that modifying array interconnections does not affect inverter/charger specifications; one single inverter can be used for all topologies. In larger installations, the LD-SP arrangement will be easier to wire because of the simplicity of the pattern compare to HC and TCT configurations. However, TCT configuration is mostly used in the PV plant to minimize MML% at the non-uniform aging condition. In this work, LD-SP configuration is recommended for the non-uniform aging condition. The cable losses in LD-SP connection is comparatively lower than TCT connection. Therefore, the proposed LD-SP configuration will be cost-effective compared to TCT configuration.

CHAPTER 4

MML Minimization by Optimal Configuration of PV Array at Partial Shading Condition

Partial shading causes multiple peak points in power-voltage (*P-V*) curves of photovoltaic (PV) arrays, and that results in mismatch power loss (MML). In vast PV arrays, output power decreases significantly with increasing the shading size. The shading effects can be minimized by changing the array. Chapter 4 investigates the performances of different PV array configurations to obtain maximum output power for six different sizes of shading patterns. The experimental investigation is carried out using a 4×6 PV array with series-parallel (SP), total-cross-tied (TCT), ladder-diagram (LD), honey-comb (HC) and bridge-linked (BL) configurations. A comparative analysis is performed among the five configurations under different shading conditions for MML reduction and improvement of the percentage of recoverable energy (%RE).

4.1 Introduction

The extraction of maximum output power from a shaded PV array has investigated by many researchers, using different interconnection topologies both for online and offline grid-connected PV systems[17, 19]. In the last two decades, a remarkable amount of research is carried out to mitigate MML due to partial shading. Partial shading causes multiple peak power points in the *P-V* curve of a PV array and results in MML. Figure 4.1 shows that a large amount of power loss is generated in a PV array by partial shading compare to without shading condition [20]. In a shaded PV array, the output power depends not only on shading size but also on module interconnection topologies [86].

In [87], three interconnection schemes (SP, BL, and TCT) are investigated using only three shading patterns for a 3×3 PV array. The experimental work is performed using an analog *I-V* tracking system. In [88], SP, TCT, HC, and BL configurations are investigated using four simple shading patterns, without any experimentation. Here, the simulation results show that the TCT configuration performed better than other arrangements for output power. In [89], partial shading is analyzed using MATLAB based simulation, for different array configurations (SP,

TCT, HC, and BL) without experimental validation. In [90], different irradiance levels (200 to 800W/m^2) are investigated using a 3×3 array with SP, TCT, and BL configurations, where TCT performed better than others. However, the experimental work is not carried out using any commercial *I-V* tracer. In [91], a simulation-based investigation is conducted to investigate SP, TCT, BL, and HC configurations under random partial shading condition using a 4×4 array. Here, the simulation result shows that minimum %MML is 15.67% obtained by TCT configuration when four modules are in a partially shaded situation.

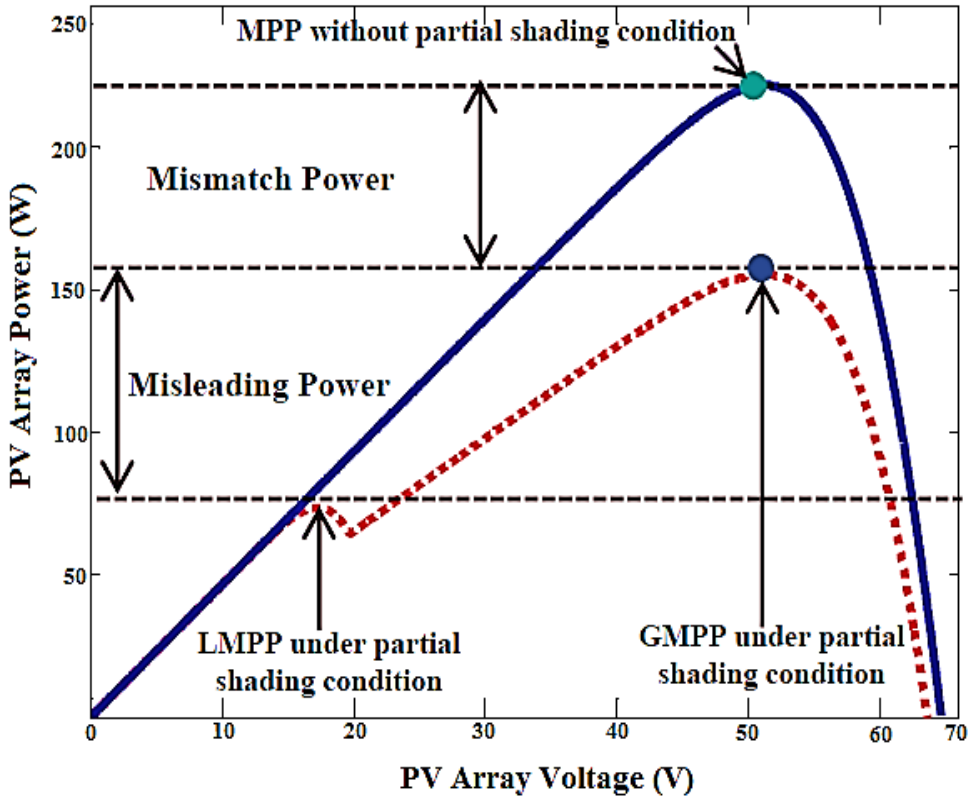

Figure 4.1: Mismatch power between unshaded and shaded PV array.

In the works cited above, investigations have been carried out to maximize the array output power by minimizing MML, under shadow condition, using the conventional array configurations (SP, TCT, BL, and HC). To the best of the author's knowledge, LD configuration is not investigated yet for different shadow conditions. Moreover, no comparative analysis is performed among the conventional topologies (SP, TCT, BL, and HC) and new LD configuration considering MML reduction and %RE under partial shading conditions. On the other hand, most of the experimental works were done by traditional *I-V* curve tracking system using a variable resistor. In

this work, the four most popular array configurations (SP, TCT, BL, and HC) and a new configuration (LD) have been investigated using six different shading patterns. A commercial *I-V* tracer is used to validate the experimental investigations. Moreover, a comparative analysis is performed for array output power maximization, %MML mitigation, and accretion of %RE.

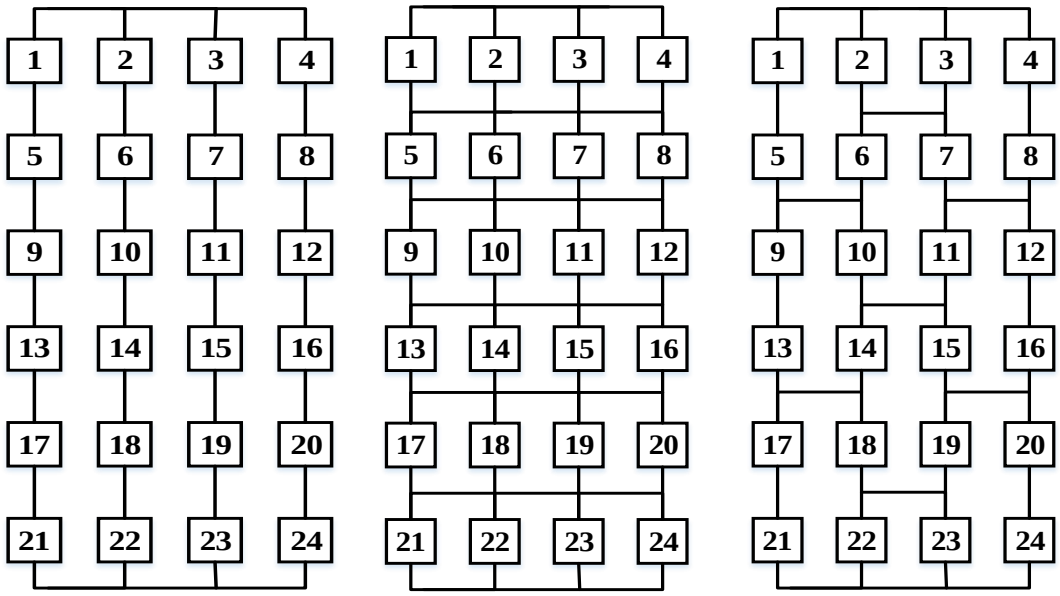

(a) SP (b) TCT (c) BL

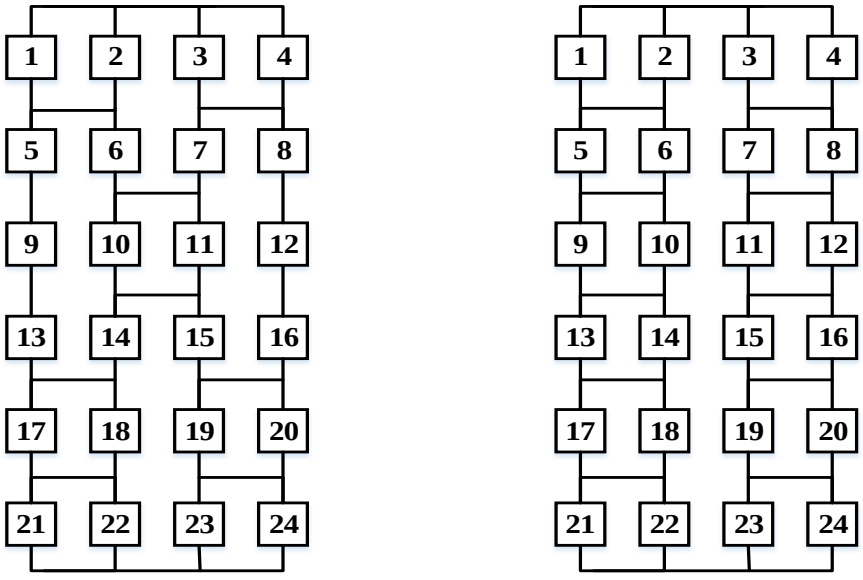

(d) HC (e) LD

Figure 4.2: Twenty four PV panels are inteconnected in (a) SP; (b) TCT; (c) BL; (d) HC and (e) LD configurations.

4.2 Methodology of the Work

In order to evaluate the performance of different array interconnection topologies to reduce mismatch loss due to shading effect, a 4×6 array is used in this study. Therefore, 24 polycrystalline PV modules are purchased from a PV module manufacturing factory. The electrical specifications of a single PV module and the array are summarized in Table 4.1. The experimental test is carried out in a renewable energy laboratory by maintaining STC (1000W/m2 and 25ºC). Six different shading patterns are used to investigate the performance of five interconnection topologies. The description of array configurations, shading patterns, and detail experimental procedure are presented in the subsequent subsections.

4.2.1 Different Array Configurations

In this work, five different interconnection topologies SP, TCT, LD, BL, and HC are investigated to evaluate their performances under different shading condition. Figure 4.2 (a), (b), (c), (d) and (e) show the electrical interconnection of 24 modules in SP, TCT, BL, HC and LD configurations respectively. In SP topology modules are joined in series to make strings and strings are attached in a parallel manner. In TCT configuration, the panels are joined in parallel to construct blocks and blocks are connected in series to create an array. Some connections are removed from the TCT configuration to make BL and HC configurations [14]. In LD configuration two strings are first joined in TCT, and then two TCT connected strings are coupled in parallel.

Table 4.1: Electrical Specifications of Module and Array

Parameter	**PV module (single)**	**PV Array (4×6)**
Open circuit voltage, *Voc (V)*	2.69	16.13
Short circuit current, *Isc (A)*	0.24	0.95
Maximum power point current, *Im (A)*	0.21	0.84
Maximum power point voltage, *Vm (V)*	2.42	14.52
Maximum power at MPP, *Pm (W)*	0.51	12.19

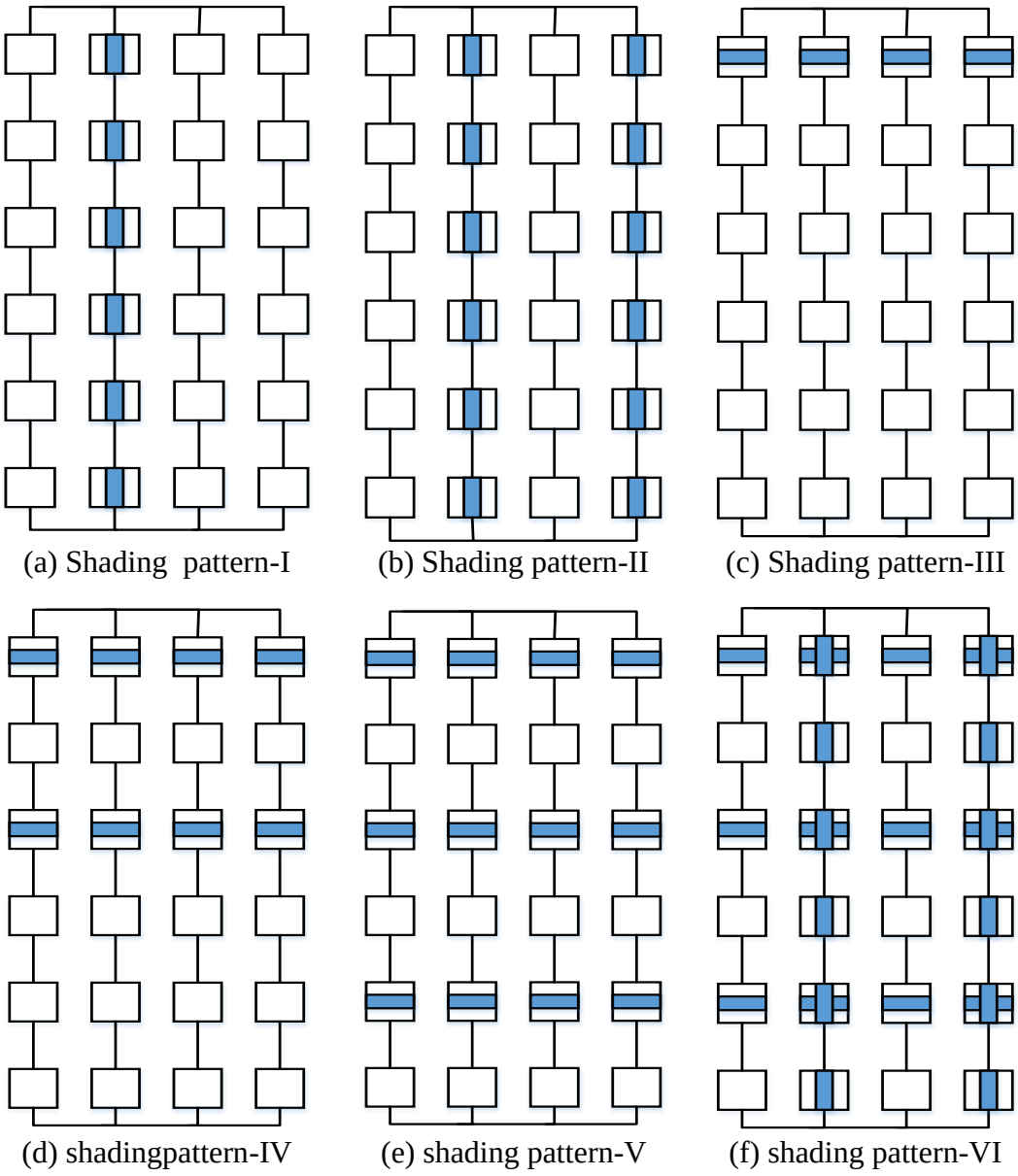

Figure 4.3: Six different partial shading patterns for SP configurations

4.2.2 Different Shading Patterns

The above mentioned five array configurations are investigated using six different shading patterns. In this work, ethylene-vinyl acetate (EVA) films are used to make the partial shading on the PV modules. Figure 4.3 shows the proposed six shading patterns, which are applied to the SP configuration. In shading pattern-I, (S-P-I) six modules are partially shaded (1/3 of each module). In shading pattern-II, (S-P-II) two strings are partially shaded as S-P-I. In shading pattern-III, (S-P-III) four modules are partially shaded (1/3 of each module) horizontally, and the modules are connected in parallel. Similar partial shading is used on eight modules and twelve modules to make partial shading-IV, (S-P-IV) and partial shading-V, (S-P-V)

respectively. Shading pattern-VI, (S-P-VI) is created by combining S-P-II and S-P-V. These six shading patterns are also applied individually on TCT, LD, BL, and HC configurations to investigate their performance. The significance of these shading patterns is evaluated using array current, array voltage, and power for each array configurations.

4.3 Experimental Work at Shading Condition

The experimental setup and data measurement procedures are described in this section. An experimental setup with 4×6 PV array is shown in Figure 4.4. Where halogen lights (0.5kW each) are used as artificial sunlight. The lights are placed parallel with the array modules. In order to make a more manageable process of interconnection, the output terminals of each PV modules are connected using flexible wires with crocodile clips. After completion of individual array interconnection, the outputs (*I-V* and *P-V* curves) of the PV array have been measured using a commercial *I-V* tracer, PROVA-1011. For a particular array configuration, the tests have been done both for without shading and partial shading conditions. The data measurement process has been repeated for each array configurations. The specifications of the *I-V* tracer are summarized in Table 4.2. Besides, an irradiance sensor device and temperature sensor are integrated with the tracer, and the device took a maximum of 15 seconds to measure the *I-V* and *P-V* curves in a single test. In this work, the experiment is performed in the laboratory at 25ºC, according to IEC 60904 [92] standard using a faster cooling system.

Table 4.2: Specifications of the I-V Tracer

Parameters of *I-V* Tracer PROVA-1011	**Measurement Range**	**Measurement Accuracy**
Voltage measurement (Volt)	1-1000	±1%
Current measurement (Amp)	0.1-12	±1%
Irradiance (W/m^2)	0-2000	±3%
Temperature (°C)	-22 to +85	±1%

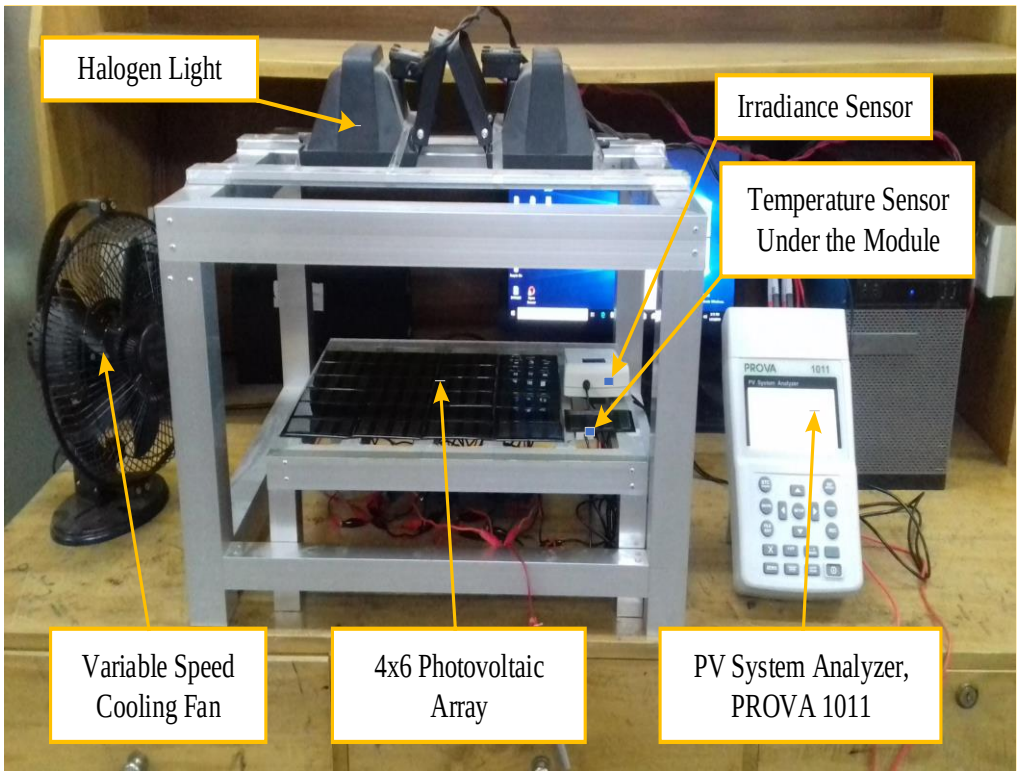

Figure 4.4: Prototype arrangement to investigate the I-V and P-V characteristics of the PV array for different interconnection topologies

4.4 Results and Discussion

The experimental results are compared and analyzed in this section. The results are analyzed using array output characteristics which are gained by five different topologies (SP, TCT, LD, HC, and BL) for without shading and with shading conditions. Table 4.3 shows the results for without shading condition, all the array configurations have generated almost the same array voltage. However, the corresponding current and power varied with array interconnection topologies. The highest array power (6.351W) is produced by LD topology due to higher array voltage, 14.56V and array current, 0.617A. Figure 4.5 shows the measured output characteristic curves for LD configuration using the *I-V* tracer, PROVA-1011. Though the array current of TCT configuration is maximum at without shading condition, its output power is lower than LD configuration due to lower array voltage. For shading pattern-I, the array outputs are summarized in Table 4.4. TCT and LD configurations yield higher output power; 5.081W and 5.006W, respectively. Where, both the voltage and current generations are higher than SP, HC, and BL interconnection schemes. Table 4.5 shows the results that are obtained for shading pattern-II. Both TCT and LD

configurations generated higher output power than SP, HC, and BL because of higher array voltage and currents. The output powers are 3.735W and 2.591W for TCT and LD configurations, respectively. However, SP configuration is generated comparatively lower output power, 3.978W and 2.415W both for shading pattern-I and shading pattern-II respectively, due to lower array voltage and current outputs.

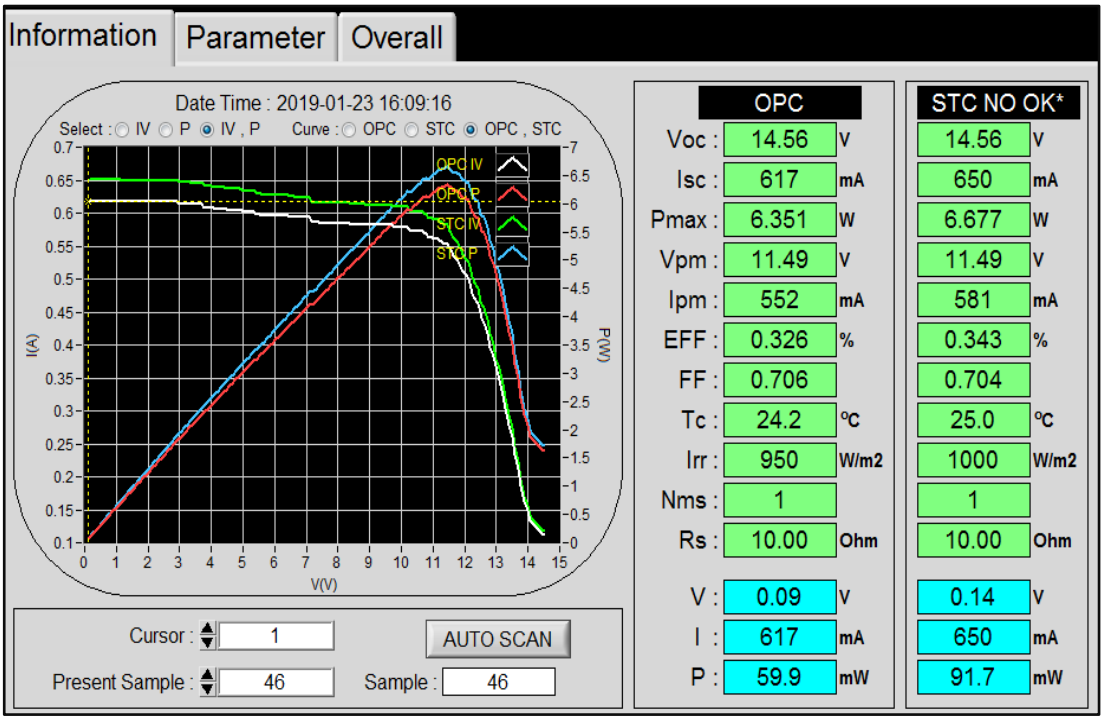

Figure 4.5: Experimental data measured by PROVA-1011 for LD configuration at without shading condition.

Table 4.3: Array Characteristics at Without Shading Condition

Array Configurations	**Array characteristics are measured at without shading condition**		
	Voltage (V)	***Current (A)***	***Power (W)***
SP	14.45	0.543	5.220
TCT	14.43	0.623	6.320
LD	14.56	0.617	6.351
HC	14.22	0.540	5.417
BL	14.41	0.530	5.216

Table 4.4: Array Outputs Obtained at Shading Pattern-I

Array Configurations	**Array characteristics are measured at shading pattern-I**		
	Voltage (V)	***Current (A)***	***Power (W)***
SP	14.19	0.418	3.978
TCT	14.36	0.530	5.081
LD	14.30	0.504	5.006
HC	13.74	0.416	3.803
BL	14.23	0.397	4.012

Table 4.5: Array Outputs Obtained at Shading Pattern-II

Array Configurations	**Array characteristics are measured at shading pattern-II**		
	Voltage (V)	***Current (A)***	***Power (W)***
SP	14.00	0.261	2.415
TCT	14.21	0.369	3.735
LD	13.95	0.309	2.591
HC	14.05	0.286	2.550
BL	14.01	0.270	2.496

The array outputs are tabulated in Table 4.6, Table 4.7, Table 4.8, and Table 4.9 for shading pattern-III, shading pattern-IV, shading pattern-V, and shading pattern-VI, respectively. For these four shading cases, both TCT and BL configurations have generated more power compare to SP, LD, and HC configurations. The lower output power is 3.939W obtained by SP configuration for shading pattern-III. The LD configuration is generated lower output power 3.845W and 1.715W for shading pattern-IV and shading pattern-VI respectively. On the other hand, for shading pattern-V, the lower power, 2.412W is obtained by HC configuration. For all the cases, TCT configuration has performed better than different configurations. Therefore, the percentage of recoverable energy by TCT configuration (%RE_TCT) is calculated with respect to the most common SP configuration using the following expression.

$$\%RE\_TCT = \frac{P_{TCT}^{array} - P_{SP}^{array}}{P_{SP}^{array}} \times 100 \quad (4.1)$$

Where P_{TCT}^{array} and P_{SP}^{array} are denoted as the maximum output power obtained by TCT and SP configurations respectively using a particular shading pattern. Fig.6 illustrates that the %RE by TCT configuration for all six shading patterns. Where, the maximum %RE (54.65%) is obtained for shading pattern-II, while the minimum %RE (17.67%) is obtained for shading pattern-V. The average %RE_TCT is also calculated for six shading patterns and found its value is 30.47%.

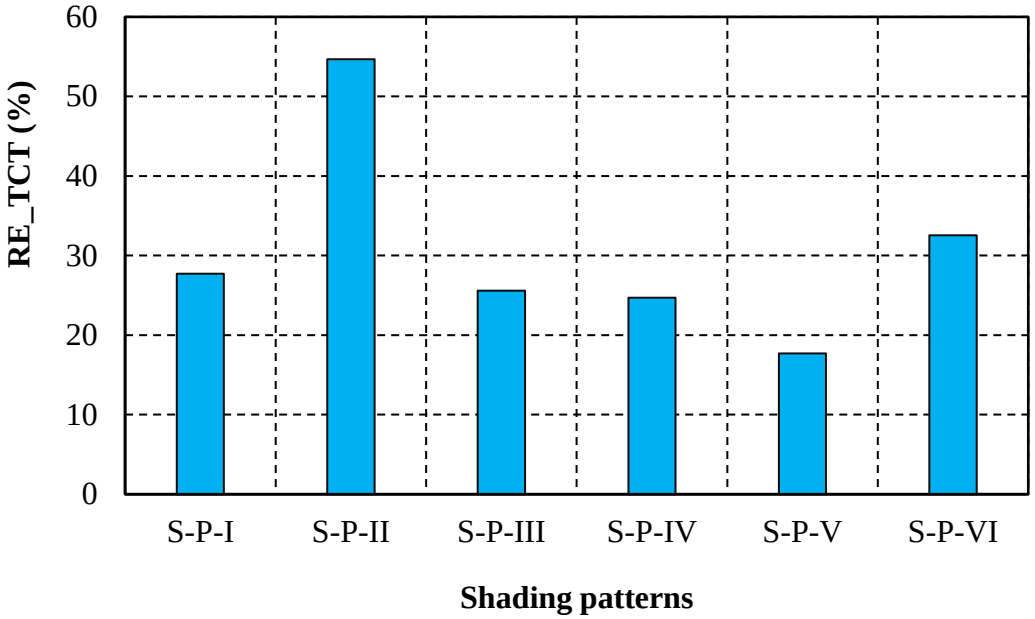

Figure 4.6: Recoverable energy obtained by TCT configuration

Table 4.6: Array Outputs Obtained at Shading Pattern-III

Array Configurations	**Array characteristics are measured at shading pattern-III**		
	Voltage (V)	***Current (A)***	***Power (W)***
SP	14.01	0.398	3.939
TCT	14.28	0.495	4.947
LD	14.03	0.443	3.991
HC	14.15	0.406	4.023
BL	14.16	0.386	4.104

Table 4.7: Array Outputs Obtained at Shading Pattern-IV

Array Configurations	**Array characteristics are measured at shading pattern-IV**		
	Voltage (V)	***Current (A)***	***Power (W)***
SP	13.93	0.399	3.905
TCT	14.35	0.492	4.869
LD	13.85	0.424	3.845
HC	13.08	0.370	3.964
BL	14.00	0.378	3.980

Table 4.8: Array Outputs Obtained at Shading Pattern-V

Array Configurations	**Array characteristics are measured at shading pattern-V**		
	Voltage (V)	***Current (A)***	***Power (W)***
SP	13.82	0.377	3.66
TCT	14.16	0.454	4.307
LD	13.61	0.371	3.499
HC	13.47	0.330	2.412
BL	13.82	0.369	3.815

Table 4.9: Array Outputs Obtained at Shading Pattern-VI

Array Configurations	**Array characteristics are measured at shading pattern-VI**		
	Voltage (V)	***Current (A)***	***Power (W)***
SP	13.65	0.208	1.980
TCT	13.81	0.300	2.624
LD	13.44	0.243	1.715
HC	13.67	0.220	1.988
BL	13.59	0.217	2.130

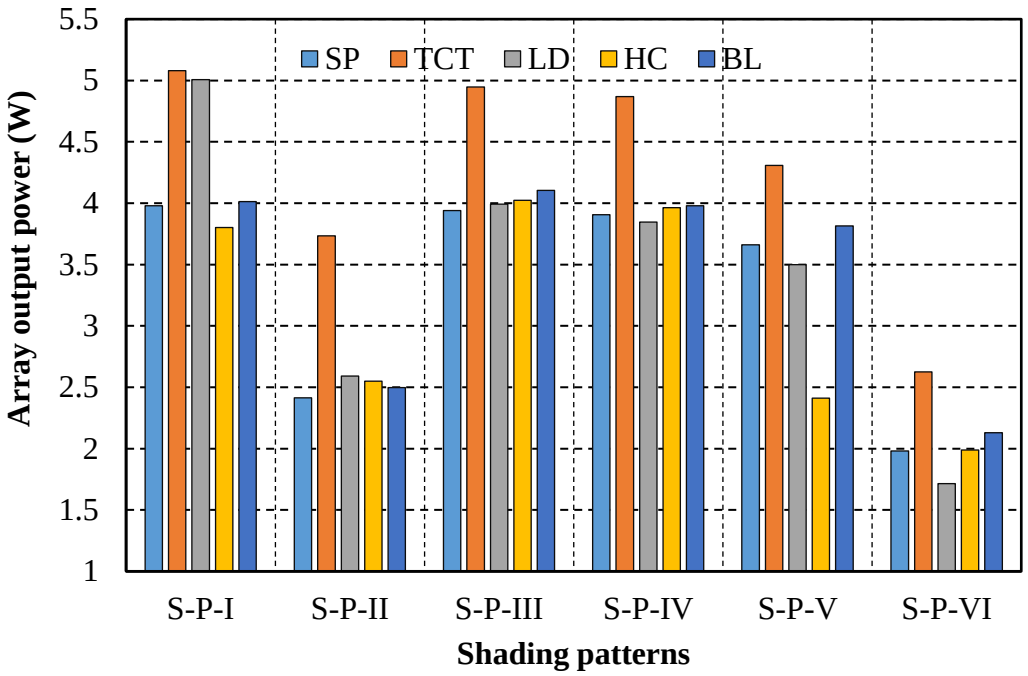

Figure 4.7: Comparison of array output power at different shading patterns using SP, TCT, LD, HC and BL configurations

Table 4.10: Average Array Output Power Calculated for Six Shading Patterns

Shading Patterns	**S-P-I**	**S-P-II**	**S-P-III**	**S-P-IV**	**S-P-V**	**S-P-VI**
Average Array Power (W)	4.38	2.76	4.20	4.11	3.54	2.09

Figure 4.7 illustrates a comparative analysis among the array configurations (SP, TCT, LD, HC, and BL) using the array output power from the six different shading patterns (S-P-I, S-P-II, S-P-III, S-P-IV, S-P-V, and S-P-VI). The shading size is maximum at S-P-VI, and the corresponding array output powers are minimum for all configurations. Similarly, due to large shading size at S-P-II, the output powers are also lower for all array configurations. On the other hand, at S-P-I, the shading size is minimum, and consequently, the array output powers are higher for different array configurations. The shading areas are increased from S-P-II to S-P-V, and accordingly, the generated powers are decreased. However, in each shading size, the TCT configuration has yielded higher output power compared to others. The average output power for six shading patterns is summarized in Table 4.10. For little shading at S-P-

I, the average power is 4.38 W while for significant shading at S-P-VI, the average power is 2.09. Also, for S-P-III to S-P-V the shading size is increased, and corresponding average array output power decreased from 4.20 W to 3.54W, respectively.

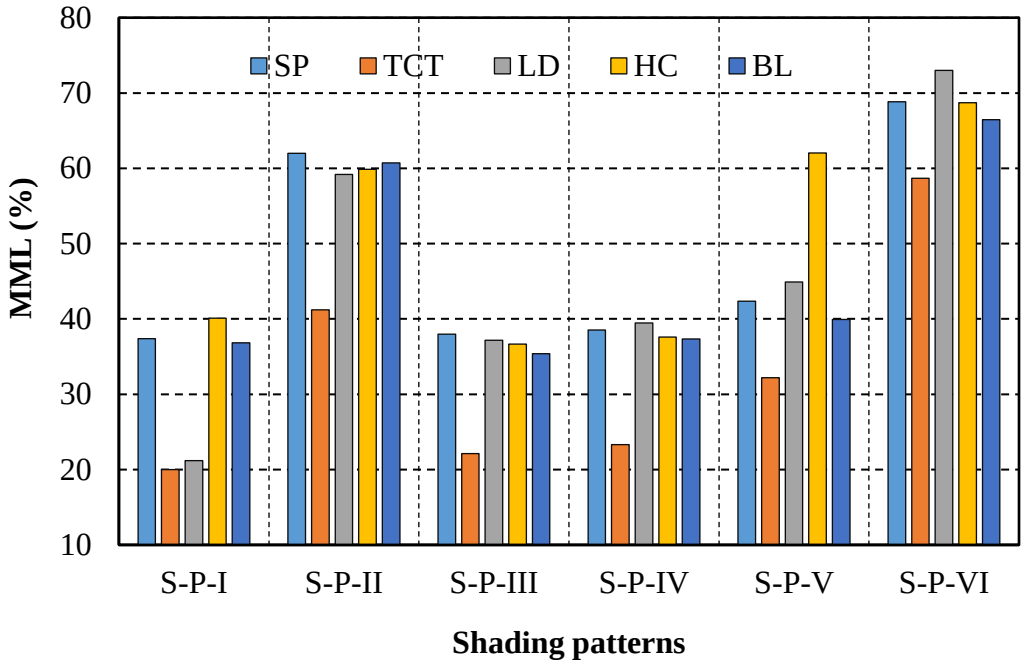

Figure 4.8: Comparison of %MML at different shading patterns using SP, TCT, LD, HC and BL configurations

Table 4.11: Average MML% of Different Array Configurations for Six Shading Conditions

Array Configurations	**SP**	**TCT**	**LD**	**HC**	**BL**
Average MML (%)	47.83	32.91	45.81	50.82	46.10

Figure 4.8 shows another comparison by MML% among the inspected array configurations with the six shading patterns. MML% is calculated as follows.

$$MML\% = \frac{P_{withoutshading}^{array} - P_{withshading}^{array}}{P_{withoutshading}^{array}} \times 100 \quad (4.2)$$

$$P_{withshading}^{array} = V_{mpp}^{array} \times I_{mpp}^{array} \quad (4.3)$$

Where the array maximum output power at without shading condition, $P_{withoutshading}^{array}$ is 6.351W, and at different shading condition the array output power, $P_{withshading}^{array}$ is calculated using the corresponding array output voltage, V_{mpp}^{array} and array output current, I_{mpp}^{array} form the experimental results. In general, the MML% depends on array configuration and also on shading size. The TCT configuration has yielded lower MML% compare to SP, LD, BL, and HC configurations for all the inspected shading patterns. The minimum and maximum values of MML% are (19.99% and 58.68%) obtained by TCT configuration for S-P-I and S-P-VI, respectively. Table 4.11 summarized the amount of average MML% for SP, TCT, LD, BL, and HC topologies. The higher value of average MML% is 50.82% for HC configuration, while the lowest value of 32.91% is obtained for TCT configuration.

4.5 Summary

In this paper, the most common array configurations (SP, TCT, HC, and BL) and a new configuration (LD) are investigated on a 4×6 PV array using different shading patterns. The experimental result shows that TCT configuration is performed better than all other configurations for array output power. The influence of shading size on array output power is also analyzed in this paper. It has been observed that the array power decreases significantly when shading increases in the parallel branches of the array modules. At shading pattern-I, the average output power is 4.38W, but at S-P-II, the average output power is 2.76W. Similarly, the output power gradually decreased for increasing shading size from S-P-III to S-P-VI. However, for all six cases of shading patterns, the TCT configuration outperformed by generating higher power and also a reduction in %MML. The average MML% of 32.91% is achieved by TCT configuration, while the average MML% of 50.82% is obtained by HC configuration. The TCT configuration yields a maximum %RE of 30.48% for a 4×6 PV array. Therefore, the TCT array configuration is suggested as the most convenient interconnection scheme for different size of partial shading.

CHAPTER 5

MML Minimization in a 28 MW PV Power Plant: A Case Study

In chapter 5 a case study is made on 28 MW grid connected PV plant to investigate the extra revenue by MML minimization in the PV plant arrays. The description of the PV arrays, MPPT charge controller, substation inverter of the 28 MW PV plant is also presented in this chapter. MML in the PV array is investigated and daily, monthly and yearly harvested energy is calculated for both at new and aged conditions of the PV array. Finally, the economic benefit is analyzed for extra energy generation by the PV plant at new and three (03) years of aged condition.

5.1 28 MW Grid Connected PV Plant in Bangladesh

A solar power plant having a power generation capacity of 28 MW has recently started its operation in Teknaf of Cox's Bazar in 2018. Accounting this, the power generation capacity from renewable energy sources exceeds five percent of the country's total demand. Technaf Solartech Energy Ltd (TSEL) has installed this power plant in Teknaf utilizing a total of 116 acres of land. Currently, the power plant is feeding 20 MW to the national grid. Figure 5.1 shows the first larger PV power plant in Teknaf, Chittagong, Bangladesh.

This power plant is situated at Aukhali area in Hinla union of Teknaf upazila. It's located at the east side of the Cox's Bazar-Teknaf highway. A total of 87,000 solar panels were used to construct the plant and the plant has 5 sub-stations, surrounded by panels. The power generated by the panels is primarily stored at the facility which is later transmitted to the substation of Palli Bidyut located at Leda area of Hinla union. The solar PV plant will cover up to 80% of the present electricity demand of the entire Teknaf region and result in a reduction in CO_2 emissions of 20,000 tonnes each year, with estimated 400,000 tonnes of carbon dioxide emissions to be prevented over the next 20 years, the solar firm noted.

Prior to the installation of this power plant, the highest capacity of a solar power plant was only 3 MW in Bangladesh. Currently, the country generates around 530 MW

of power from renewable sources, where almost half of the power comes from hydro-power. The power generation capacity from renewable sources is likely to raise up to 600 MW within next year. According to the master plan of Bangladesh Power Development Board or BPDB, there is a target to generate 2,235 MW of power from renewable sources within the year of 2021.

Figure 5.1: Bangladesh's first larger PV power plant in Teknaf, Chittagong is started in 2018.

5.1.1 Project Description

The schematic diagram of 28MW grid connected PV plant at Cox-Bazar, Bangladesh is shown in Figure 5.2. In a single DC connection box total 441 PV modules are connected in (21×21) SP configuration has shown in Figure 5.3. Where a single PV module power is 325 W(peak). Eight (08) DC connection boxes are connected with a single MPPT charge controller and two (02) similar MPPT charge controllers are connected with a single 2244 KW power station inverter. Figure 5.4 shows the schematic diagram of 2244 KW Power Station Inverter. Table 5.1 summarizes about the 2244 KW power station inverter. Total twelve (12) inverters are connected with a 11 KV grid line via step-up transformers to feed 20 MW (peak) power during the day time at full-sun.

Table 5.1: 2244 KW Power Station Specifications

SI No	Item	Quantity	Status
01	Inverter	01	Inverter is connected with a step-up transformer
02	MPPT	02	Two MPPT charge controllers are connected inside a single inverter
03	DC combiner box	16	Eight DC combiner boxes are connected with a single MPPT charge controller
04	PV module	7056	(21×21) = 441 modules are connected in SP configuration with a single DC combiner box.

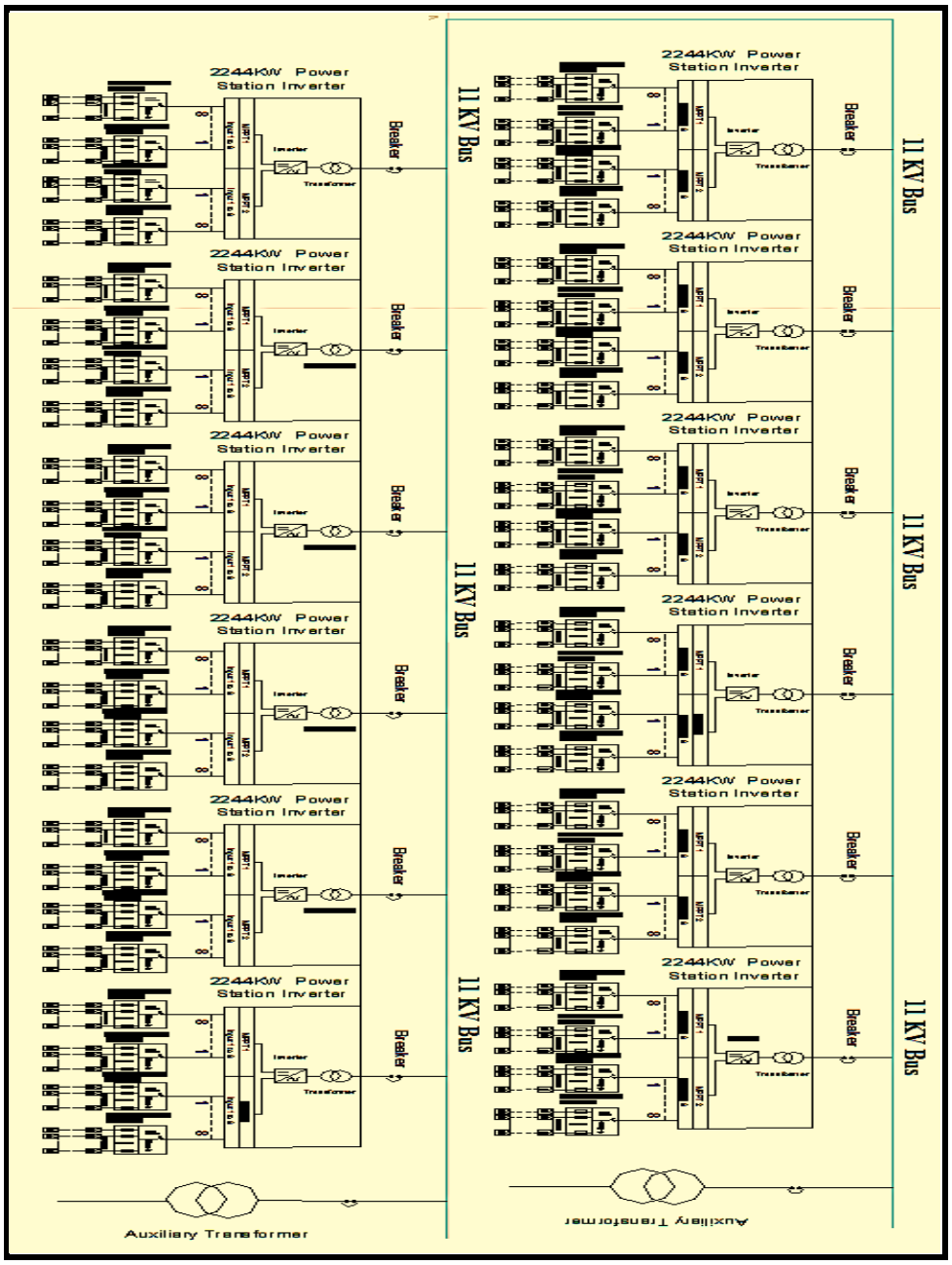

Figure 5.2: Schematic Diagram of 28 MW grid tied PV Plant

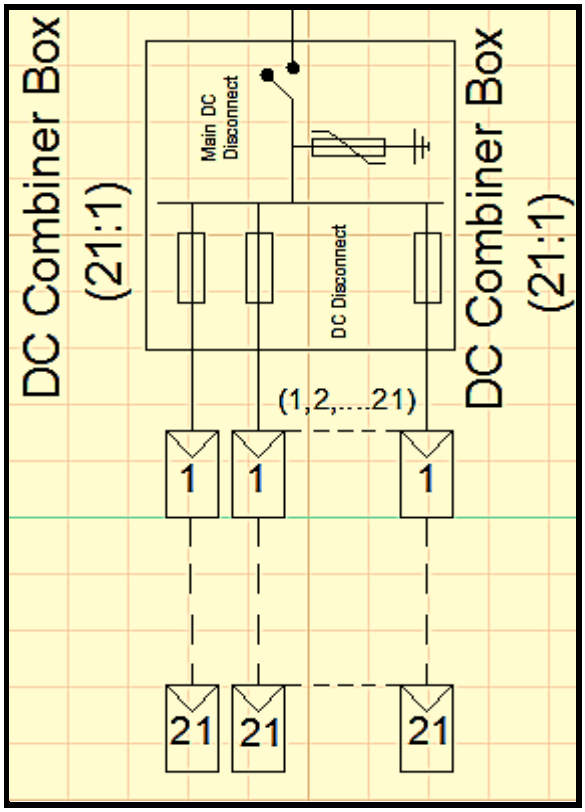

Figure 5.3: Schematic Diagram of a DC Combiner Box in 2244 KW Power Station Inverter

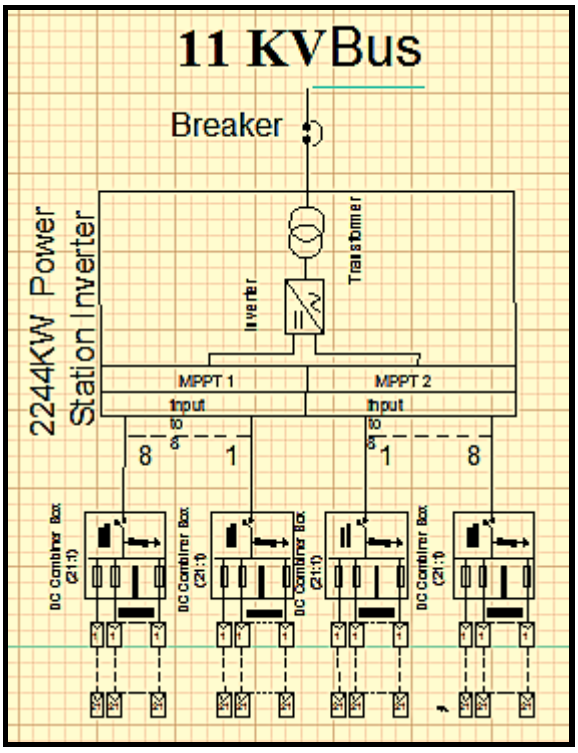

Figure 5.4: Schematic Diagram of 2244 KW Power Station Inverter in 28 MW grid tied PV Plant

5.1.2 PV Module Characteristics

In the 28 MW PV plant total 87000 PV modules of 325 W are installed. Among them 84672 modules are used to feed the power in the national grid and 2328 modules are used to charge batteries as a back-up power supply for the PV power plant. The PV modules are manufactured by Solarland. The electrical characteristics of 325 W Multi-crystalline PV module is shown in Table 5.2. Figure 755 shows the 325 W Multi-crystalline PV module made by Solarland.

Table 5.2: Electrical Characteristics of 325 W Multi-crystalline PV module made by Solarland

Items	Specification
Power Output (W)	325W
Max Power Tolerance (W)	0~+5W
Voltage MPP Vmpp (V)	37.31V
Current MPP Impp (A)	8.71A
Voltage Open Circuit Voc (V)	45.67V
Short Circuit Current Isc (A)	9.27A
No of PV cell	72
Fill Factor	0.7675

Figure 5.5: 325 W Multi-crystalline PV module made by Solarland

5.2 Mismatch Loss Analysis in the 28 MW PV Plant

In order to investigate the MML in a particular PV array, it is essential to get the electrical characteristics of all modules of that array. In the 28 MW PV plant the number of PV modules are 87000, which is quite large. However, in this PV plant a single array unit contains only 441 PV modules and the corresponding array dimension is (21×21). Where, all the PV modules are manufactured by a single manufacturer company, named Solarland. Which is a China based multinational company. In this case study the MML% of the single unit (21×21) PV array has been calculated and considered the similar MML% for the other array units of the PV plant. In this chapter the datasets of new PV array modules (441) of 325W are first collected from the manufacturer company. After that the same PV modules, their aged (03 years) datasets are generated using statistical calculation by subtracting the degradation factors from the corresponding new modules dataset. The degradation factors which have been used to calculated the 3 years aged PV modules data sets are summarized in Table 5.3. Finally, the MML% is calculated for the (21×21) PV array both at new and three (03) years of aged condition.

Table 5.3: Degradation factors of three years aged PV modules.

SI No	Pmpp (%)	Isc (%)	Voc (%)	Vmpp (%)	Impp (%)	FF (%)
1	3.019831	-0.41667	0.325598	2.440998	0.565157	3.119983
2	2.964414	-0.3981	0.290182	2.637902	0.315338	3.077738
3	1.258575	-0.27257	0.339997	1.521279	-0.26135	1.188156
4	1.532768	-0.65524	0.225316	1.485186	0.046638	1.96968
5	3.381951	-0.37156	0.468352	2.51547	0.842621	3.277351
6	3.216762	-0.71475	0.358512	2.595147	0.607249	3.578298
7	1.371646	-1.60691	0.417725	1.798395	-0.42086	2.59782
8	0.812326	-1.4404	0.243981	1.561183	-0.73583	2.038866
9	2.874658	-0.31583	0.398099	2.13815	0.716228	2.785748
10	2.734248	-0.60754	0.304735	2.205875	0.516162	3.041554
.	.	.	.	.	.	.
.	.	.	.	.	.	.
.	.	.	.	.	.	.
440	2.667973	-0.35829	0.261164	2.374112	0.283804	2.769964
441	4.652341	-0.43888	0.134087	3.379027	1.191746	4.983263

5.2.1 Dataset of Multi-Crystalline PV Modules

The relation between the Vmpp and Impp of the 441 PV modules are shown in Figure 5.6 at new condition. The corresponding histogram of Vmpp and Impp are illustrated in Figure 5.7. Where the average value of Vmpp and Impp are 37.56 V and 8.71 A respectively. On the other hand, the aged PV modules datasets are shown in Figure 5.8 and corresponding histogram of Vmpp and Impp are illustrated in Figure 5.9. Where the ideal location represents as the average value of *Vmpp* and *Impp*. And the values are 36.72 V and 8.68 A respectively.

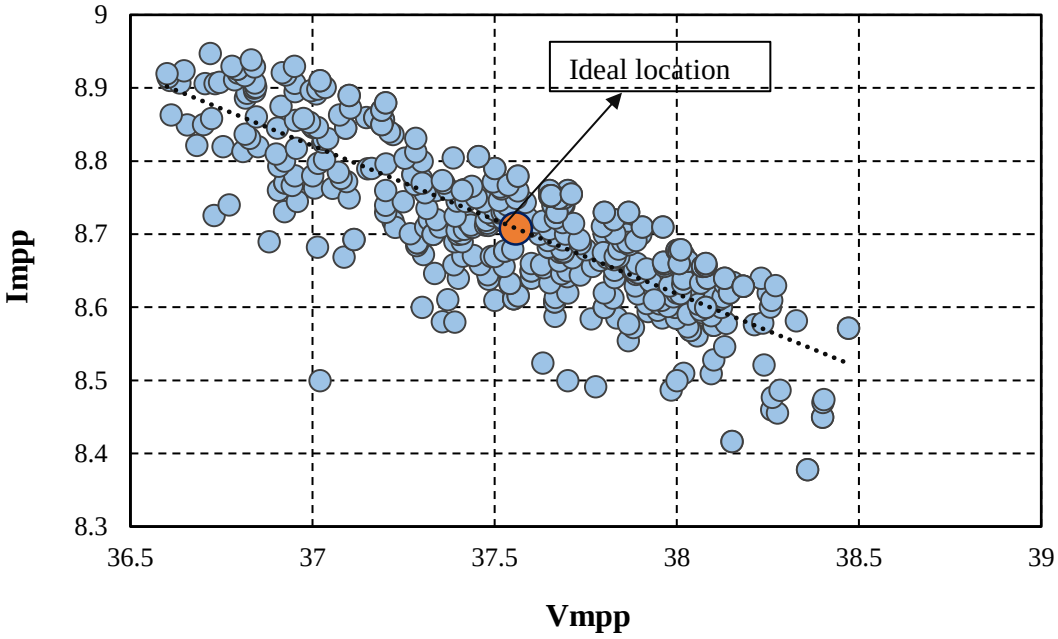

Figure 5.6: Datasets of 441 pieces multi-crystalline PV modules at new condition.

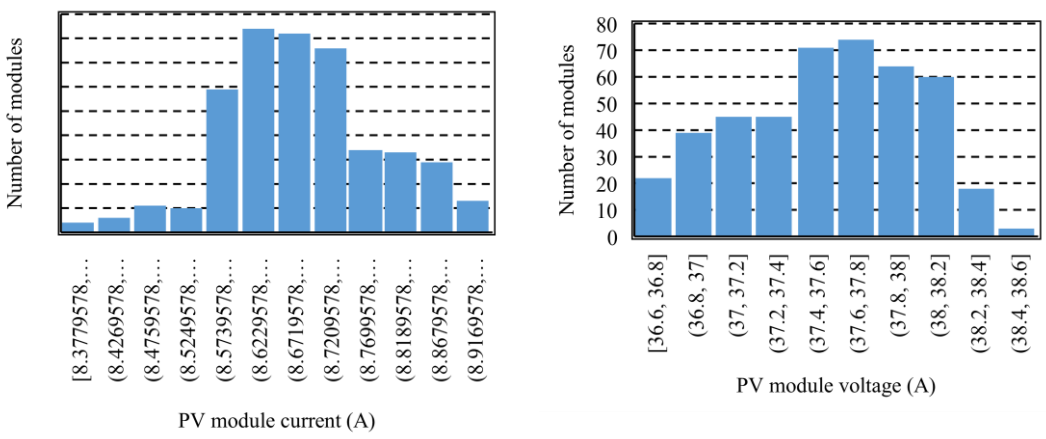

(A) Impp (B) Vmpp

Figure 5.7: Histogram of Vmpp and Impp of PV modules datasets at new Condition

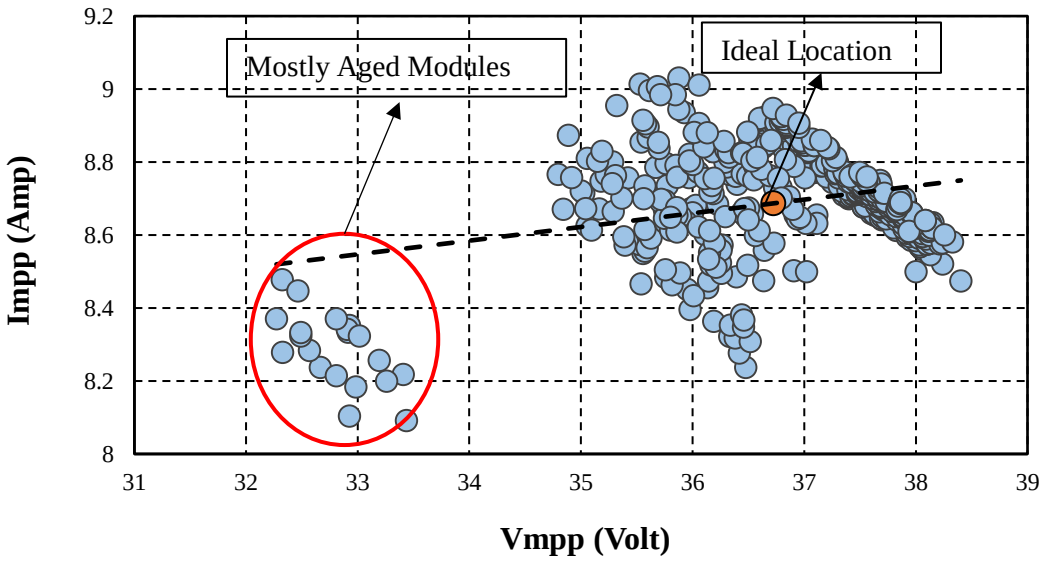

Figure 5.8: Estimated datasets of multi-crystalline PV modules after 3 years aged

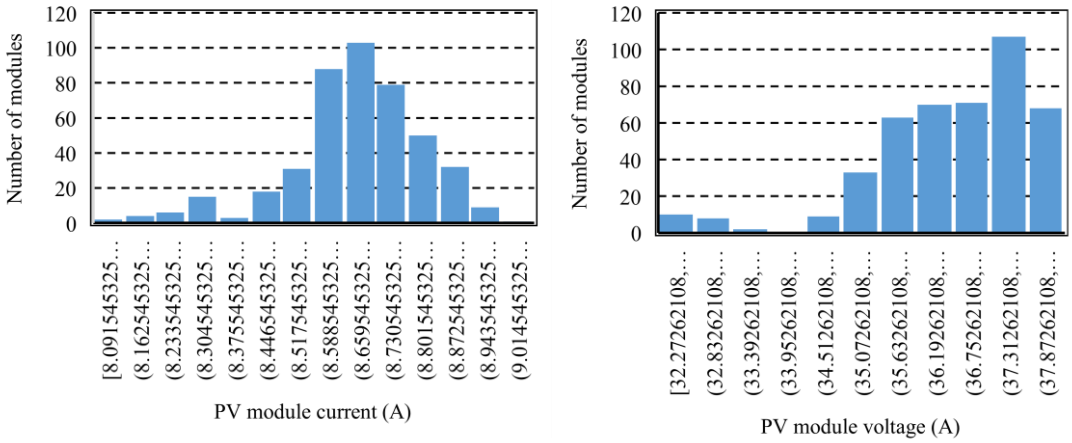

(C) Impp (D) Vmpp

Figure 5.9: Histogram of Vmpp and Impp of PV modules datasets after 3 years of aged

5.2.2 Analysis of Simulation Results

In order to minimize the MML% of the 28 MW PV plant GA based module rearrangement technique is applied and economic benefits are analyzed by comparing with randomly module rearrangement method. Simulation results are summarized at Table 5.4 for both GA and Ra based techniques. In both cases for (21×21) PV array the summation of modules power is 144213.664 W. For GA based technique the array voltage, current and power are 783.624 V, 182.233 A and 142802.475 W respectively. The corresponding MML% is 0.978 for GA based technique. On the other hand, for

Ra based method the output voltage, current and power are 782.850 V, 180.234 A and 141096.968 W respectively. The MML% is obtained 2.161% for random arrangement. However, GA based technique is performed better than RA based technique with respect to MML%. Hence, the energy is increased by 1.2%, by applying GA based rearrangement technique. The simulation results are summarized in table 7.5 for three years of aged (21×21) PV array. Where the array output power is 135281.049 W and 133275.926 W for GA and Ra based techniques respectively. The MML% is obtained 3.857% and 5.282% by GA and Ra based techniques respectively. Though at aged condition the GA based technique is performed better than Ra based technique by increasing the %RE by 1.5%, but the array output power is decreased significantly compare to new condition due to non-uniform aging.

Table 5.4: Simulation Results of a single unit (21×21) PV array at new condition

Parameters	**New (21×21) PV array parameters for different technique**	
	GA based	***RA based***
Varray (V)	783.624	782.850
Iarray (A)	182.233	180.234
Parray (W)	142802.475	141096.968
Pmodule (W)	144213.664	144213.664
MML (%)	0.978	2.161
%RE	1.2	----

Table 5.5: Simulation Results of a single unit (21×21) PV array at Aged condition

Parameters	**Aged (21×21) PV array parameters for different technique**	
	GA based	***RA based***
Varray (V)	743.604	743.604
Iarray (A)	181.926	179.229
Parray (W)	135281.049	133275.926
Pmodule (W)	140708.711	140708.711
MML (%)	3.857	5.282
%RE	1.5	----

5.3 Estimation of Generated Energy and Extra Energy

In this section the energy generation is calculated for both GA and RA based techniques. The corresponding energy harvesting by GA based technique is also

calculated for daily, monthly and yearly basis. Table 5.6 and Table 5.7 summarize the energy harvesting by GA based method at new and aged condition respectively.

For both condition the effective day time is considered as 4 hours and per unit energy cost is 13.86 BDT. At new condition the annual energy increases 475141.676 kWhr and corresponding extra revenue is 6585463.641 BDT. After three years of aged for the same PV plant the annual energy harvesting is 572527.36 kWhr and the corresponding extra income is 7935229.22 BDT. Though the energy generation is lower at aged condition but the %RE is higher and consequently increases the extra income also. Therefore, the GA based rearrangement technique is more effective and very much necessary for the PV array at aged condition.

Table 5.6: Extra energy and income of 28MW plant at new condition

Period of Time	**Energy Generated by GA Technique (kWhr)**	**Energy Generated by RA Technique (kWhr)**	**Extra Energy (kWhr)**	**Extra Revenue (BDT)**
Daily	108996.485	107694.727	1301.758	18042.366
Monthly	3269894.573	3230841.832	39052.740	541270.984
Annual	39783717.3	39308575.62	475141.676	6585463.641

Table 5.7: Extra energy and income of 28MW plant after three years of aged condition

Period of Time	**Energy Generated by GA Technique (kWhr)**	**Energy Generated by RA Technique (kWhr)**	**Extra Energy (kWhr)**	**Extra Revenue (BDT)**
Daily	105827.6	104259.08	1568.56	21740.35
Monthly	3174829	3127772.44	47057.04	652210.62
Annual	38627092	38054564.70	572527.36	7935229.22

5.4 Summary

This case study shows that GA based module rearrangement technique is economically beneficial for the PV arrays of 28 MW PV plant both at new and aged condition. Therefore, the GA based optimal rearrangement technique presented in the work can be applied to any online grid connected PV plant of any array dimension.

CHAPTER 6

Conclusion and Future Works

6.1 Summary and Conclusions

In this work, a new technique of module arrangement in PV arrays using adaptive GA is experimentally validated both for LSS-SP (4×10, 5×8) and LPB-SP (10×4, 8×5) configurations by minimizing MML. The performance of the proposed GA based technique is tested and also compared with the previous work, regarding the array output power and %MML. The tested simulation results are compared in Table 6.1. Where the proposed GA based technique minimizes MML by 0.265% (average) more than the previous work. Besides the proposed technique is also compared with other five conventional module sorting techniques. The traditional current-based methods (Im, Isc) show better performance than the voltage-based methods (Vm, Voc); however, the proposed GA based technique outperforms the conventional ones in every array configuration. The GA technique minimizes the MML by maximizing the array output power, thus increases %RE, both for LSS-SP and LPB-SP array configurations. Additionally, it is observed that the LSS-SP configurations are providing significantly lower %MML than the LPB-SP configurations.

Table 6.1: Tested Results of Previous and Proposed Technique

Array size	Proposed technique		Previous technique [31]	
	Parray_OX (W)	MML_OX(%)	Parray_PMX (W)	MML_PMX (%)
3×6	1695.795	0.669	1689.801	1.02
4×10	3779.044	0.448	3767.968	0.74
5×13	6138.312	0.477	6122.130	0.74
5×18	8507.228	0.476	8494.065	0.63
Avg.	5030.095	0.518	5018.491	0.783

In addition, for aged PV array modules the performance of the proposed GA based module rearrangement technique is compared with SCC and Ra based technique in terms of array output power and MML. The performance comparison is made by simulation and validated by experimental investigation. The proposed GA shows better performance in both cases. Additionally, the proposed GA based rearrangement technique also shows superiority for MML reduction in both small and large-size of

aged PV arrays with different dimensions. To the best of the authors' knowledge, this is the first time that the influences of rearrangement techniques to minimize MML% in real aged SP-PV array configurations are compared experimentally. The proposed GA based optimal rearrangement technique presented in this work can be applied to offline aged PV arrays of any size or dimension.

Moreover, a comparative analysis of aged PV module rearrangement techniques is analyzed using SP, TCT, BL, and HC configurations to extract the maximum array output power by minimizing the MML. One of the main contributions of this work illustrates that the Im based technique is performed better for all array configurations with respect to array output power. Additionally, it is observed that TCT, B, and HC configurations are outperformed than SP configuration. Besides, BL performed better than TCT configuration. According to the indoor experimental results, HC configuration is recommended as the best conventional configuration for the aged PV array.

Furthermore, a comparative analysis of different hybrid array configurations is performed to minimize the MML by generating more array power. Experimental investigation illustrates that hybrid array configurations are performed better than conventional array configurations with respect to array output power. The hybrid array configuration can also reduce MML more effectively than traditional interconnection topologies for non-uniformly aged PV array. Experimental analysis of twelve different array configurations is carried out using a 400W non-uniformly aged PV array. The experimental result shows that the maximum %RE is 15.94% for the hybrid, LD-SP configuration.

Additionally, a case study is performed to investigate the GA based MML reduction technique on the PV arrays of a 28MW grid connected PV plant. The simulation results show that the %RE of the PV arrays is 1.2% and 1.5% at new and aged condition respectively. Finally, it is recommended that the GA based module rearrangement technique is economically beneficial both at new and aged condition of the PV arrays.

6.2 Future Work

In this work, module rearrangement techniques SCC and GA have proven for MML reduction in aged PV arrays. But long term (10 years) investigation is needed to establish the closed-loop link between nonuniform aging and mismatching. Therefore, future work is needed to clarify that mismatching is also responsible for the premature aging of PV modules.

On the other hand, in this work, GA based rearrangement technique has proven as an optimal module arrangement technique both for new and aged PV array with SP configuration. However, GA is not investigated for TCT, BL, HC, LD, and another hybrid array configuration. Therefore, applying and validating this new technique with other array configurations can contribute the future work regarding this study.

Appendix A

A.1 Simulation Platform for PV Array Rearrangement

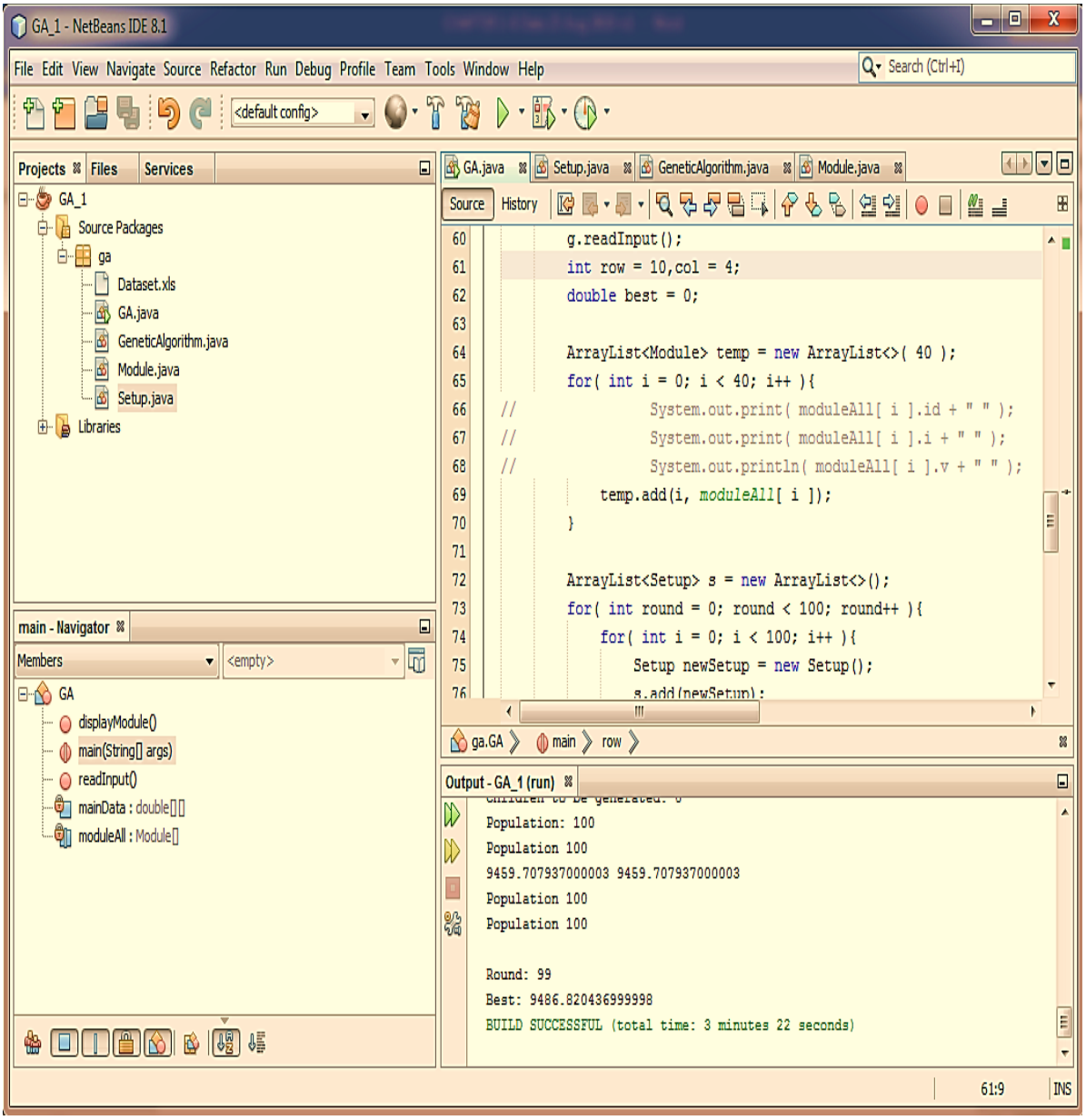

Figure A.1: Simulation window in NetBeans IDE 8.1 software

A.2 Simulation Platform for PV Array Rearrangement

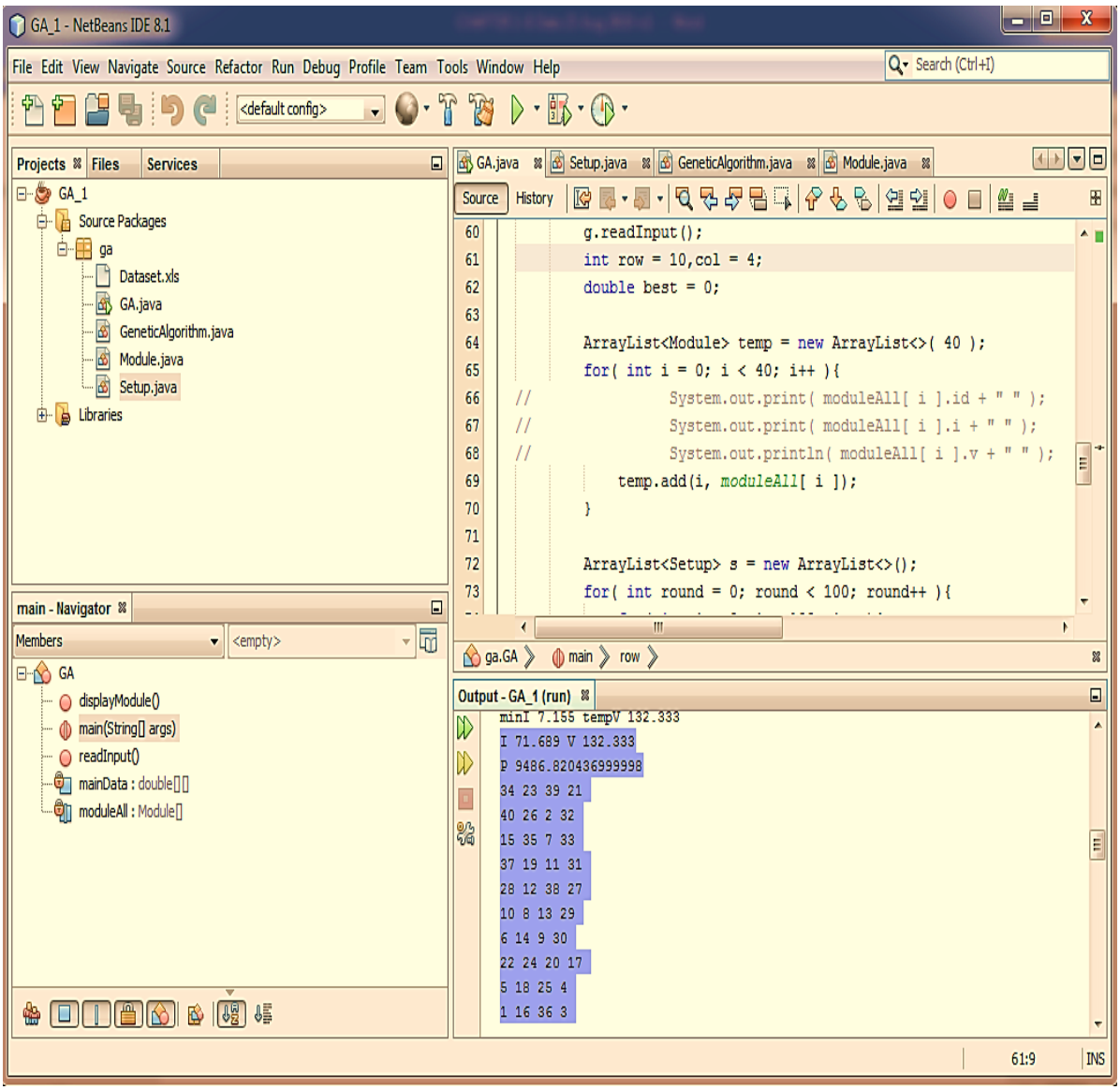

Figure A.2: Simulation window in NetBeans IDE 8.1 software with results

References

[1] L. L. Bucciarelli Jr, "Power loss in photovoltaic arrays due to mismatch in cell characteristics," *Solar Energy*, vol. 23, pp. 277-288 %@ 0038-092X, 1979.

[2] *Mismatch Effects*. Available: https://www.pveducation.org/pvcdrom/modules-and-arrays/mismatch-effects

[3] J. Bishop, "Computer simulation of the effects of electrical mismatches in photovoltaic cell interconnection circuits," *Solar cells*, vol. 25, pp. 73-89, 1988.

[4] E. Faldella, G. C. Cardinali, and P. U. Calzolari, "Architectural and design issues on optimal management of photovoltaic pumping systems," *IEEE Transactions on Industrial Electronics*, vol. 38, pp. 385-392, 1991.

[5] S. Deutsche Gesellschaft für, *Planning and installing photovoltaic systems: a guide for installers, architects and engineers*: Routledge, 2013.

[6] M. R. Maghami, H. Hizam, C. Gomes, M. A. Radzi, M. I. Rezadad, and S. Hajighorbani, "Power loss due to soiling on solar panel: A review," *Renewable and Sustainable Energy Reviews*, vol. 59, pp. 1307-1316 %@ 1364-0321, 2016.

[7] N. Kaushika and A. K. Rai, "An investigation of mismatch losses in solar photovoltaic cell networks," *Energy*, vol. 32, pp. 755-759, 2007.

[8] I. Tigo Energy, "SOURCES OF MISMATCH IN UNSHADED PHOTOVOLTAIC COMMERCIAL ARRAYS," May, 2012.

[9] A. Skoczek, T. Sample, and E. D. Dunlop, "The results of performance measurements of field-aged crystalline silicon photovoltaic modules," *Progress in Photovoltaics: Research and applications*, vol. 17, pp. 227-240 %@ 1062-7995, 2009.

[10] F. A. Silva, "Power Electronics and Control Techniques for Maximum Energy Harvesting in Photovoltaic Systems (Femia, N. et al; 2013)[Book News]," *IEEE industrial electronics magazine*, vol. 7, pp. 66-67 %@ 1932-4529, 2013.

[11] N. Femia, G. Petrone, G. Spagnuolo, and M. Vitelli, *Power electronics and control techniques for maximum energy harvesting in photovoltaic systems*: CRC press, 2017.

[12] D. C. Jordan, B. Sekulic, B. Marion, and S. R. Kurtz, "Performance and aging of a 20-year-old silicon PV system," *IEEE Journal of Photovoltaics*, vol. 5, pp. 744-751, 2015.

[13] M. Köntges, S. Kurtz, C. Packard, U. Jahn, K. A. Berger, and K. Kato, *Performance and reliability of photovoltaic systems: Subtask 3.2: Review of failures of photovoltaic modules: IEA PVPS task 13: External final report IEA-PVPS*: International Energy Agency, Photovoltaic Power Systems Programme, 2014.

[14] C. Tubniyom, R. Chatthaworn, A. Suksri, and T. Wongwuttanasatian, "Minimization of Losses in Solar Photovoltaic Modules by Reconfiguration under Various Patterns of Partial Shading," *Energies*, vol. 12, p. 24, 2019.

[15] G. Spagnuolo, S. Kouro, and D. Vinnikov, "Photovoltaic Module and Submodule Level Power Electronics and Control," *IEEE Transactions on Industrial Electronics,* vol. 66, pp. 3856-3859, 2019.

[16] J. D. Bastidas-Rodríguez, J. M. Cruz-Duarte, and R. Correa, "Mismatched Series–Parallel Photovoltaic Generator Modeling: An Implicit Current–Voltage Approach," *IEEE Journal of Photovoltaics*, 2019.

[17] G. S. Krishna and T. Moger, "Reconfiguration strategies for reducing partial shading effects in photovoltaic arrays: State of the art," *Solar Energy,* vol. 182, pp. 429-452, 2019.

[18] D. Picault, B. Raison, and S. Bacha, "Reducing mismatch losses in grid-connected residential BIPV arrays using active power conversion components," 2010.

[19] R. Pachauri, R. Singh, A. Gehlot, R. Samakaria, and S. Choudhury, "Experimental analysis to extract maximum power from PV array reconfiguration under partial shading conditions," *Engineering Science and Technology, an International Journal,* vol. 22, pp. 109-130, 2019.

[20] P. R. Satpathy and R. Sharma, "Power and mismatch losses mitigation by a fixed electrical reconfiguration technique for partially shaded photovoltaic arrays," *Energy conversion and Management,* vol. 192, pp. 52-70, 2019.

[21] R. Evans, M. Boreland, and M. A. Green, "A holistic review of mismatch loss: From manufacturing decision making to losses in fielded arrays," *Solar Energy Materials and Solar Cells,* vol. 174, pp. 214-224 %@ 0927-0248, 2018.

[22] T. Kohno, K. Gokita, H. Shitanishi, M. Toyosaki, T. Nakamura, K. Morikawa, and M. Hatano, "Fault-Diagnosis Architecture for Large-Scale Photovoltaic Power Plants That Does Not Require Additional Sensors," *IEEE Journal of Photovoltaics,* vol. 9, pp. 780-789, 2019.

[23] H. Saha, G. Bhattacharya, and D. Mukherjee, "Mismatch losses in series combinations of silicon solar cell modules," *Solar cells,* vol. 25, pp. 143-153, 1988.

[24] N. L. Chang, A. W. Yi Ho-Baillie, P. A. Basore, T. L. Young, R. Evans, and R. J. Egan, "A manufacturing cost estimation method with uncertainty analysis and its application to perovskite on glass photovoltaic modules," *Progress in Photovoltaics: Research and applications,* vol. 25, pp. 390-405 %@ 1062-7995, 2017.

[25] R. Evans, K. H. Kim, X. Wang, A. Sugianto, X. Chen, R. Chen, and M. A. Green, "Simplified technique for calculating mismatch loss in mass production," *Solar Energy Materials and Solar Cells,* vol. 134, pp. 236-243 %@ 0927-0248, 2015.

[26] J. Bany, J. Appelbaum, and A. Braunstein, "The influence of parameter dispersion of electrical cells on the array power output," *IEEE Transactions on Electron Devices,* vol. 24, pp. 1032-1040 %@ 0018-9383, 1977.

[27] R. Zilles and E. Lorenzo, "An analytical model for mismatch losses in PV arrays," *International journal of solar energy,* vol. 13, pp. 121-133 %@ 0142-5919, 1992.

[28] L. L. Bucciarelli Jr, "Power loss in photovoltaic arrays due to mismatch in cell characteristics," *Solar energy,* vol. 23, pp. 277-288, 1979.

[29] J. Webber and E. Riley, "Mismatch loss reduction in photovoltaic arrays as a result of sorting photovoltaic modules by max-power parameters," *ISRN Renewable Energy,* vol. 2013, 2013.

[30] D. G. Lorente, S. Pedrazzi, G. Zini, A. Dalla Rosa, and P. Tartarini, "Mismatch losses in PV power plants," *Solar Energy,* vol. 100, pp. 42-49, 2014.

[31] S. Shirzadi, H. Hizam, and N. I. A. Wahab, "Mismatch losses minimization in photovoltaic arrays by arranging modules applying a genetic algorithm," *Solar Energy,* vol. 108, pp. 467-478, 2014.

[32] Y. Hu, B. Gao, X. Song, G. Y. Tian, K. Li, and X. He, "Photovoltaic fault detection using a parameter based model," *Solar Energy,* vol. 96, pp. 96-102, 2013.

[33] M. C. Di Piazza, M. Luna, G. Petrone, and G. Spagnuolo, "Translation of the single-diode PV model parameters identified by using explicit formulas," *IEEE Journal of Photovoltaics,* vol. 7, pp. 1009-1016, 2017.

[34] A. Skoczek, T. Sample, and E. D. Dunlop, "The results of performance measurements of field-aged crystalline silicon photovoltaic modules," *Progress in Photovoltaics: Research and applications,* vol. 17, pp. 227-240, 2009.

[35] J. D. Bastidas-Rodriguez, E. Franco, G. Petrone, C. A. Ramos-Paja, and G. Spagnuolo, "Model-based degradation analysis of photovoltaic modules through series resistance estimation," *IEEE Transactions on Industrial Electronics,* vol. 62, pp. 7256-7265, 2015.

[36] N. Femia, G. Petrone, G. Spagnuolo, and M. Vitelli, *Power electronics and control techniques for maximum energy harvesting in photovoltaic systems*: CRC press, 2012.

[37] D. C. Jordan and S. R. Kurtz, "The dark horse of evaluating long-term field performance—Data filtering," *IEEE Journal of Photovoltaics,* vol. 4, pp. 317-323, 2013.

[38] P. Manganiello, M. Balato, and M. Vitelli, "A survey on mismatching and aging of PV modules: The closed loop," *IEEE Transactions on Industrial Electronics,* vol. 62, pp. 7276-7286, 2015.

[39] E. R. Sanseverino, T. N. Ngoc, M. Cardinale, V. L. Vigni, D. Musso, P. Romano, and F. Viola, "Dynamic programming and Munkres algorithm for optimal photovoltaic arrays reconfiguration," *Solar Energy,* vol. 122, pp. 347-358, 2015.

[40] A. Al Mansur, M. R. Amin, and K. K. Islam, "Determination of Module Rearrangement Techniques for Non-uniformly Aged PV Arrays with SP, TCT, BL

and HC Configurations for Maximum Power Output," in *2019 International Conference on Electrical, Computer and Communication Engineering (ECCE)*, 2019, pp. 1-5.

[41] Y. Hu, J. Zhang, P. Li, D. Yu, and L. Jiang, "Non-uniform aged modules reconfiguration for large-scale pv array," *IEEE Transactions on Device and Materials Reliability*, vol. 17, pp. 560-569, 2017.

[42] P. Udenze, Y. Hu, H. Wen, X. Ye, and K. Ni, "A Reconfiguration Method for Extracting Maximum Power from Non-Uniform Aging Solar Panels," *Energies*, vol. 11, p. 2743, 2018.

[43] Y. Hu, J. Zhang, J. Wu, W. Cao, G. Y. Tian, and J. L. Kirtley, "Efficiency improvement of nonuniformly aged PV arrays," *IEEE Transactions on Power Electronics*, vol. 32, pp. 1124-1137, 2016.

[44] A. A. Mansur, M. Amin, and K. K. Islam, "Performance Comparison of Mismatch Power Loss Minimization Techniques in Series-Parallel PV Array Configurations," *Energies*, vol. 12, p. 874, 2019.

[45] N. Belhaouas, M. S. A. Cheikh, P. Agathoklis, M. R. Oularbi, B. Amrouche, K. Sedraoui, and N. Djilali, "PV array power output maximization under partial shading using new shifted PV array arrangements," *Applied energy*, vol. 187, pp. 326-337 %@ 0306-2619, 2017.

[46] R. Kadri, H. Andrei, J.-P. Gaubert, T. Ivanovici, G. Champenois, and P. Andrei, "Modeling of the photovoltaic cell circuit parameters for optimum connection model and real-time emulator with partial shadow conditions," *Energy*, vol. 42, pp. 57-67 %@ 0360-5442, 2012.

[47] A. Peled and J. Appelbaum, "Minimizing the current mismatch resulting from different locations of solar cells within a PV module by proposing new interconnections," *Solar Energy*, vol. 135, pp. 840-847 %@ 0038-092X, 2016.

[48] E. Kandemir, N. S. Cetin, and S. Borekci, "A comprehensive overview of maximum power extraction methods for PV systems," *Renewable and Sustainable Energy Reviews*, vol. 78, pp. 93-112 %@ 1364-0321, 2017.

[49] D. Picault, B. Raison, S. Bacha, J. De La Casa, and J. Aguilera, "Forecasting photovoltaic array power production subject to mismatch losses," *Solar Energy*, vol. 84, pp. 1301-1309 %@ 0038-092X, 2010.

[50] D. Picault, "Reduction of mismatch losses in grid-connected photovoltaic systems using alternative topologies," 2010.

[51] M. Balato, L. Costanzo, and M. Vitelli, "Series–Parallel PV array re-configuration: Maximization of the extraction of energy and much more," *Applied energy*, vol. 159, pp. 145-160 %@ 0306-2619, 2015.

[52] M. Balato, L. Costanzo, and M. Vitelli, "Multi-Objective Optimization of PV arrays performances by means of the dynamical reconfiguration of PV modules connections," 2015, pp. 1646-1650 %@ 1479999822.

[53] D. Picault, B. Raison, S. Bacha, J. Aguilera, and J. De La Casa, "Changing photovoltaic array interconnections to reduce mismatch losses: a case study," 2010, pp. 37-40 %@ 1424453704.

[54] M.-C. Alvarez-Hérault, D. Picault, R. Caire, B. Raison, N. HadjSaid, and W. Bienia, "A novel hybrid network architecture to increase DG insertion in electrical distribution systems," *IEEE Transactions on Power Systems,* vol. 26, pp. 905-914 %@ 0885-8950, 2010.

[55] S. R. Potnuru, D. Pattabiraman, S. I. Ganesan, and N. Chilakapati, "Positioning of PV panels for reduction in line losses and mismatch losses in PV array," *Renewable Energy,* vol. 78, pp. 264-275 %@ 0960-1481, 2015.

[56] M. Balato, L. Costanzo, and M. Vitelli, "Reconfiguration of PV modules: A tool to get the best compromise between maximization of the extracted power and minimization of localized heating phenomena," *Solar Energy,* vol. 138, pp. 105-118 %@ 0038-092X, 2016.

[57] S. R. Pendem and S. Mikkili, "Modelling and performance assessment of PV array topologies under partial shading conditions to mitigate the mismatching power losses," *Solar Energy,* vol. 160, pp. 303-321 %@ 0038-092X, 2018.

[58] S. Mohammadnejad, A. Khalafi, and S. M. Ahmadi, "Mathematical analysis of total-cross-tied photovoltaic array under partial shading condition and its comparison with other configurations," *Solar Energy,* vol. 133, pp. 501-511 %@ 0038-092X, 2016.

[59] E. Karatepe, M. Boztepe, and M. Colak, "Development of a suitable model for characterizing photovoltaic arrays with shaded solar cells," *Solar Energy,* vol. 81, pp. 977-992 %@ 0038-092X, 2007.

[60] S. Bana and R. P. Saini, "Experimental investigation on power output of different photovoltaic array configurations under uniform and partial shading scenarios," *Energy,* vol. 127, pp. 438-453 %@ 0360-5442, 2017.

[61] A. S. Yadav, R. K. Pachauri, Y. K. Chauhan, S. Choudhury, and R. Singh, "Performance enhancement of partially shaded PV array using novel shade dispersion effect on magic-square puzzle configuration," *Solar Energy,* vol. 144, pp. 780-797 %@ 0038-092X, 2017.

[62] N. Mishra, A. S. Yadav, R. Pachauri, Y. K. Chauhan, and V. K. Yadav, "Performance enhancement of PV system using proposed array topologies under various shadow patterns," *Solar Energy,* vol. 157, pp. 641-656 %@ 0038-092X, 2017.

[63] C. Deline, B. Marion, J. Granata, and S. Gonzalez, "A performance and economic analysis of distributed power electronics in photovoltaic systems," *Contract*, vol. 303, pp. 275-3000, 2011.

[64] Y. Du, K. Yan, Z. Ren, and W. Xiao, "Designing localized MPPT for PV systems using fuzzy-weighted extreme learning machine," *Energies*, vol. 11, p. 2615, 2018.

[65] C. Ramos-Paja, D. Gonzalez Montoya, and J. Bastidas-Rodriguez, "Sliding-Mode Control of Distributed Maximum Power Point Tracking Converters Featuring Overvoltage Protection," *Energies*, vol. 11, p. 2220, 2018.

[66] H. Islam, S. Mekhilef, N. Shah, T. Soon, M. Seyedmahmousian, B. Horan, and A. Stojcevski, "Performance evaluation of maximum power point tracking approaches and photovoltaic systems," *Energies*, vol. 11, p. 365, 2018.

[67] M. Hammami and G. Grandi, "A Single-Phase Multilevel PV Generation System with an Improved Ripple Correlation Control MPPT Algorithm," *Energies*, vol. 10, p. 2037, 2017.

[68] L.-Y. Chang, Y.-N. Chung, K.-H. Chao, and J.-J. Kao, "Smart Global Maximum Power Point Tracking Controller of Photovoltaic Module Arrays," *Energies*, vol. 11, p. 567, 2018.

[69] K.-H. Chao and M.-C. Wu, "Global maximum power point tracking (MPPT) of a photovoltaic module array constructed through improved teaching-learning-based optimization," *Energies*, vol. 9, p. 986, 2016.

[70] T. Pei, X. Hao, and Q. Gu, "A Novel Global Maximum Power Point Tracking Strategy Based on Modified Flower Pollination Algorithm for Photovoltaic Systems under Non-Uniform Irradiation and Temperature Conditions," *Energies*, vol. 11, p. 2708, 2018.

[71] E. Koutroulis and F. Blaabjerg, "A new technique for tracking the global maximum power point of PV arrays operating under partial-shading conditions," *IEEE Journal of Photovoltaics*, vol. 2, pp. 184-190, 2012.

[72] F. Spertino and J. S. Akilimali, "Are Manufacturing $ I $–$ V $ Mismatch and Reverse Currents Key Factors in Large Photovoltaic Arrays?," *IEEE Transactions on Industrial Electronics*, vol. 56, pp. 4520-4531, 2009.

[73] R. Zilles and E. Lorenzo, "Statistical analysis of current voltage characteristics of PV modules," *International journal of solar energy*, vol. 9, pp. 233-239, 1991.

[74] P. Devices—Part, "Measurement of Photovoltaic Current-Voltage Characteristics," *CEI/IEC*, pp. 60904-1.

[75] I. Standard, "60891. Photovoltaic Devices. Procedures for Temperature and Irradiance Corrections to Measured IV Characteristics," *International Electrotechnical Commission*, 2009.

[76] D. G. f. Sonnenenergie, *Planning and installing photovoltaic systems: a guide for installers, architects and engineers*: Routledge, 2013.

[77] P. Bakas, A. Marinopoulos, and B. Stridh, "Impact of PV module mismatch on the PV array energy yield and comparison of module, string and central MPPT," in *Photovoltaic Specialists Conference (PVSC), 2012 38th IEEE*, 2012, pp. 001393-001398.

[78] A. Harrag and S. Messalti, "Adaptive GA-based reconfiguration of photovoltaic array combating partial shading conditions," *Neural Computing and Applications,* vol. 30, pp. 1145-1170, 2018.

[79] S. Bana and R. Saini, "Experimental investigation on power output of different photovoltaic array configurations under uniform and partial shading scenarios," *Energy,* vol. 127, pp. 438-453, 2017.

[80] C. Han and H. Lee, "A field-applicable health monitoring method for photovoltaic system," *Reliability Engineering & System Safety,* vol. 184, pp. 219-227 %@ 0951-8320, 2019.

[81] E. Roumpakias and A. Stamatelos, "Performance analysis of a grid-connected photovoltaic park after 6 years of operation," *Renewable Energy,* vol. 141, pp. 368-378 %@ 0960-1481, 2019.

[82] C. Han and H. Lee, "Investigation and modeling of long-term mismatch loss of photovoltaic array," *Renewable Energy,* vol. 121, pp. 521-527 %@ 0960-1481, 2018.

[83] E. D. Dunlop and D. Halton, "The performance of crystalline silicon photovoltaic solar modules after 22 years of continuous outdoor exposure," *Progress in Photovoltaics: Research and applications,* vol. 14, pp. 53-64 %@ 1062-7995, 2006.

[84] I. Standard, "60904-1, Photovoltaic Devices, Part 1: Measurement of Photovoltaic Current–Voltage Characteristics," *International Electrotechnical Commission, Geneva, Switzerland,* 2006.

[85] R. Zilles and E. Lorenzo, "An analytical model for mismatch losses in PV arrays," *International journal of solar energy,* vol. 13, pp. 121-133, 1992.

[86] P. R. Satpathy, A. Sarangi, S. Jena, B. Jena, and R. Sharma, "Topology alteration for output power maximization in PV arrays under partial shading," in *2018 Technologies for Smart-City Energy Security and Power (ICSESP)*, 2018, pp. 1-6.

[87] P. R. Satpathy, S. Jena, B. Jena, and R. Sharma, "Comparative study of interconnection schemes of modules in solar PV array network," in *2017 International Conference on Circuit, Power and Computing Technologies (ICCPCT)*, 2017, pp. 1-6.

[88] S. Vijayalekshmy, G. Bindu, and S. R. Iyer, "Estimation of power losses in photovoltaic array configurations under moving cloud conditions," in *2014 Fourth*

International Conference on Advances in Computing and Communications, 2014, pp. 366-369.

[89] L. El Iysaouy, M. Lahbabi, and A. Oumnad, "Enhancing the Performances of PV Array Configurations Under Partially Shaded Conditions: A Comparative Study," *International Journal of Renewable Energy Research (IJRER)*, vol. 8, pp. 1779-1790 %@ 1309-0127, 2018.

[90] P. S. Rao, P. Dinesh, G. S. Ilango, and C. Nagamani, "Laboratory course on solar photovoltaic systems based on low cost equipment," 2013, pp. 146-151 %@ 1479916269.

[91] B. Nayak, A. Mohapatra, and P. Das, "Optimal hybrid array configuration scheme to reduce mismatch losses of photovoltaic system," 2017, pp. 1-7 %@ 1509032398.

[92] C. International Electrotechnical, "Standard IEC 60904-3: photovoltaic devices," *Part 3: Measurement Principles for Terrestrial Photovoltaic (PV) Solar Devices with Reference Spectral Irradiance Data*, 1987.

Publications

[1] Ahmed Al Mansur, Ruhul Amin, Kazi Khairul Islam, "Performance Comparison of Mismatch Power Loss Minimization Techniques in Series-Parallel PV Array Configurations" -Energies 2019, 12, 874.

[2] Ahmed Al Mansur, Md Ruhul Amin, Kazi Khairul Islam, "Comparative Analysis of Mismatch Power Loss Reduction Techniques for Photovoltaic Series Parallel Array Configurations"- IAPE '19, Oxford, United Kingdom ISBN: 978-1-912532-05-6, March, 2019.

[3] Ahmed Al Mansur, Ruhul Amin, Kazi Khairul Islam "Determination of Module Rearrangement Techniques for Non-uniformly Aged PV Arrays with SP, TCT, BL and HC Configurations for Maximum Power Output"- International Conference on Electrical, Computer and Communication Engineering (ECCE), 7-9 Feb. 2019.

[4] Ahmed Al Mansur, Ruhul Amin, "Performance Investigation of Different PV Array Configurations at Partial Shading Condition for Maximum Power Output", International Journal of Renewable Energy Research- IEEE Conf. STI, Dec, 24-25, 2019 (Accepted).

Paper Under Review

[5] Ahmed Al Mansur, Ruhul Amin, "Performance Comparison of Mismatch Power Loss Reduction Techniques for Aged PV Arrays", IEEE Transactions on Industrial Electronics. (Under Review)

[6] Ahmed Al Mansur, Ruhul Amin, "The Effects of Non-Uniformly Aged Photovoltaic Array on the Mismatch Power Loss: A Practical Investigation towards Novel Hybrid Array Configurations", Energy Conversion and Management-Journal-Elsevier.